# DERIVING THE DENSITY OF STATES FOR GRANULAR CONTACT FORCES

by

PHILIP TILLMAN METZGER
B.E.E. Auburn University, 1985
M.S. University of Central Florida, 2000

A dissertation submitted in partial fulfillment of the requirements
for the degree of Doctor of Philosophy
in the Department of Physics
in the College of Arts and Sciences
at the University of Central Florida
Orlando, Florida

Spring Term
2005

Major Professor: Aniket Bhattacharya

## ABSTRACT

The density of single grain states in static granular packings is derived from first principles for an idealized yet fundamental case. This produces the distribution of contact forces $P_f(f)$ in the packing. Because there has been some controversy in the published literature over the exact form of the distribution, this dissertation begins by reviewing the existing empirical observations to resolve those controversies. A method is then developed to analyze Edwards' granular contact force probability functional from first principles. The derivation assumes Edwards' flat measure—a density of states (DOS) that is uniform within the metastable regions of phase space. A further assumption, supported by physical arguments and empirical evidence, is that contact force correlations arising through the closure of loops of grains may be neglected. Then, maximizing a state-counting entropy results in a transport equation that can be solved numerically. For the present it has been solved using the "Mean Structure Approximation," projecting the DOS across all angular coordinates to more clearly identify its predominant features in the remaining stress coordinates. These features are: (1) the Grain Factor $\overline{\Psi}$ related to grain stability and strong correlation between the contact forces on the same grain, and (2) the Structure Factor $\overline{\Upsilon}$ related to Newton's third law and strong correlation between neighboring grains. Numerical simulations were then performed for idealized granular packings to permit a direct comparison with the theory, and the data including $P_f(f)$ were found to be in excellent agreement. Where the simulations and theory disagree, it is primarily due to the coordination number $Z$ because the theory assumes $Z$ to be a constant whereas in disordered packings it is not. The form of the empirical DOS is discovered to have an elegant, underlying pattern related to $Z$. This pattern consists entirely of the functional forms correctly predicted by the theory, but with only slight parameter changes as a function of $Z$. This produces significant physical insight and suggests how the theory may be generalized in the future.

*To my beloved wife, Gigi, whose love and patient support made this work possible.*

## ACKNOWLEDGEMENTS

I gratefully acknowledge many enlightening discussions with Dr. Aniket Bhattacharya, Dr. Lee Chow, Dr. Michael Johnson, Dr. Weili Luo, and Dr. Boris Zel'dovich of the University of Central Florida, Dr. Nadine Barlow of the University of Northern Arizona, and Dr. Robert Youngquist of NASA's John F. Kennedy Space Center.

## TABLE OF CONTENTS

## LIST OF FIGURES

# CHAPTER 1

# INTRODUCTION

## 1.1 The Importance of Granular Physics

Humanity has had arguably more experience working with sand (through agriculture) than with any other material in nature, and beginning from the time of Coulomb we have scientifically investigated its rheological behaviors with intense interest due to the wide range of practical applications. Nevertheless, we still do not fundamentally understand sand's behaviors, many of which have a surprisingly complex and fascinating phenomenology [5, 6, 7]. As it now stands, we have equations for the mechanics of solids, liquids and gases; the dynamics of heat, electromagnetism and quantum mechanics; the behavior of the universe in its earliest moments and the formation of galaxies and stars—but ironically we cannot explain the pouring or squeezing of an ordinary pile of sand.

Traditionally, granular materials have been modeled as continua using various plasticity equations [8]. These are not a true rheological theory because they lack a first-principles explanation and because they contain numerical parameters which are chosen *ad hoc* to match the material's empirical behavior. These equations implicitly assume that the microstate behaviors of the individual grains can be coarse-grained into a continuum description at the macroscopic scale. However, recent studies have demonstrated that the microstate behaviors are self-organizing so that they produce effects observable at the largest spatial scales—resulting in pattern formation [6]—and thus the actual macroscopic behavior of granular materials may be more complex than simplistic continuum models can predict. Clearly, the continuum mechanics approach is neither satisfying nor illuminating from a fundamental perspective.

With the advancement of digital computing, which allows us to see the internal state

of a simulated granular packing, granular materials have re-emerged as a topic of intense interest to physicists in the past two decades. An example of a simulated granular packing from a particular technique called Discrete Element Modeling (DEM) is shown in Figure 1. In this technique the grains overlap very slightly at their contacts and a repulsive force is applied to each grain contact proportional to the amount of overlap. The simulation then solves Newton's equations of motion for each individual grain, dissipating energy through several numerical methods until static equilibrium is attained. The complete set of contact forces and geometric descriptors of the microstate can then be harvested. This computationally intensive technique is possible as long as the number of grains is not too large. Innovative experimental techniques have also been developed in recent years (for example, see References [9] and [10]), and these have worked together with the numerical simulations to produce a consistent picture of key granular phenomena.

Perhaps the most surprising discovery to emerge from these numerical simulations is the fact that a static granular packing under stress is *bimodal*, that it contains two populations of grains having rather distinct characteristics, distinguishable as those which have at least one contact force $f$ greater than the average $\langle f \rangle$, versus those that do not [11]. The former population is solid-like in that it supports shear stress just like a normal solid. The latter is liquid-like in that it supports essentially none of the shear stress of the packing. Not only does the solid-like mode carry the shear stress, it also carries the majority of the normal stresses in the packing. Its grains are organized into *force chains* which demonstrate long-range order even when the material itself is disordered with vanishing geometric correlation at very short distance. The force chains can be seen in Figure 1, where the thickness of the lines connecting grain centroids is proportional to the force at the corresponding grain contact. It is the percolation of these force chains that allows the overall packing to *jam* [12, 13] and act macroscopically like a solid despite the presence of the liquid-like mode within its bulk. That liquid-like mode consists of

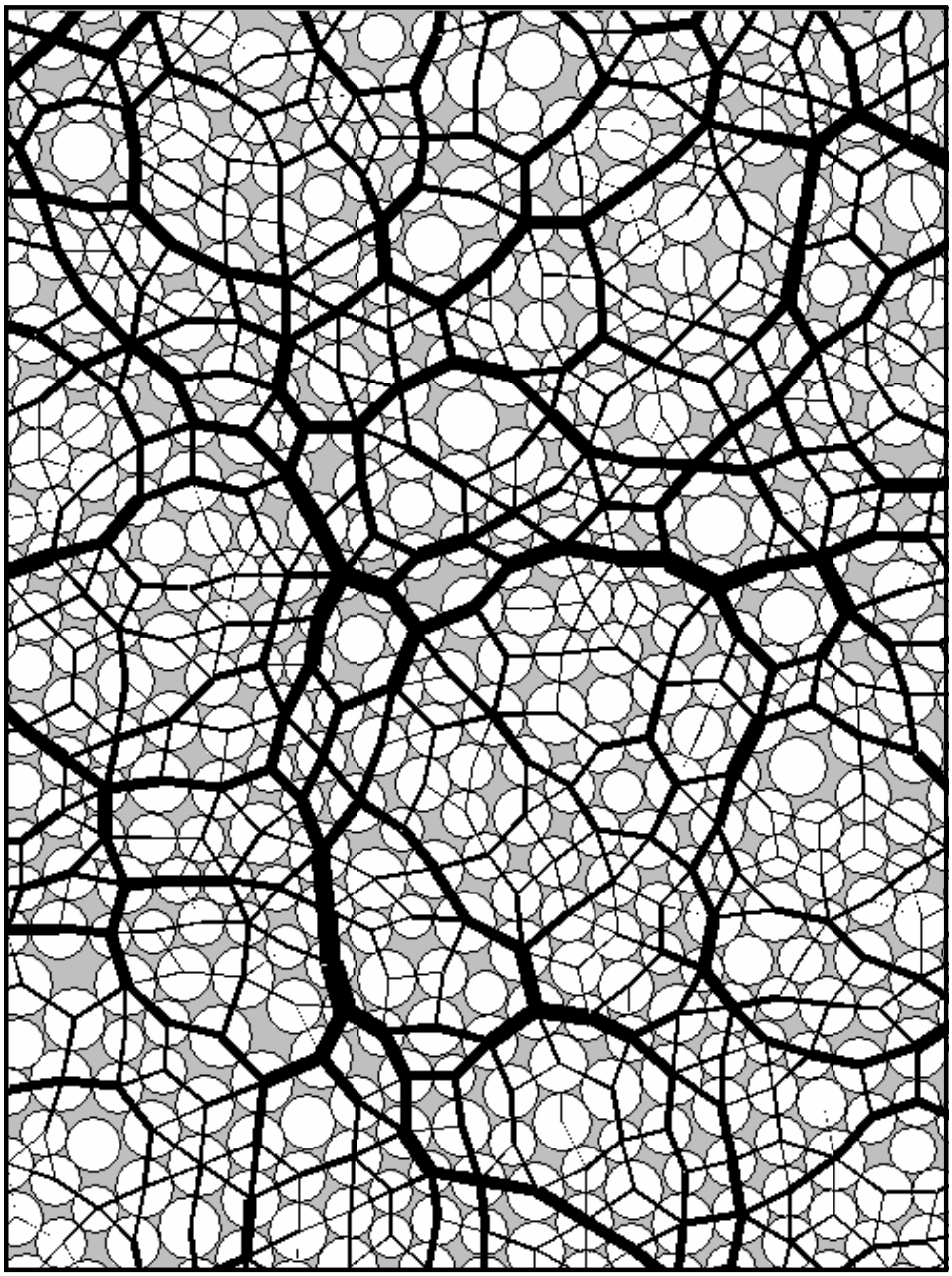

Figure 1: Portion of a computer-simulated granular packing. Line width is proportional to the compressive force between the grains.

approximately half the grains carrying a minority of the total load and none of the shear stress. They act like an interstitial fluid between the force chains, providing them with lateral support so that they do not buckle and collapse. The ability of the grains to rapidly exchange between the two modes as the force chains break and reorganize into new percolating networks [10, 11] is the essence of granular *fragility* [14] and the underlying mechanism of granular rheology. These concepts of jamming and fragility have emerged as central concepts in granular materials research.

Recently it has been conjectured that granular physics may fall within the purview of statistical mechanics, despite the fact that granular materials are athermal—gravity dominates over thermal vibrations so that they cannot explore a phase space—and have a small particle count relative to typical thermal ensembles. Edwards stated this in the 1980's when he hypothesized that a powder material may be represented by a statistical ensemble with a flat measure such that every metastable arrangement of grains (a *blocked* state) is equally probable [15]. This led to a statistical mechanics theory predicting the vibration-induced evolution of a powder's volume. Since then, Edwards' hypothesis has emerged as probably the main focus among granular theorists as it has passed a number of empirical tests. This shall be further discussed in section 3.2.1 as Edwards' flat measure is a part of the basis for this dissertation.

Edwards' hypothesis created significant interest in applying statistical mechanics to granular materials, and this interest increased after the probability density function (or *distribution*) of granular contact forces $P_f(f)$ had been measured. A typical $P_f(f)$, normalized so that $\langle f \rangle = 1$, is shown in Figure 2. It starts from a finite $P_f(0) > 0$, rises to a peak near $f = 1$, and then decays with an asymptotically exponential tail as demonstrated in Figure 3. This set of features is somewhat similar to those found in thermal distributions, implying that the same mathematical framework might apply. To see why this is so important, we may note that although the stress in a solid is properly represented by a rank two tensor, in a granular material all the stress information must

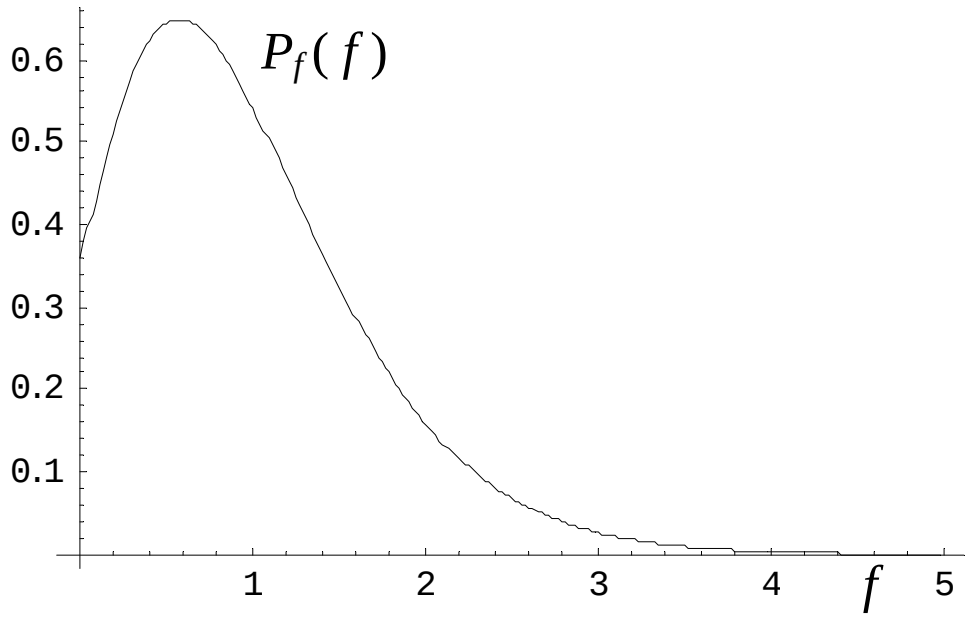


Figure 2: The typical form of $P_f(f)$ normalized so that $\langle f \rangle = 1$, showing the finite $P_f(0) > 0$, the rise to a peak near $f \approx \langle f \rangle$, and the decay at high forces.

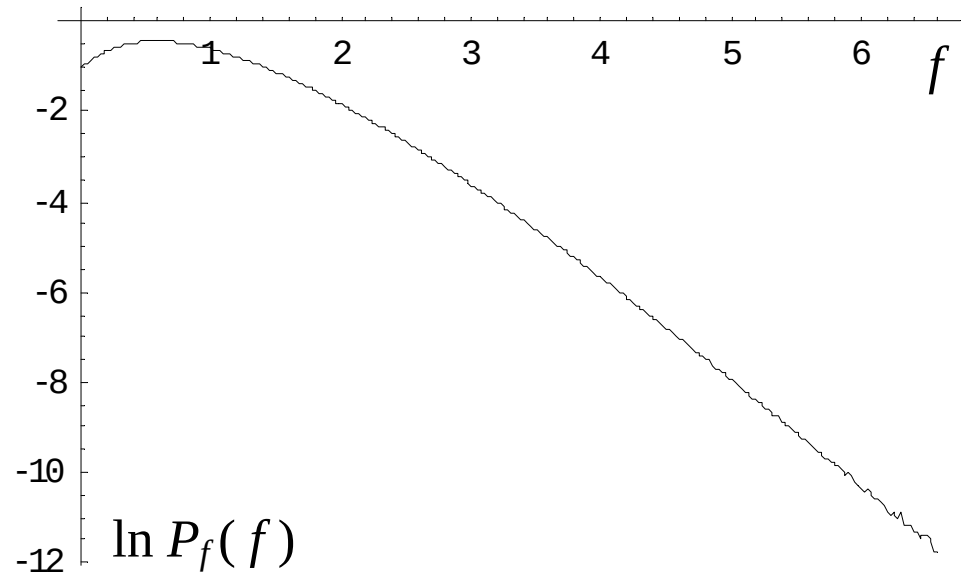


Figure 3: Semi logarithmic plot of the typical form of $P_f(f)$ showing the tail becoming increasingly straight at high forces, thereby indicating that the decay is asymptotically exponential.

be passed from a grain to its neighboring grains through the contact surfaces between them. To excellent approximation these contacts are point-like and unable to transmit torque. Hence, the stress field within the dissected medium of a granular material may be represented, without loss of information, by the forces between the grains. In other words, in granular materials the rank-two tensor field is reducible to a rank-one tensor field. Furthermore, this vector field is discretized rather than continuous; it consists of a summation of delta functions, one for each grain contact in the packing. Given only the magnitudes and directions of this finite number of force vectors, along with their physical locations in the medium, the stress tensor may be computed by coarse-graining over any spatial scale [16]. Hence, just as the discovery of the atom in the nineteenth century reshaped our view of matter from the continuum to the discretized description, so the consideration of grain contacts reshapes our view of the stress field in granular solids from a continuum to a discretized description. Just as the discretization of matter produced the statistical mechanics revolution and successfully explained thermal phenomena, so the discretization of the granular stress field may produce a statistical mechanics revolution and produce a theory of granular stress propagation. Since forces are what drive sand's dynamics, it is even possible that this could complete the work initiated by Coulomb: we just might find a way to explain the pouring and squeezing of sand. Hence, it is fundamentally important to understand the physics and mathematics that give rise to the form of $P_f(f)$ along with the other, related distributions. A successful theory of $P_f(f)$ will be tangible progress toward a statistical mechanics theory of granular materials. Because of this, there were several prior attempts to derive $P_f(f)$ [17, 18, 19, 20], but none of them successfully explained all of its features as described in the next chapter.

## 1.2 Organization of this Dissertation

This dissertation is organized as follows. This chapter has explained the significance of the granular contact force distribution in the larger context of granular physics. Chapter 2 will review what is known about the granular contact force distribution. Chapter 3 will analyze the density of states (DOS) for two-dimensional granular packings from first principles. This uses the ensemble methods of statistical mechanics: starting from Edwards' hypothesis it counts states, defines and maximizes an entropy, and produces a transport equation that can be solved numerically. Chapter 4 will introduce an approximation that significantly simplifies the transport equation as well as providing physical insight into the form of the DOS. Chapter 5 will solve the simplified transport equation and work out the key predictions of the theory. These predictions are shown to be in qualitative agreement with the existing experimental and simulation data, although these data are of limited value in this context because they were not obtained in cases formulated to match the theory. Chapter 6 presents the results of new dynamic simulations that were formulated specifically to test this theory. These results are compared to the theory, demonstrating excellent agreement. Furthermore, several elegant, underlying patterns in the DOS are identified. Chapter 7 summarizes the dissertation and states the major conclusions.

# CHAPTER 2

# THE FORM OF THE CONTACT FORCE DISTRIBUTION

This chapter will review the empirical observations of $P_f(f)$ and attempt to clear up some disagreements over its form. This will clear the way to derive a theory of $P_f(f)$ in the next chapter.

## 2.1 The Tail of the Distribution

Researchers have discovered, both in experiments [9, 21, 22, 23, 24] and in numerical simulations [25, 26, 27, 28, 29, 30, 31], that the distribution of contact force magnitudes has an exponential tail reminiscent of the energy distributions in thermal systems. This was contrary to the existing naïve expectation that stress fluctuations in a disordered solid should take on a Gaussian distribution around the mean, thereby demonstrating central limit theorem behavior like a random process. This unexpected result encourages the hope of a statistical mechanics theory. Whenever a thermal system is maximally entropic subject to energy conservation, the result is an exponential tail. Perhaps the tail in granular force distributions is likewise indicating maximal randomness subject to a global force conservation law of some kind.

Another way to look at the unexpected broadness in the tail is that it is an indicator of the existence of force chains [10, 11], because an unexpectedly large fraction of the grains carry forces significantly higher than the mean. It indicates that force fluctuations above mean die out exponentially slow rather than with Gaussian quickness, resulting in long-range order of the force chains.

### *2.1.1 Gaussian versus Exponential Tails*

There are some factors that complicate the interpretation of the tail. First, there is usually some downward curvature in the tail when plotted semi-logarithmically, and this has caused some discussion [3, 19, 32] whether the asymptotic behavior of the tail $\sim \exp(-\beta f^{\alpha})$ is Gaussian ($\alpha = 2$) or compressed exponential ($1 < \alpha < 2$) rather than truly exponential ($\alpha = 1$). However, this curvature can be explained simply by noting how slowly the asymptotic behavior develops. Normally it becomes apparent only beyond several multiples of the average value of force, $\langle f \rangle$, and this seems to be dependent upon the dimensionality of the packing. For example, Figures 2 and 5 of reference [26] shows exponential behavior beginning at $f \approx 3 \langle f \rangle$ for two dimensional (2D) packings and $f \approx 2 \langle f \rangle$ for three dimensional (3D) packings. There may be other factors which hasten or delay the onset of exponentiality as well, such as the presence or absence of friction. A number of the semi logarithmic plots in the published literature lack statistical precision for a sufficient range beyond the exponential onset and thus may appear Gaussian. This is because the eye tends to extrapolate the curvature it sees just prior to the loss of precision. However, the author has seen no case that is truly inconsistent with an exponential tail beyond the reasonable range of onsets except when there are large deformations [19, 23, 33] or a very small number of grains [34]. On the other hand, there are numerous examples which clearly show an exponential tail inconsistent with a Gaussian or other curved form. These examples include 2D frictional simulations using contact dynamics (CD) and molecular dynamics [26]; 3D frictional simulations using CD [26], a Hertzian contact law [30], and a Hookean contact law [30, 31]; 3D frictionless simulations using two versions of the Lennard-Jones potential [27]; 3D frictional experiments [9, 22]; and 3D frictionless experiments with emulsions [23].

Second, some studies have shown that as packings are increasingly compressed, causing large deformations at the grain contacts, the tails continuously evolve from a more apparently exponential to a more downwardly curved form [19, 23, 33]. This behavior has

not been observed in every relevant case [21]. Because of this, it is the author's opinion that the important physical dependencies have not been experimentally identified, yet, and more experimental work is needed on this topic before a theory can be reasonably formulated. This paper will therefore focus exclusively on cases with perfectly rigid grains and will leave this topic of large deformations to future research.

Third, it has been hypothesized [19, 32] that the form of the tail depends on the form of the work function $W(f)$ at the grain contacts. These hypotheses predict Gaussian and/or compressed exponential tails for some of the typical work functions used in numerical modeling. However, a simple argument can prove that, for frictionless packings in the limit of small deformations, the contact force distribution *cannot* be a functional of $W(f)$. This is due to the *isostatic* character of such packings [35], as explained below.

Isostaticity means that the number of equations (mechanical degrees of freedom) for all the grains equals the number of unknowns (contact forces) in the overall packing. Then, all the forces can be derived strictly as a linear algebra problem given the geometry of the contact network and the imposed mechanical loading at the boundaries, alone. For packings of $N$ round, rigid, frictionless grains in $d$ spatial dimensions there are only $d$ translational degrees of freedom per grain (i.e., no rotational modes can be activated) and hence there must be $Nd$ unknowns for the packing to be isostatic. Since each frictionless contact provides only one unknown (the normal force, with no tangential force permitted), there must be $Nd$ contacts in the packing. The *coordination number* $Z$ is the number of contacts that an individual grain has with neighboring grains. Since each contact is shared by two grains, the packing must have an average coordination number $\langle Z \rangle = 2d$ for it to be isostatic. Likewise, for frictional grains, which have rotational degrees of freedom, it can be shown that isostaticity requires $\langle Z \rangle = d + 1$. Packings with too many contacts are called *hyperstatic*.

It has been shown that packings of frictionless, rigid, round grains are actually isostatic [35], whereas frictional packings appear to be hyperstatic. In the isostatic case,

where all the forces in the packing are solvable as a function of the contact geometry and the loading at the boundaries, the only role that $W(f)$ can play is in helping to decide what the geometry of the contact network shall be. If $W(f)$ is relatively soft so that deformations are large, then the geometry of the contact network will be perturbed significantly as the loading is increased, and then $W(f)$ may indeed affect the resulting forces. However, in the limit when the deformations become vanishingly small relative to the diameters of the grains, then the geometry of the contact network becomes independent of the form of $W(f)$ and the contact forces must also become independent of the form of $W(f)$. Therefore, the force distributions resulting from every $W(f)$ must approach a universal form in this limit. This conclusion is corroborated by Bouchaud's argument involving the $q$ model, as discussed below.

### *2.1.2 The Tail Derived in the $q$ Model*

The most influential model to study contact force distributions was the $q$ model introduced by Coppersmith, *et al.* [36, 37] For simplicity Figure (4) shows only the two-dimensional diamond lattice version of the $q$ model with two contacts above and below each grain. Each node represents a grain and the legs represent contacts between grains. A scalar value is propagated through each leg representing the *vertical component* of the force at a contact, $f_x$. The sum of all such inputs at the top of a grain plus the grain's gravitational weight $w_0$ form the *Cartesian load*, or simply the *load*, of each grain, $w$. Omitting $w_0$ represents a packing without gravity. Random $q$ variables are assigned to each grain according to a specified probability distribution $\eta(q)$, $0 \leq q \leq 1$, to determine what fraction of its load is transmitted to the contact on its lower right, the remainder going to the lower left. The calculations proceed layer-by-layer from top to bottom so that all information flows in the same direction. If $\eta(q) \equiv 1$, then the model is called the "uniform" $q$ model. If $q$ can only take on values of exactly 0 or 1, then it is called the "critical" $q$ model. In all cases except the critical case, after some tens

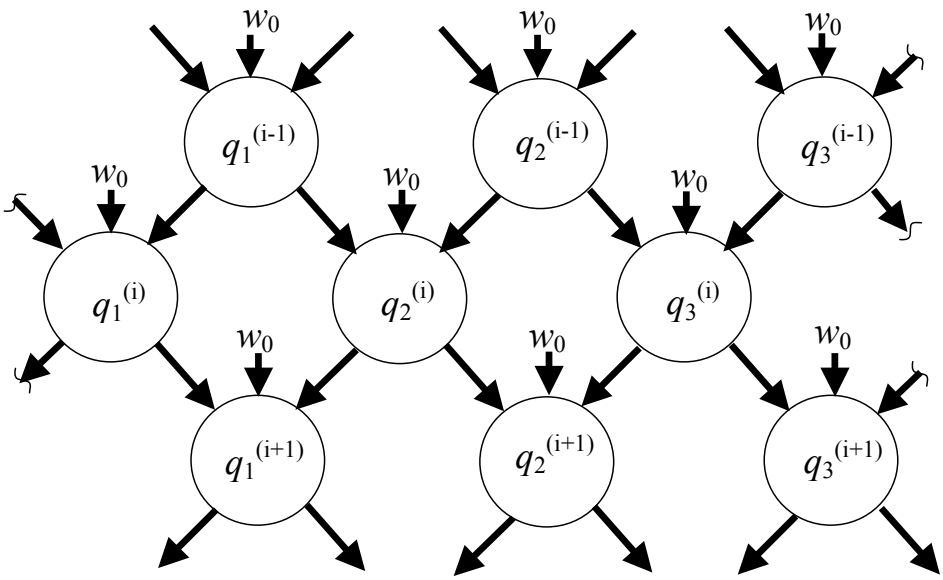


Figure 4: A version of the $q$ model.

of layers into the packing the distribution of vertical forces relaxes to a monotonically decreasing form having an exponential tail. The critical $q$ model, being the sole exception, produces a power law tail, and the uniform $q$ model produces a purely exponential (Gibbs) distribution of the vertical forces.

It should be remembered that since the $q$ model only propagates the vertical component of force it cannot predict the distribution of $f$, which is a vector magnitude. Thus, the $q$ model is often called the *scalar* model. It predicts $P_x(f_x)$ where $f_x$ is the vertical component of force, and $P_w(w)$ where $w$ is the total vertical load supported by each grain. Numerical simulation data have agreed with the $q$ model that $P_x(f_x)$ should indeed be monotonically decreasing [38] (in contrast to $P_f(f)$ which usually is not monotonic). Also, the exponential tail in $P_x(f_x)$ has been understood to imply the same asymptotic behavior in $P_f(f)$, and so the model is relevant to understanding the tail of $P_f(f)$ despite being a scalar model.

The $q$ model introduced a new way to think about granular media: the statistical relaxation of the force distribution does not occur dynamically through the time dimension

as it does in thermal systems; rather it is a necessary feature of the *internal*, layer-by-layer static equilibrium relationships, where the spatial dimensions play a role analogous to the time dimension for the corresponding set of Cartesian components of force [37]. In the weightless case, the total of all the vertical forces in a layer of grains is conserved layer-by-layer across the model. It is possible to count states in the uniform $q$ model and maximize the entropy using a Lagrange multiplier to conserve that total force. The exponential decay constant in the resulting distribution derives from that Lagrange multiplier, and this shows a commonality between granular and thermal systems: in both cases the exponential tail is due to maximal randomness subject to a global conservation law. Several vectorial generalizations of the $q$ model, as well as other lattice-based models, have been developed [39] but none has received the same attention nor produced same the degree of insight as the $q$ model.

Bouchaud has shown that the sufficient condition for an exponential tail to occur in any noncritical version of the $q$ model is merely that some grains be allowed to tip all of their load into one contact [7]. This allows arbitrarily large forces to accumulate along particular force chains. This argument applies to all cohesionless granular media regardless of $W(f)$, except for cases where the grains cannot freely tip. This demonstrates that there must be a universal, asymptotic form of the tail, regardless of $W(f)$, and that it is exponential. We may draw another important inference: when deformations become large, the formation of additional contacts increases the stability of the grains so that they may not tip, hence allowing the forces to be more evenly distributed through space [33]. This may erode the exponential tail so that it transits to the more rapidly decreasing form.

Chapter 3 will develop a way to generalize the entropy maximization inherent in the $q$ model. It will count states and maximize entropy for the fully vectorial set of forces while enforcing conservation of the overall stress tensor. It will be shown that this produces the asymptotically exponential tail along with the other features of $P_f(f)$ that the $q$ model

was not able to predict.

### 2.2 The Region of Weak Forces

While the empirical form of $P_f(f)$ has an exponential tail reminiscent of the energy distributions of thermal systems, its overall form is not found in thermal systems. It generally has a peak or plateau near the average force and a nonzero value at zero force as illustrated in Figure (2). In contrast to this form, the prototypical distributions found in thermal systems are either monotonically decreasing (e.g., the Gibbs energy distribution), or begin from zero probability density at the origin before rising to a peak (e.g., the Planck and the Maxwell-Boltzmann distributions). In the nonmonotonic cases the rising slope is due to the degeneracy of states. The degeneracies reflect the spatial dimensionality of the system and dominate the form of the distribution at weak energies beginning from the origin. Since the forces in a granular medium are vector magnitudes composed from several Cartesian components—implying degeneracy in the force magnitudes—this raises the question why $P_f(f)$ does not likewise begin from the origin $P_f(0) = 0$ before rising to its peak? Indeed, a recent model predicts that it should [20]. Perhaps the empirical $P_f(0) > 0$ is merely an artifact of the methods since weak forces are the most difficult to simulate and measure; perhaps the theoretical model with $P_f(0) = 0$ provides the clearer view into the physics.

It seems to the author that this is not the case for two reasons. First, it has been shown that the form in the region of weak forces evolves in a predictable way as a function of stress and/or fabric anisotropy, which may be induced through shearing [28]. This is illustrated in Figure 5. The curve with the lowest intercept on the vertical axis is the isotropic case. The other curves qualitatively illustrate the evolution of its form with increasing anisotropy.

This anisotropy dependence probably explains the variations in $P_f(f)$ seen among the different empirical studies, in that some jammed packings have displayed peaks while

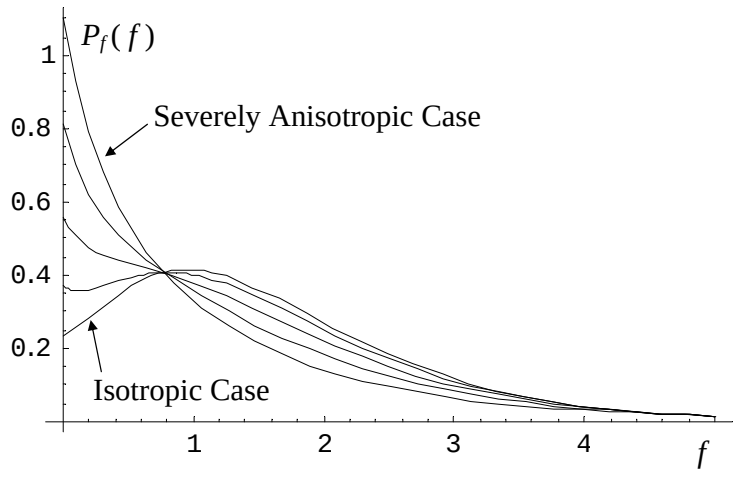


Figure 5: Evolution of $P_f(f)$ under anistropy. To separate the graphs for clarity, their vertical axes are not normalized.

others have displayed plateaus or monotonic forms. For a packing of grains originally in an isotropic state, $P_f(f)$ displays a form similar to Figure (2). As the packing is quasi-statically sheared the distribution smoothly evolves to having a plateau in the region of weak forces and then on to becoming a monotonically decreasing function. After the packing achieves peak shear strength, continued shearing reduces the stress anisotropy and causes the distribution to retrace its evolution most of the way, ending with a small peak again. This behavior affects the distribution well above the region of numerical uncertainty and cannot be dismissed as the result of dynamical or transient forces since the shearing is quasi-static. It is difficult to see how this smooth variation of forms—including plateaus and monotonic forms—could be explained if the finite $P_f(0) > 0$ were merely an artifact.

Second, the unique features of the distribution have been obtained using a wide range of empirical techniques, and it does not seem reasonable that all of them are incorrect in the region of weak forces. These techniques include experiments with frictional grains [9, 21], numerical simulations with frictional grains [25, 26, 28, 30, 31] or purely frictionless grains [32, 38, 40], hyperstatic ensembles [34, 41], and adaptive network models [42]. The simulation techniques have included contact dynamics (CD), discrete element

modeling (DEM), and molecular dynamics (MD) quenched beneath the glass transition [27], all of which are well-established techniques. The contact laws in these simulations have included Hertzian, Hookean, and Lennard Jones potentials. Simulations have been done with and without gravity and under a wide variety of conditions. The transitions between the boundary and bulk have been thoroughly examined [38, 40]. The numerical techniques have demonstrated the ability to distinguish between distributions that begin at the origin and those that do not [38, 40]. Although experiments with frictionless emulsions [23] and some numerical simulations [29] have been fitted to forms that begin with $P_f(0) = 0$, arguably those data would be fit as well or better by forms with nonzero $P_f(0)$.

The rise in $P_f(f)$ to a peak before decaying cannot be explained as a degeneracy of states, so how do we explain this behavior? The answer emerges from the most important organizing feature of granular packings: the requirement that the grains be individually stable. There is no analogous requirement in classical thermal systems, and it turns out that this requirement biases the density of states against weaker forces. An explanation of the bias begins by noting that any two contact forces on the same grain are strongly correlated, increasingly so as the contacts are further away from each other toward opposite sides of the grain [30]. To develop physical intuition for this, this chapter will demonstrate the effect of these correlations using only a simplified case as shown in Figure 6.

For an isotropic packing of frictionless 2D grains, consider one grain which has two of its contacts exactly opposite one another, $\psi_1 = 0$ and $\psi_2 = \pi$ as shown in Fig. 6. The force $f_1$ is clearly related to $f_3$, but not generally equal to it because of the contact forces $f_2$ and $f_4$ located in $\pi/3 < \psi_1 < 2\pi/3$ and $4\pi/3 < \psi_4 < 5\pi/3$, respectively. Note that steric exclusion keeps the contacts arranged fairly predictably around a grain, which prevents the statistically averaged general case from deviating too far from this special

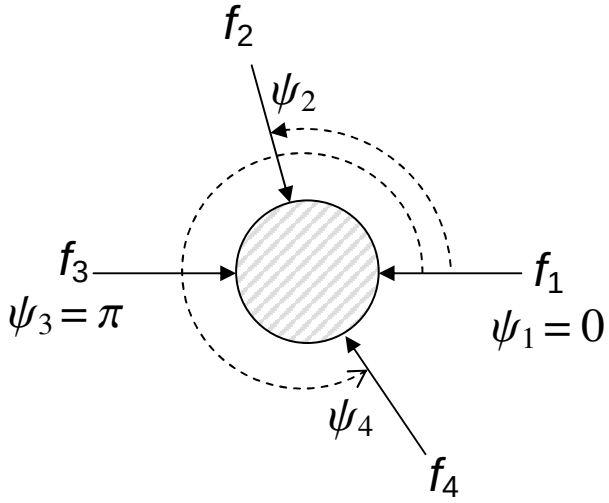


Figure 6: Special case to illustrate why grains with below-average forces correspond to fewer stable locations in phase space than do grains with average forces.

case. Static equilibrium requires

$$\begin{aligned} f_2 \sin\psi_2 &= -f_4 \sin\psi_4, \\ f_1 &= f_3 - G, \end{aligned} \tag{1}$$

where

$$G = f_2 \cos\psi_2 + f_4 \cos\psi_4 \tag{2}$$

is the difference between $f_1$ and $f_3$. Then $G = J^{-1} f_4$,

$$J^{-1} = \cos\psi_4 - \cos\psi_2 \frac{\sin\psi_4}{\sin\psi_2}. \tag{3}$$

We assume that the distribution of $f_4$ is representative of all the forces in the packing. These have a distribution $P_f(f)$, which we want to derive. By changing variables the distribution of $G$ in terms of $P_f$ is

$$P_G(G) = \int_{\pi/3}^{2\pi/3} \mathrm{d}\psi_2 \int_{4\pi/3}^{5\pi/3} \mathrm{d}\psi_4 \; |J| \; P_f\left(G \; J\right), \tag{4}$$

where $J$ is identified as the Jacobian. All we know about $P_f$ is that it is zero for negative arguments (tensile forces), but positive valued and normalized for positive arguments.

Assuming it is a continuous function its normalization implies that it has a bounded tail. Over the range of integration, $J$ has odd symmetry in the sense that $J(\psi_2, \psi_4) = -J(\pi - \psi_2, 3\pi - \psi_4)$. Hence, $P_G(G)$ must be an even function which is positive valued over $-\infty < G < \infty$, having a bounded tail in both extremes. We cannot solve the distribution of $f_1$ by directly changing variables from $(G, f_3)$ to $(f_1, f_3)$ because the pairs are not statistically independent and we do not know their joint probability distributions. However, we know that the only stable configurations of this grain are those in which $G \leq f_3$ because of Eq. (1). We can therefore calculate the proportions of the volume of phase space that include only the stable configurations of this grain with a particular value of $f_3$. Since there are two equations of stability there are only two degrees of freedom in the force dimensions. Integrating across only one of these to find the size of stable space as a function of the other,

$$\begin{aligned} V(f_3) &\propto \iint \mathrm{d}^2\psi \int_0^\infty \mathrm{d}f_4 \;\; \Theta(f_1)\, P_f(f_4) \\ &\propto \int_{-\infty}^{\infty} \mathrm{d}G \;\; \Theta(f_3 - G)\, P_G(G) \\ &\propto \int_{-\infty}^{f_3} \mathrm{d}G \;\; P_G(G), \end{aligned} \tag{5}$$

where $\Theta$ is the Heaviside (unit step) function. Hence, $V$ is a monotonically increasing function of $f_3$, which (because $P_G(G)$ is an even function) has a finite value at $f_3 = 0$. This illustrates that the volume of the stable regions in phase space is biased against weaker forces, but is not vanishing for zero force. Neglecting that Figure 6 is a special case, the $P_f$ corresponding to the maximum volume of stable phase space is, therefore,

$$P_f(f) = e^{-\beta f} \int_{-\infty}^{f} \mathrm{d}G \;\; P_G(G), \tag{6}$$

which is a recursion equation in $P_f$ through Eq. (4). Thus, the relative slope of the exponential factor and the integral will determine the behavior of $P_f$ in the region of weak forces, and this provides the mechanism to explain variations in that region as a function of the anisotropy of the packing [28].

Stated more simply, the absence of tensile forces produces a discontinuity in $P_f(f)$ at $f = 0$. Forces that are very close to this cliff may not survive the perturbing effect of the other forces that share the same grain, and as a result they may be pushed over the cliff causing the contact to open. Therefore, forces near $f = 0$ are found on fewer grain configurations than forces just slightly farther from that cliff. The general solution will be obtained in Chapter 3, although it will not produce the clear physical insight provided by this simple picture.

## 2.3 The Form of Related Distributions

Two other distributions are related to $P_f(f)$ and these will be discussed throughout this dissertation. These are the distribution of Cartesian loads and the distribution of contact force Cartesian components.

### *2.3.1 Distribution of Cartesian Loads*

The "Cartesian loads" (or simply the "loads"), $w$, are the total quantities of force borne by a grain in the direction of each Cartesian axis (specified arbitrarily). Without gravity, $w$ is computed as the sum of all the parallel Cartesian components of the contact forces acting on a particular hemisphere. The Cartesian load borne by one hemisphere of a grain is of course the same as the load borne by the opposite hemisphere (due to the requirements of static equilibrium), where the "equator" dividing the two hemispheres is defined by a plane normal to the Cartesian axis under consideration. In $d$ spatial dimensions, each grain therefore has $d$ distinct Cartesian loads. The distribution of the loads, $P_w(w)$, is scientifically interesting and has been confused with $P_f(f)$ in the published literature.

The historical reason for the interest in the loads lies with the $q$ model (see Figure 4). The published predictions of the $q$ model [37] were in terms of $P_w(w)$ rather than $P_x(f_x)$. The $q$ model's predictions were then compared to the carbon paper experiments performed at the University of Chicago [9]. In those experiments, a packing of beads

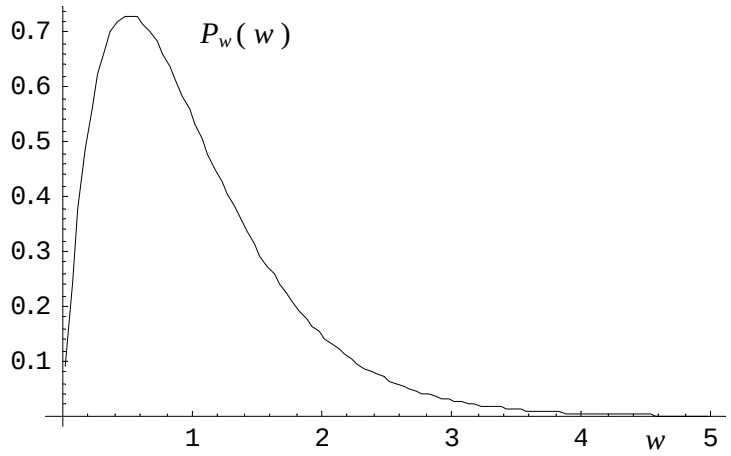


Figure 7: The $q$-Model's Distribution of Cartesian Loads, $P_w(w)$.

or ball bearings in a cylinder is compressed by a piston at the top, and carbon paper at the bottom (or sides or top) of the cylinder record the force between each bead and the boundary of the container. By calibrating the carbon paper imprints to actual force values, an empirical $P_f(f)$ is obtained. Because these measurements are performed at the flat boundaries of the container, the sampled forces are located on contacts that are all parallel to one another, normal to the boundary. Because the beads all have the same (or nearly the same) diameter, each of these grain contacts is the only one on its own hemisphere. As a result, the sampled forces are identical to the sampled Cartesian loads, and $P_w(w) = P_f(f)$ in that special geometry. In the bulk, however, the two distributions may be dissimilar. The failure to recognize these distinctions has injected some confusion into the published discussion of $P_f(f)$.

In the $q$ model, where every grain has a fixed number of contacts $n > 1$ on each hemisphere, the form of $P_w(w)$ is shown in Figure 7.[1] It has a form with $P_w(0) = 0$ in contrast to $P_f(0) > 0$. The relationship between $P_w$ and $P_f$ both near the boundary and in the bulk have been thoroughly studied in numerical simulations [38] and it was shown there that grains at the bottom of a container supporting $n > 1$ grain on their

[1]The data shown in Figure 7 were obtained by the author using a version of the $q$ model implemented in MATHEMATICA.

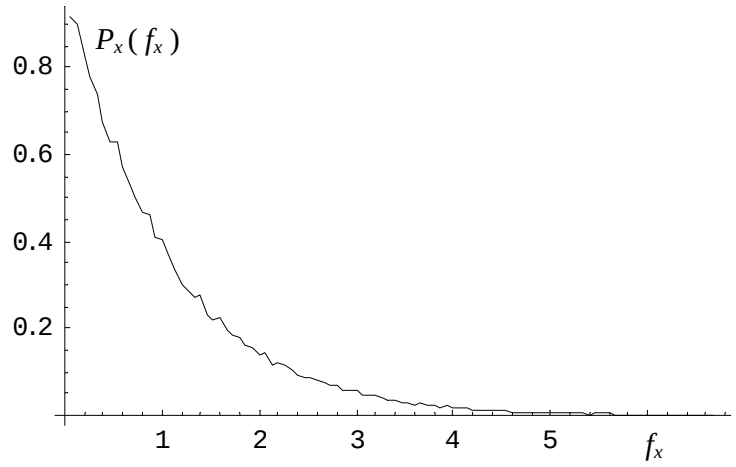


Figure 8: The $q$-Model's Distribution of Contact Force Cartesian Components, $P_x(f_x)$.

upper hemisphere display $P_w(0) = 0$ in agreement with the $q$ model, whereas gains supporting only $n = 1$ grain on their upper hemisphere display $P_w(0) > 0$ due to the direct relationship between $w$ and $f$ in that case. As a result, the composite $P_w(w)$ in the bulk of a granular packing looks qualitatively similar to $P_f(f)$ as shown in Figure 2, in contrast to the form shown in Figure 7.

### *2.3.2 Distribution of Contact Force Cartesian Components*

Because the $q$ model propagates only the Cartesian components of force $f_x$ that are parallel to the direction of propagation, it is not able to predict the contact force magnitudes or their distribution $P_f(f)$. The $q$ model predicts that the distribution of the Cartesian components on the individual contacts $P_x(f_x)$ shall be monotonically decreasing, as shown in Figure 8.[2] Dynamic computer modeling of amorphous granular packings have validated the $q$ model's predictions, measuring monotonically decreasing $P_x(f_x)$ [38].

Recently, a pair of integral transforms was developed by Youngquist [43] to convert between $P_{f\theta}(f, \theta)$ and $P_x(f_x \mid \phi)$. The first of these is the joint probability density of contact force magnitudes and their corresponding vector angles. The second of these

[2]The data shown in Figure 8 were obtained by the author using a version of the $q$ model implemented in MATHEMATICA.

is the conditional probability density of $f_x$ where the $x$ axis is oriented at the angle $\phi$. For the isotropic case, when the stress in the packing is purely hydrostatic and the contact angles in the packing form a contact network that is geometrically isotropic (in the statistical sense, averaged over a large packing), then the angle dependence can be integrated out of the integral transforms and it reduces to a conversion between $P_x(f_x)$ and $P_f(f)$. These transforms increase the importance of $P_x(f_x)$ because it is now possible to compare the $q$ model's predicted $P_x(f_x)$ to the $P_f(f)$ measured in granular packings, both for isotropic and anisotropic cases. Even more importantly, it shall be shown in Chapters 5 and 6 that $P_x(f_x)$ for real packings has a functional form that is naturally described by a series of modified Bessel functions of the second kind.[3] Using the integral transform on this series allows us to discover the natural functional form for $P_f(f)$ as well. The agreement between the empirical distributions from dynamic simulation and the theoretical distributions predicted in Chapter 5, and the ability to transfer back and forth between the Cartesian component and vector magnitude forms, strongly implies that the correct functional forms have been identified. This confirms that the tail of $P_f(f)$ truly is exponential and that the behavior in the region of weak forces truly has $P_f(0) > 0$ as discussed above.

## 2.4 Summary of the Distribution's Form

The form of $P_f(f)$ is unique to granular physics, and therefore the DOS must be organized in some way that is unique, not found in any of the typical thermal systems that have been studied by physicists. As explained in references [1] and [2], the prior attempts [17, 18, 19, 20] to derive $P_f(f)$ or $P_x(f_x)$ did not incorporate various elements of the physics and hence did not produce all of the expected features in the distributions. $P_f(f)$ has an exponential tail when the grains are not too deformed (indicating that the forces are maximally entropic subject to some global force conservation law). The distribution

[3]The author has found that careful selection of $\eta(q)$ will cause the $q$ model, also, to produce a $P_x(f_x)$ that is well-fitted by a sum of modified Bessel functions of the second kind.

displays a peak near the average value of force, but it has a finite $P_f(0) > 0$ unlike the Planck or Maxwell-Boltzmann distributions, indicating that it is not dominated by spatial degeneracies in the region of weak forces. This form evolves under increasing stress and fabric anisotropy so that it becomes monotonically decreasing. The behavior in the region of weak forces arises due to intra-grain correlation that discriminate against the weakest of forces. This form for $P_f(f)$ is surprisingly consistent. It occurs in packings with crystalline order, as well as in amorphous, disordered packings [9]. It occurs with or without friction. It occurs in a packing that has just been deposited into a container, without first experiencing any dynamic exploration of a phase space. Because of these unique features, an overly simplistic appeal to thermal analogies will not be sufficient to explain its form. The DOS of a static granular packing should be considered on the basis of its own first principles.

# CHAPTER 3

# ENSEMBLE THEORY

The universality of the observed form of $P_f(f)$ shows that its unique features are not associated with a specific type of model or the (non)existence of friction, but are fundamental characteristics of static granular packings. Perhaps the explanation lies in a unique generalization of statistical mechanics. Just as the DOS for ideal Bose and Fermi gases are organized differently than the classical dilute gas and therefore produce their own unique energy distributions, so the DOS of granular packings must be organized in some unique way to produce this distinctive distribution.

## 3.1 Nomenclature

When writing the arguments for densities of states, the notation in this paper is to use a vertical midline to distinguish between two types of arguments, $\rho\{x, y \mid z, w\}$: the ensemble is distributed across the domain of all the arguments that are written prior to the midline ($x$ and $y$ in this example), which are the phase space axes; the ensemble exists at only a specified value of each of the arguments written after the midline ($z$ and $w$), which are the conditions that define the accessible region of the phase space. A similar convention is used for probability distributions. If they have arguments after a midline, $P_{f\theta}(f, \theta \mid \sigma_{ij})$, then it is understood to be a conditional density; it is normalized to unity when integrated across the domains of all the arguments prior to the midline ($f$ and $\theta$ in this example), regardless of the evaluation of the conditions after the midline ($\sigma_{ij}$).

## 3.2 Theoretical Basis

The following ensemble analysis is based upon two of Edwards' theories: (1) Edwards' ensemble theory, and (2) the stress propagation theory. These are both introduced here

before proceeding with the analysis.

### *3.2.1 Edwards' Ensemble Theory*

A generalization of statistical mechanics to explain granular physics has been taking shape [44], beginning with Edwards' hypothesis that all metastable packings are equally probable in the statistical ensemble [15]. Edwards treated the powder's volume $V$ as analogous to the energy of a thermal system. The microcanonical DOS $\rho$ is defined in terms of the collective coordinates $\{\zeta_i\}$. These coordinates remain unspecified but are written to represent the complete set of microscopic geometrical information in the packing [20]. The microcanonical DOS is written as

$$\rho_\zeta(\zeta_i \mid V) \triangleq \delta\left[V - W(\zeta_i)\right]\ \Theta_\zeta(\zeta_i) \tag{7}$$

where $\delta$ is the Dirac delta function, $W$ is a function analogous to the Hamilton that calculates the overall volume of the packing, and $\Theta_\zeta$ is a function that evaluates to either 1 or 0, enforcing geometric self-consistency on the packing by requiring that each grain just touch its neighbors without overlapping. Then, the entropy $S$ and the compactivity $\chi$ (analogous to inverse temperature) are defined as

$$\begin{aligned} S &\triangleq -k \ln \int \rho(\zeta_i \mid V)\ \mathcal{D}\zeta \\ \chi &\triangleq \frac{\partial S}{\partial V}, \end{aligned} \tag{8}$$

where $k$ is some constant having units of volume. The theory asserts that if two powders labeled $A$ and $B$ are in physical contact sharing a container which is being shaken or tapped, then the steady state partition of volume between $A$ and $B$ is the one that satisfies $\chi_A = \chi_B$. This theory has made some successful predictions when applied to idealized models of compaction behavior [45] or to the mobility-diffusivity behavior of individual grains in a simulated packing that is slowly sheared [46].

### *3.2.2 Stress Propagation Theory of Edwards and Coworkers*

Edwards and co-workers are also studying the propagation of stress in a static granular material [47], as have others [48]. Here, the word "propagation" is taken to mean the spatial distribution of stresses in the material since the packing is in fact static and nothing propagates in the temporal sense. Experiments have discovered that stress propagation is a nontrivial concern in granular materials, because (for example) the stress beneath a conical sandpile depends upon the local "fabric" of the sand (its predominant contact orientation), directing the forces in one direction of another depending on how the pile was constructed [49]. Edwards and co-workers focused on isostatic packings and wrote the "probability functional" for the force microstate, which enforces Newton's laws explicitly grain-by-grain. With round, rigid, frictionless grains (no torques to balance) this probability functional reduces to,

$$\rho_f\left(\vec{f}^{\alpha\beta} \mid \zeta_i, \vec{g}^{\alpha}\right) = \mathcal{N} \prod_{\alpha} \delta\left(\sum_{\beta \in \text{c.n.}} \vec{f}^{\alpha\beta} - \vec{g}^{\alpha}\right) \prod_{\beta \in \text{c.n.}} \delta\left(\vec{f}^{\alpha\beta} + \vec{f}^{\beta\alpha}\right) \Theta\left(f^{\alpha\beta}\right) \qquad (9)$$

where $\mathcal{N}$ is for normalization, $\Theta$ is the Heaviside (unit step) function, $\alpha$ and $\beta$ index the grains, and $\vec{g}^{\alpha}$ is the external force applied to a grain (either a contact force from the container's boundary to the grain and/or the gravitational force acting on the grain). The sums and products in $\beta$ are taken only over contacting neighbors (c.n.). The first set of delta functions enforces Newton's second law at each grain, and the second set of delta functions enforces Newton's third law between grains. The Heaviside function enforces the lack of tensile forces at the grain contacts, since the idealized granular medium is noncohesive. Some progress has been made toward using this to derive a complete set of stress propagation equations, solvable given $\{\zeta_i\}$.

Before proceeding, we note that Edwards' flat measure only applies to $\rho_\zeta$, not to $\rho_f$. Edwards, *et al.*, applied Equation 9 only to isostatic packings, those in which there exists exactly one valid $\{\vec{f}\}$ state for each specified $\{\zeta_i\}$ when subjected to loading $\{\vec{g}\}$. Hence,

$\rho_f$ is a delta function and the question of a measure in $\{\vec{f}\}$ was not addressed. In particular, they applied $\rho_f$ to isostatic packings of *frictional* grains. Numerical simulations with frictional grains have shown such packings to be generally hyperstatic rather than isostatic, having more contact force unknowns than mechanical degrees of freedom in the geometry. Hence, for such a packing there exists a hypersurface of nonzero volume in $\{\vec{f}\}$ corresponding to stable states for each $\{\zeta\}$ given $\{\vec{g}\}$. Furthermore, it has been reported recently that different numerical simulation methods sample this hypersurface in $\{\vec{f}\}$ with different nonflat measures, depending on the choice of numerical simulation techniques [50]. Whether or not nature samples that space with a nonflat measure is an important question. However, this paper will instead focus on isostatic packings of *frictionless* grains for a practical advantage: numerical simulations have shown that packings of round, rigid, frictionless grains really do organize themselves to be isostatic, having exactly as many contact force unknowns as mechanical degrees of freedom. This choice will allow the theory developed in this paper to be tested empirically through comparison with numerical simulations, neatly bypassing the question of a measure in $\rho_f$.

### 3.3 Synthesis of Edwards' Theories

The object of this analysis is to begin with the flat measure in $\{\zeta_i\}$ and the stress propagation equation in $\{\vec{f}\}$ of Edwards, *et al.*, and then to derive the contact force distribution. Following Edwards and coworkers this paper focuses upon amorphous, isostatic packings of cohesionless, rigid grains wherein there is a fixed coordination number for every grain [47]. The problem shall be further idealized by using only 2D, smooth, round, frictionless grains so that the coordination number is $Z = 4$. Among other benefits, these choices make it very easy to specify fabric. Although this ensemble is highly idealized, it is a good starting point because packings of cohesionless, round grains that are perfectly rigid [25, 26] and/or frictionless [13, 23, 27, 30, 32, 38, 40] are known to have force distributions with the same qualitative features as the more generalized packings and hence must

be subject to the same organizational constraints in the statistics. Therefore they are sufficient to elucidate the origin of those constraints in the physics.

The use of exactly $Z = 4$ for every grain does not occurs in typical numerical simulations, which have significant populations of grains for each of $Z = 3$, $Z = 4$ and $Z = 5$. Nevertheless, it is acceptable as a beginning point in a theory for three reasons. First, four is indeed the average coordination number and the majority coordination number measured in these types of packings [7, 35]. Second, it will be shown that the $P_f(f)$ predicted in the theory matches the $P_f(f)$ obtained in simulations. Third, we will compare the theory against each of the $Z = 3$, $Z = 4$, and $Z = 5$ populations individually to obtain new physical insights. The fixed coordination number may then be generalized in future extensions of the theory.

We begin simply by multiplying Edwards' DOS, Equation 7, with Edwards' probability functional, Equation 9, to obtain the DOS in the direct product space $\{\vec{f}^{\alpha}\} \otimes \{\zeta_i\}$,

$$\rho(\vec{f}^{\alpha}, \zeta_i \mid V, \vec{g}^{\alpha}) = \rho_f(\vec{f}^{\alpha} | \zeta_i, \vec{g}^{\alpha}) \; \rho_\zeta(\zeta_i \mid V). \tag{10}$$

Some adaptations are needed to proceed. The two defining issues for the ensemble are (1) how to specify the fabric $\{\zeta_i\}$, and (2) how to apply stress to it $\{\vec{g}^{\alpha}\}$. We have three guiding principles. First, this paper is concerned primarily with the derivation of $P_f(f)$, and its form is known to evolve with stress and fabric anisotropy under shearing. Therefore, a useful ensemble must be sufficiently general to accommodate anisotropy in each. Second, since this paper does not address the more ambitious problem of stress propagation, the ensemble need not accommodate the large-scale stress and fabric inhomogeneities that break the symmetry of stress propagation. In this paper, only actions such as shaking, shearing and compressing are assumed to have occurred in the construction history because these may be done in a way to produce homogeneous stress and fabric states in the bulk of the packing; statistical fluctuations away from homogeneity vanish

in the ensemble average. Third, we specify fabric and stress with an eye toward the eventual development of a first-principles theory of rheology. Like the Navier-Stokes equation, such a theory should not track every particle but only the coarse-grained behavior over a larger spatial scale. Therefore, fabric and stress should be specified as macroscopic, continuum variables, or if that is not possible then using the simplest practical statistics to represent the microstate.

Specifically, stress will be specified as the tensor which is a volume average over the entire packing. The source of stress will be mechanical at the boundaries to allow for the full range of possible states, something which gravity alone cannot do. Gravity will be eliminated both because it is unnecessary and because it breaks a symmetry of the ensemble and may thus tend to obscure the organizational features of the physics. Also, since we are working in the bulk in the thermodynamic limit, we do not want to specify particular force vectors along the boundary of the packing. Hence, in Equation 10, the $\vec{g}^{\alpha}$ terms shall be omitted and new delta function factors shall be included to constrain the ensemble onto the hypersurface having the specified the stress state. It is the opinion of the author that this formulation of the ensemble will better support the eventual development of a full statistical mechanics theory of rheology.

This leaves the question how to specify the fabric. In the two theories mentioned above (for $\rho_{\zeta}$ and $\rho_f$), fabric was treated very differently. In $\rho_{\zeta}$ only the scalar $V$ was specified. On the other hand, the analysis of $\rho_f$ showed that two fabric tensors are required to produce the complete set of stress propagation equations. For the present purposes, something is needed that is more than the simple scalar treatment of compaction but less than the full tensorial treatment of stress propagation. We select the joint probability distribution $P_{4\theta}(\theta_1, \ldots, \theta_4)$ studied in reference [51]. This distribution correlates the contact angles that share the same grain. It can be collapsed to the more commonly

used fabric distribution $P_\theta(\theta)$,

$$P_\theta(\theta) = \frac{1}{4}\sum_{\beta=1}^{4} \iiint_0^{2\pi} \mathrm{d}^4\theta \; P_{4\theta}(\theta_1, \ldots, \theta_4) \; \delta(\theta - \theta_\beta). \tag{11}$$

The use of the uncollapsed $P_{4\theta}$ is deemed necessary because the physics of fragile media are grain-centered and the intra-grain correlations turn out to be the heart of the statistical physics, as shall be shown here. However, $P_{4\theta}$ is not sufficient to relate the packing state to the specified stress tensor, because it tells nothing of the number and size of voids created in the arrangement of neighboring grain configurations. For the present, the voids may be quantified simply by assuming a linear grain density in each direction. These tell the number of grains per unit distance in a cross-section of the packing in each orthogonal spatial dimension. Since we are working in the bulk of a packing with an eye toward rheology in the thermodynamic limit, these quantities are expected to have well defined averages. These quantities along with $P_{4\theta}$ are assumed to have been specified in the ensemble rather than predicted. Rheological evolution of the fabric is beyond the present study.

Finally, for convenience the idea of "quartered fabric" is introduced at several points. It is defined such that $P_{4\theta}(\theta_1, \ldots, \theta_4)$ is zero everywhere except where the $j^{\text{th}}$ contact is on the $j^{\text{th}}$ quadrant of every grain in the packing. For the specific case of "quartered isotropy," collapsing the quartered fabric by Equation (11) produces $P_\theta(\theta) = 1/2\pi$. This mimics true isotropy but the anisotropic quartering is apparent in the joint distribution. As in the case of nonquartered fabric, $P_{4\theta}$ enforces steric exclusion. To achieve quartered isotropy with steric exclusion in a random sampling process it is necessary to weight the distribution of attempted angles to emphasize the regions close to the edges of each quadrant. Otherwise, steric exclusion would cause notches to appear in $P_\theta(\theta)$ near the boundary of each quadrant. The use of quartered fabric in this analysis is only to provide insight into the expressions. It is always possible to write and numerically solve them for the more general case, and it was found that numerical solutions were identical (to

within the statistical accuracy of the data) with or without quartered fabric.

### 3.4 The Phase Space

The locus in phase space of a classical dilute monatomic gas completely defines its state. We seek specificity in $\{\vec{f}^{\alpha}, \zeta_i\}$ that is similarly complete. An isostatic packing of $N$ round, rigid, frictionless grains contains $2N$ contacts. The phase space therefore requires at least $4N$ phase space axes, half of which define the force on each contact and half of which define the contact angles, $\{f_k, \theta_k \mid k = 1, \ldots, 2N\}$, which is labeled $\mathbb{S}_1$ and has DOS $\rho^{(1)}$. It is possible to define the ordering of the axes so that it is understood which four contacts correspond to the same grain and therefore which grains contact one another. It will not prove necessary to do so explicitly, although this ordering is implicitly assumed to exist.

Newton's third law is automatically satisfied in $\mathbb{S}_1$, since each contact is represented by only one force and one angle axis. However, enforcing Newton's second law will prove simpler if redundant axes are created to account for each contact force twice, one time with each grain that shares the contact, $\{f_{\alpha\beta}, \theta_{\alpha\beta} \mid \alpha = 1, \ldots, N; \beta = 1, \ldots, 4\}$, where $\alpha$ subscripts the grain and $\beta$ subscripts the contact on the grain. This space is labeled $\mathbb{S}_2$. In this new space it will be necessary to enforce Newton's third law. Again, it is possible to define the ordering of the axes so that it is understood which contacts are redundant to one another and therefore which grains are contacting neighbors. This ordering information is contained in the *construction list* $\mathcal{C} = \{(\gamma\delta, \kappa\lambda)\}$, which says that the grain indexed by $\gamma$ has a contact indexed by $\delta$ connecting to a grain $\kappa$ at its contact $\lambda$.

Rewriting Equation 10 in the coordinates of $\mathbb{S}_2$, with $\delta(V - W)$ replaced by the more

specific fabric constraint $P_{4\theta}$ and $\vec{g}^{\alpha}$ replaced by the stress state delta functions,

$$\rho^{(2)}\{f_{\alpha\beta},\theta_{\alpha\beta}\mid\mathcal{C},W_x,W_y,P_{4\theta}\}\triangleq\left\{\prod_{\mathcal{C}}\delta\Big(\vec{f}_{\gamma\delta}+\vec{f}_{\kappa\lambda}\Big)\right\}\prod_{\alpha=1}^{N}\delta\Big(\sum_{\beta=1}^{4}\vec{f}_{\alpha\beta}\Big)\prod_{\beta=1}^{4}\Theta\left(f_{\alpha\beta}\right)$$
$$\times\,\delta\left[P_{4\theta}-Q_{4\theta}\{\theta_{\alpha\beta}\}\right]\;\delta\Big(\sum_{\alpha}w_{x\alpha}-W_x\Big)\,\delta\Big(\sum_{\alpha}w_{y\alpha}-W_y\Big).\quad(12)$$

The six constraints which define the accessible regions of phase space are described below.

1. Newton's third law is satisfied between every pair of contacting grains.

$$\vec{f}_{\gamma\delta}=-\vec{f}_{\kappa\lambda}\;\forall\;(\gamma\delta,\kappa\lambda)\in\mathcal{C},\tag{13}$$

2. Newton's second law for static equilibrium must be satisfied at each grain individually,

$$\sum_{\beta=1}^{4}\vec{f}_{\alpha\beta}=0\;\forall\;\alpha.\tag{14}$$

3. $\Theta$ enforces no tensile contacts anywhere in the packing, which restricts the DOS to the first "quadrant" of the force axes.

4. $P_{4\theta}$ is specified by a delta function. $Q$ is a function, analogous to the Hamiltonian, which computes the joint fabric distribution given $\{\theta\}$ (thereby taking over the role of $W\{\zeta\}$ from Edwards' microcanonical DOS). Actually, at finite $N$ there should be a statement relating the continuum $P_{4\theta}(\theta_1,\theta_2,\theta_3,\theta_4)$ with the discretized distribution of angles $\mu_{klmn}(\theta_{1k},\ldots,\theta_{4n})$, but the meaning is nonetheless clear.

5. (and 6.) At each locus in phase space the relationship exists between the Cartesian loads these loads and the Cauchy stress tensor. (See for example reference [16].) For simplicity the sum over these Cartesian loads is specified. Hence,

$$\sum_{\alpha=1}^{N}w_{x\alpha}=W_x,\quad\sum_{\alpha=1}^{N}w_{y\alpha}=W_y,\tag{15}$$

where the loads are defined by,

$$w_{x\alpha}=\left(w_{x\alpha}^{\text{left}}+w_{x\alpha}^{\text{right}}\right)/2,\qquad w_{y\alpha}=\left(w_{y\alpha}^{\text{top}}+w_{y\alpha}^{\text{bottom}}\right)/2,\tag{16}$$

and, using nonquartered fabric,

$$\begin{aligned} w_{x\alpha}^{\text{left}} &= -\sum_{\beta=1}^{4} L_{\alpha\beta} f_{\alpha\beta} \cos\theta_{\alpha\beta}, \\ w_{x\alpha}^{\text{right}} &= +\sum_{\beta=1}^{4} R_{\alpha\beta} f_{\alpha\beta} \cos\theta_{\alpha\beta}, \\ w_{y\alpha}^{\text{top}} &= +\sum_{\beta=1}^{4} T_{\alpha\beta} f_{\alpha\beta} \sin\theta_{\alpha\beta}, \\ w_{y\alpha}^{\text{bott.}} &= -\sum_{\beta=1}^{4} B_{\alpha\beta} f_{\alpha\beta} \sin\theta_{\alpha\beta}. \end{aligned} \tag{17}$$

The operator $L_{\alpha\beta}$ multiplies the expression by 1 if the $\beta^{\text{th}}$ contact is on the left half of the grain ($\pi/2 \leq \theta_{\alpha\beta} < 3\pi/2$), else it multiplies it by 0. Likewise $R_{\alpha\beta}$, $T_{\alpha\beta}$ and $B_{\alpha\beta}$ test for contacts on the right, top and bottom side of the grain, respectively. For stable grains, $w_{x\alpha} = w_{x\alpha}^{\text{left}} = w_{x\alpha}^{\text{right}}$, but the hemispheric distinctions shall be useful in the analysis. Since $w_{\xi\alpha}^{\text{hem.}} = w_{\xi\alpha}^{\text{hem.}}(f_{1\alpha}, \ldots, f_{4\alpha}, \theta_{1\alpha}, \ldots, \theta_{4\alpha})$ for all hemispheres ($\xi = x$ with hem. $=$ left, right; $\xi = y$ with hem. $=$ top, bott.), then its argument shall be written more compactly as $w_{\xi\alpha}^{\text{hem.}}(\cdot)$.

This ensemble does not enforce the shear stress but relies on the fact that its ensemble average is zero and in the thermodynamic limit the fraction of packings in which the shear deviates from zero by more than some arbitrarily small amount will vanish. The Cartesian axes of the packings are taken to be aligned with the principle stress axes so that the off-diagonal elements of the stress tensor should indeed be zero.

The one key omission from these constraints is discussed in the next section.

### 3.5 The First Shell Approximation

To make the stress propagation problem tractable, Edwards and coworkers omitted the noncohesion Heaviside function from Equation 9. It cannot be omitted in the present work because we are using Equation 9 to define an ensemble, and noncohesion is a crucial part of the ensemble's physics. The choice here is to omit $\Theta_\zeta(\zeta_i)$ instead. A cluster of real grains must just touch one another, forming closed loops as illustrated in Figure 9. Omitting $\Theta_\zeta(\zeta_i)$ removes that geometric constraints for grains outside the first coordination shell. ($P_{4\theta}$ maintains steric exclusion for grains inside the first coordination shell.)

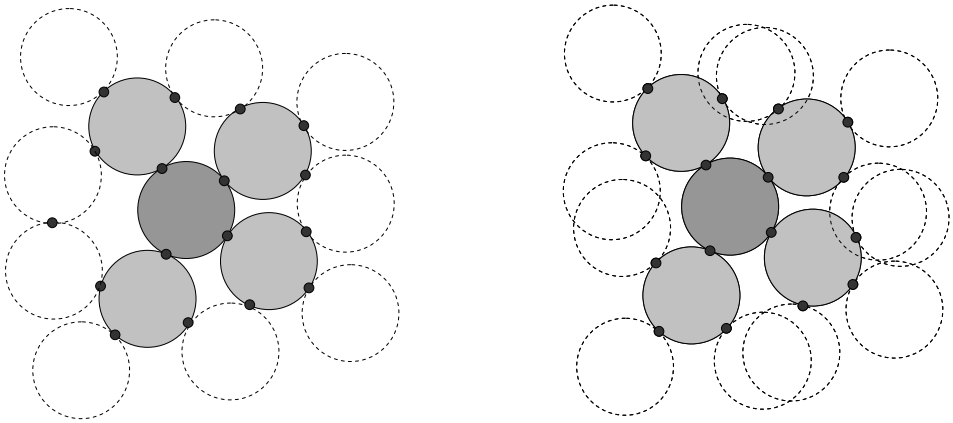

Figure 9: Illustration of closed loops or unclosed loops in the second coordination shell. The light gray grains are the first coordination shell of the dark gray grain. The white grains with dashed lines are the second coordination shell of the dark gray grain. The black spots are the contacts between grains. (Left) A packing with closed loops satisfying $\Theta_\zeta(\zeta_i) = 1$. (Right) A packing with improperly overlapping grains in the second coordination shell, $\Theta_\zeta(\zeta_i) = 0$.

Edwards and Grinev discussed this *First Shell Approximation* (FSA) in a geometric context to predict the volume occupied by grains in a packing [20]. In the present context the FSA asserts that only negligible correlative information travels all the way around closed loops of grains in the ensemble average. In other words, the DOS is adequately characterized for the present purposes by the two-point (intra-grain) force correlations and the resulting correlation of loads in neighboring grains. Therefore, the geometric closure of force loops can be ignored when deriving the statistics of single-grain states.

Without this closure, however, the chains of contacting grains are allowed to branch out ever increasingly in all directions and overlap into one another's space. Geometrically, then, omitting $\Theta_\zeta(\zeta_i)$ does not produce a good approximation to a packing. However, it may still be an excellent approximation as far as the statistics of single-grain states are concerned.

It has been shown [30] that contact forces on the same grain are strongly correlated with one another. There is anti-correlation for contacts closer together than $\Delta\theta \approx 0.4\pi$

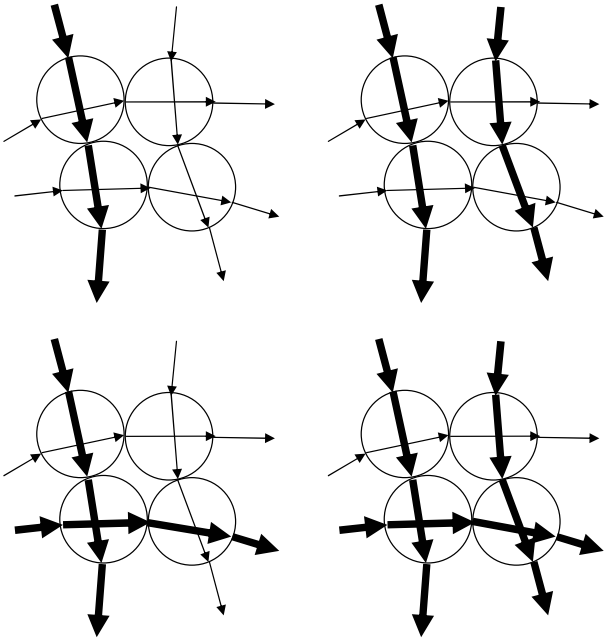

Figure 10: Illustration of the statistical independence of neighboring force chains. The four force paths shown here become exactly independent when the contact angles are all exactly orthogonal.

radians of angular separation, and a positive correlation when the angular separation is greater than that. The correlation continues to increase as the contacts are increasingly distant from one another but still on the same grain. The correlation dramatically drops immediately thereafter when the distance between contacts becomes greater than one grain diameter.

These correlations are easily understood by examining the mechanics localized within the first coordination shell. Contacts on the same hemisphere of a grain compete for a share of the same load and hence are anti-correlated. Contacts on opposite hemispheres transmit load through one another and hence are correlated. Simplistically we could expect $\Delta\theta = \pi/2$ to be the crossover point of no correlation as illustrated in Figure (10). This is approximately correct according to the $\Delta\theta \approx 0.4\pi$ (in the only published measurement to-date), and the difference is probably attributable to the existence of three-grain loops, history-dependent frictional effects, and so on.

Furthermore, the sudden drop in correlation after one grain diameter of separation is easily understood because this puts the contacts on different grains. It is true that neighboring grains share a common contact so that the *other* contacts on those two grains are just two sequential two-point correlations away from one another. However, the net of two sequential such correlations must be much weaker than a single intra-grain correlation, hence the sudden drop in correlation after one grain diameter.

Higher-order constraints are not found in the packing until entirely closed loops of grains are considered so that the sequential two-point correlations come all the way around the loop back to the original grain, again. In 2D the typical closed loop consists of four grains, each grain being a vertex between a pair of contacts that form the loop. The four-point correlation constructed as three sequential two-point correlations going the long way around a loop would undoubtedly be very weak compared to the single two-point correlation going the short way around the same loop, since the short way is intra-grain. Hence, the extra correlation information imposed going the long-way around the loop must be very weak compared to the information already present intra-grain. It should therefore be an excellent approximation to neglect this additional information and consider only the intra-grain relationships in defining the DOS.

This is not a rigorous argument because we should consider the sum of information from *all* the loops in the packing that contain the grain in question, and it is conceivable that the sum of very many weak contributions may be strong. However, due to the randomness of the packing, and the large number of amorphous packings that may exist in the configuration space, it is expected that the contributions from increasingly larger loops of grains will be increasingly decoherent and largely cancel one another. Hence, there is good reason to assume that only the intra-grain contribution to the correlations is significant as asserted by the FSA.

If correct, the FSA is an important statement of the physics because it fundamentally characterizes the DOS. The significance of this can be seen in the analogy to thermal

statistical mechanics. In thermal systems the momenta into and out from a particle collision are in some ways similar to the forces on a static grain. If the outgoing momentum vectors are reversed then the sum of momentum vectors are zero on every collision analogous to Newton's second law on each grain. However, there are several differences, the most important of which are that information in a thermal system propagates only in the direction from incoming to outgoing momentum vectors and that momentum vectors are not subject to steric exclusion. Any pair of incoming particles are allowed to collide regardless of their incoming momenta, and they always produce some valid pair of outgoing momentum vectors. Hence there is no "intra-grain" source of correlation between the incoming pair of momenta. This enabled Boltzmann's assumption of molecular chaos (AMC), which was needed to solve the Boltzmann transport equation and which characterizes the DOS as being uniform without significant momentum correlations. With granular packings the AMC would be unsatisfactory because it would throw away the strong two-point correlations that propagate symmetrically in all spatial directions away from each grain. However, by including only this next higher level in the approximation, that is, only the intra-grain effects, and assuming that all higher correlations exist strictly as a sequence of such two-point correlations, we will obtain excellent results as shown in the remainder of this paper. The two-point correlations therefore appear to be the essence of the physics.

### 3.6 Phase Space Operations to Quantify the Non-Uniformity

The previous section was discussing the states of individual contacts sharing the same grain. Here we return to Edwards' flat measure, which deals not with states of individual contacts nor even the states of individual grains but rather with states of entire, metastable granular packings. A locus in $\mathbb{S}_2$ defines an entire packing and we have assumed the DOS to be uniform across all the accessible regions of that space. Although the DOS may be uniform across the accessible regions, those regions may themselves be

nonuniformly distributed throughout the space. We wish to quantify that lack of uniformity because that is what shapes $P_f(f)$ and the other distributions if Edwards' hypothesis is correct. However, the lack of continuity in the DOS, caused by the highly restrictive delta functions, makes the analysis difficult. The program therefore is to change coordinates in a way that eliminates delta function constraints from the right-hand side of Equation (12), trading the lack of continuity in the coordinates for a lack of flatness in the measure. When only extensive, conserved quantities remain in the list of constraints, then the method of the most probable distribution may be used, relying on the method of Lagrange multipliers to conserve those quantities.

### *3.6.1 Newton's Third Law*

In this context the term "grain configuration" refers not only to a grain's contact geometry but also to the set of forces upon those contacts as defined by the locus in phase space. The form of $\mathbb{S}_2$ itself does not require neighboring grains to satisfy Newton's third law, and so the vast majority of loci include neighboring grain configurations with physically unrealizable forces. This mathematical abstraction enables the analysis.

If we wished to neglect Newton's third law then we could proceed with the remainder of the analysis, obtaining the hypothetical DOS for regions of this space having stable, cohesionless grains, write the state-counting entropy and then maximize it subject to the conservation of total loads and fabric. This would produce the most probable distribution for all possible permutations of $N$ stable grain configurations where the grains are mechanically *independent*. However, it turns out that Newton's third law is not negligible: by considering instead all the possible *combinations* (rather than all possible *permutations*) of $N$ stable, independent grain configurations, we note that some of these combinations can be mechanically connected into a greater number permutations satisfying Newton's third law than can other combinations. Hence, those combinations are the more entropic ones, the ones which represent the greater number of metastable

packings in the phase space. Therefore, to find the most entropic combination of stable, independent grain configurations, we will map $\mathbb{S}_2 \rightarrow \mathbb{S}_3$, a space where the axes are the same as in $\mathbb{S}_2$ except that they are not sequenced to represent a particular permutation of the grains. Whereas a locus in $\mathbb{S}_2$ represents a single state (a single packing permutation of a set of grain configurations), a locus in $\mathbb{S}_3$ represents a set of mechanically disconnected grain configurations that may or may not be permutable into some number of stable states. We shall call the latter an "assembly space" to distinguish it from a phase space that identifies every grain's location in the packing. The mapping is performed by summing over all possible construction lists $\mathcal{C}_i$ $(i = 1, 2, \ldots, N!)$ to include all possible packing permutations.

$$\begin{aligned}\tilde{\rho}^{(3)}\{f_{\alpha\beta}, \theta_{\alpha\beta} \mid W_x, W_y, P_{4\theta}\} &= \sum_{i=1}^{N!} \rho^{(2)}\{f_{\alpha\beta}, \theta_{\alpha\beta} \mid \mathcal{C}_i, W_x, W_y, P_{4\theta}\} \\ &= \left\{ \sum_i \prod_{\mathcal{C}_i} \delta\left(\vec{f}_{\gamma\delta} + \vec{f}_{\kappa\lambda}\right) \right\} \prod_{\alpha=1}^{N} \delta\left(\sum_{\beta=1}^{4} \vec{f}_{\alpha\beta}\right) \prod_{\beta=1}^{4} \Theta\left(f_{\alpha\beta}\right) \\ &\times \delta\left[P_{4\theta} - Q_{4\theta}\{\theta_{\alpha\beta}\}\right] \; \delta\left(\sum_{\alpha} w_{x\alpha} - W_x\right) \delta\left(\sum_{\alpha} w_{y\alpha} - W_y\right). \end{aligned} \tag{18}$$

where the tilde on $\tilde{\rho}$ indicates that this density is in an assembly space. However, most of these permutations $\mathcal{C}_i$ are physically unrealizable because they do not satisfy Newton's third law and hence do not contribute to the sum. The fraction that do satisfy Newton's third law may be quantified in the thermodynamic limit to simplify the first term in this expression.

To verify that a particular permutation of a given combination of stable grains $\{f_{\alpha\beta}, \theta_{\alpha\beta}\}$ satisfies Newton's third law, it is necessary to check every contact in the permutation. All permutations of this combination have the same joint distribution of forces and contact angles, $P_{f\theta}(f, \theta) = P_{f\theta}(f, \theta \mid \{f_{\alpha\beta}, \theta_{\alpha\beta}\})$, whatever its form may be. Randomly choosing one contact from the set of these permutations, a contact force $f_{\alpha\beta}$ at angle $\theta_{\alpha\beta}$ therefore has the probability $P_{f\theta}(f_{\alpha\beta}, \theta_{\alpha\beta})\mathrm{d}f\mathrm{d}\theta$ that it will satisfy Newton's third law with its neighbor. (The two differentials reflect the fact that Newton's third

law reduces the solution space by two dimensions per contact, thereby taking out the extra dimensions introduced in $\mathbb{S}_1 \rightarrow \mathbb{S}_2$.) The probability that grain $\alpha$ drawn randomly from $\{\mathcal{C}_i\}$ will satisfy Newton's third law with its four neighbors will be called $\Upsilon^2(f_{\alpha 1}, \ldots, f_{\alpha 4}, \theta_{\alpha 1}, \ldots, \theta_{\alpha 4})\ \mathrm{d}^4 f\ \mathrm{d}^4\theta$, written for compactness as $\Upsilon^2(f_{\alpha\beta}, \theta_{\alpha\beta})\ \mathrm{d}^4 f\ \mathrm{d}^4\theta$. It may be written as a functional of $P_{f\theta}$,

$$\Upsilon^2(f_{\alpha\beta}, \theta_{\alpha\beta}) \;=\; \prod_{\beta} P_{f\theta}\left(f_{\alpha\beta}, \theta_{\alpha\beta}\right). \tag{19}$$

This expression treats the contacts on the neighboring grains as if they are uncorrelated because this is a packing that was drawn randomly from $\{\mathcal{C}_i\}$, including those $\mathcal{C}_i$ that are physically unrealizable. Therefore there are no *a priori* correlations between neighboring grains; such correlations arise *a posteriori* by selecting the subset of packings that satisfy Newton's third law.

Because of this statistical independence, the fraction of packings that satisfy Newton's third law for all of its grains is likewise simply the product over the probabilities that each of the individual grains will satisfy Newton's third law with its own local neighbors. (The FSA appears implicitly in this statement.) However, the product of $\Upsilon^2(f^{\alpha\beta}, \theta^{\alpha\beta})$ over all $\alpha$ accounts for every contact in the packing twice, once with each grain sharing the contact. For the cases where Newton's third law is in fact satisfied, the double accounting of contacts will appear as pairs of $P_{f\theta}$ factors having identical arguments. Hence, the probability that the entire packing will satisfy Newton's third law is the square root of that product—explaining the use of the square exponent in Equation (19). The fraction of permutations that satisfy Newton's third law is therefore,

$$\begin{aligned}
\Phi_{\mathrm{N3L}}\{f_{\alpha\beta}, \theta_{\alpha\beta}\} \;&=\; \prod_{\alpha=1}^{N} \Upsilon(f^{\alpha\beta}, \theta^{\alpha\beta})\ \mathrm{d}^{2N} f\ \mathrm{d}^{2N}\theta \\
&=\; \prod_{\alpha=1}^{N} \prod_{\beta=1}^{4} P_{f\theta}^{1/2}(f^{\alpha\beta}, \theta^{\alpha\beta})\ \mathrm{d}^{2N} f\ \mathrm{d}^{2N}\theta
\end{aligned} \tag{20}$$

This calculation does not handle the boundaries of the packing (unless they are periodic), but we are concerned with the statistics in the bulk in the thermodynamic limit where

the boundaries are pushed out toward infinity.

Now the DOS may be mapped from the phase space to the assembly space, $\mathbb{S}_2 \rightarrow \mathbb{S}_3$,

$$\tilde{\rho}^{(3)}\{f_{\alpha\beta}, \theta_{\alpha\beta} \mid W_x, W_y, P_{4\theta}\} = \prod_{\alpha=1}^{N} \Upsilon(f_{\alpha\beta}, \theta_{\alpha\beta}) \; \mathrm{d}^{2N}f \; \mathrm{d}^{2N}\theta \; \delta\left(\sum_{\beta=1}^{4} \vec{f}_{\alpha\beta}\right) \; \prod_{\beta=1}^{4} \Theta\left(f_{\alpha\beta}\right)$$
$$\times \delta\left[P_{4\theta} - Q_{4\theta}\{\theta_{\alpha\beta}\}\right] \; \delta\left(\sum_{\alpha} w_{x\alpha} - W_x\right) \; \delta\left(\sum_{\alpha} w_{y\alpha} - W_y\right). \quad (21)$$

### *3.6.2 Newton's Second Law*

To quantify the effects of Newton's second law, note that Equation (17) with $w_x = w_x^{\text{left}} = w_x^{\text{right}}$ and $w_y = w_y^{\text{top}} = w_x^{\text{bott.}}$ can be used as a many-to-one mapping from $\mathbb{S}_3 \rightarrow \mathbb{S}_4$, which will have coordinates $\{w_{\xi\alpha}, \theta_{\alpha\beta} \mid \xi = x, y; \alpha = 1, \ldots, N; \beta = 1, \ldots, 4\}$ and is another assembly space, representing combinations of mechanically-independent grain configurations. Thus, the mapping reduces the dimensionality of the space by two per grain, just as Newton's second law reduces the dimensionality of the solution space by two per grain. However, the reverse mapping is one-to-one because the localized isostacy of the grains determines the four contact forces when the two loads and four contact angles are specified. Thus, of all the points in $\mathbb{S}_3$ that map to the same point in $\mathbb{S}_4$, at most only one represents a stable packing and is occupied, the one which is specified by solving Equation (17) for $f_{\alpha\beta}$ with $w_x = w_x^{\text{left}} = w_x^{\text{right}}$ and $w_y = w_y^{\text{top}} = w_x^{\text{bott.}}$. This system of equations is nonsingular except for some precise alignments of contacts on a grain which we can safely ignore. The Jacobian of transformation for $\mathbb{S}_3 \rightarrow \mathbb{S}_4$ is simple to write and is a functional of the fabric. Instead, $\Upsilon$ is re-defined to produce the Jacobian via delta functions,

$$\begin{aligned} \Upsilon^2(w_{x\alpha}, w_{y\alpha}, \theta_{\alpha\beta}) \;\; = \;\; & \iiiint_o^{\infty} \mathrm{d}^4 f \prod_{\beta} P_{f\theta}\left(f_{\alpha\beta}, \theta_{\alpha\beta}\right) \\ & \times \; \delta\left(w_{x\alpha} - w_{x\alpha}^{\text{right}}(\cdot)\right) \; \delta\left(w_{x\alpha} - w_{x\alpha}^{\text{left}}(\cdot)\right) \\ & \times \; \delta\left(w_{y\alpha} - w_{y\alpha}^{\text{top}}(\cdot)\right) \; \delta\left(w_{y\alpha} - w_{y\alpha}^{\text{bott.}}(\cdot)\right). \end{aligned} \quad (22)$$

With this, the DOS in $\mathbb{S}_4$ may be written,

$$\tilde{\rho}^{(4)}\{w_{\xi\alpha},\theta_{\alpha\beta}\mid W_x,W_y,P_{4\theta}\}=\prod_{\alpha=1}^{N}\Upsilon(w_{x\alpha},w_{y\alpha},\theta_{\alpha\beta})\ \mathrm{d}^{2N}\theta\ \prod_{\beta=1}^{4}\Theta\left[f_{\alpha\beta}(w_{x\alpha},w_{y\alpha},\theta_{\alpha\beta})\right]$$
$$\times\delta\left[P_{4\theta}-Q_{4\theta}\{\theta_{\alpha\beta}\}\right]\ \delta\left(\sum_{\alpha}w_{x\alpha}-W_x\right)\delta\left(\sum_{\alpha}w_{y\alpha}-W_y\right). \tag{23}$$

### *3.6.3 Cohesionless Grains*

The product over Heaviside functions may simply be omitted if it is remembered that the $P_{f\theta}(f,\theta)$ factors contained within $\Upsilon$ must be zero for negative arguments $f$. On the other hand, it will prove convenient to define

$$\Psi(w_{x\alpha},w_{y\alpha},\theta_{\alpha\beta})=\prod_{\beta=1}^{4}\Theta(f_{\alpha\beta}) \tag{24}$$

where $f_{\alpha\beta}=f_{\alpha\beta}(w_{x\alpha},w_{y\alpha},\theta_{\alpha\beta})$. Then,

$$\tilde{\rho}^{(4)}\{w_{\xi\alpha},\theta_{\alpha\beta}\mid W_x,W_y,P_{4\theta}\}=\prod_{\alpha=1}^{N}\Upsilon(w_{x\alpha},w_{y\alpha},\theta_{\alpha\beta})\ \Psi(w_{x\alpha},w_{y\alpha},\theta_{\alpha\beta})\ \mathrm{d}^{2N}\theta$$
$$\times\delta\left[P_{4\theta}-Q_{4\theta}\{\theta_{\alpha\beta}\}\right]\ \delta\left(\sum_{\alpha}w_{x\alpha}-W_x\right)\delta\left(\sum_{\alpha}w_{y\alpha}-W_y\right). \tag{25}$$

## 3.7 State-Counting Entropy and Its Maximum

The density $\tilde{\rho}^{(4)}\{w_{\xi\alpha},\theta_{\alpha\beta}\mid W_x,W_y,P_{4\theta}\}$ is continuous but nonuniform. We wish to extract from it the most probable density of single grain states $\rho_g(w_x,w_y,\theta_1,\ldots,\theta_4\mid W_x,W_y,P_{4\theta}\}$. For now we shall suppress the conditions in $\rho_g$ to the right of the midline. This density contains all that can be known about the state of individual grains to within the FSA. Because the frictionless $Z=4$ grains are locally isostatic, the forces may be obtained deterministically $f_\gamma=f_\gamma(w_x,w_y,\theta_1,\ldots,\theta_4)\ \forall\ \gamma=1,\ldots,4$, henceforth written more compactly as $f_\gamma=f_\gamma(\cdot)$. Therefore, $\rho_g$ contains the joint distribution of contact

forces and angles,

$$\begin{aligned} P_{f\theta}(f,\theta) &= \frac{1}{4}\sum_{\beta=1}^{4}\iint_0^\infty \mathrm{d}^2w \iiint_0^{2\pi} \mathrm{d}^4\theta\ \rho_g(w_x,w_y,\theta_1,\ldots,\theta_4)\ \delta(\theta-\theta_\beta)\ \delta\left[f-f_\beta(\cdot)\right] \\ &= P_{f\theta}(f,\theta \mid \rho_g). \end{aligned} \tag{26}$$

$\rho_g$ can also be collapsed to obtain $P_{4\theta}$ by integrating out $w_x$ and $w_y$.

Randomly drawing packings from the regions of $\mathbb{S}_4$ that have a specified $\rho_g$ (and hence a specified fabric and a specified $P_{f\theta}(f,\theta)$), the fraction of packing permutations in which all grains will satisfy Newton's second law without cohesion *and* satisfy Newton's third law with its neighbors is,

$$\begin{aligned} \Phi\{w_{\xi\alpha},\theta_{\alpha\beta}\}\left[P_{f\theta}\right] &= \prod_\alpha \Upsilon(w_{x\alpha},w_{y\alpha},\theta_{\alpha\beta})\left[P_{f\theta}\right]\cdot\Psi(w_{x\alpha},w_{y\alpha},\theta_{\alpha\beta})\ \mathrm{d}^{2N}\theta \\ &= \prod_i\prod_j\prod_k\prod_l\prod_m\prod_n\Big[\Upsilon(w_{xi},w_{yj},\theta_{1k},\ldots,\theta_{4n})\left[P_{f\theta}\right] \\ &\quad\times\ \Psi(w_{xi},w_{yj},\theta_{1k},\ldots,\theta_{4n})\Big]^{\nu_{ijklmn}}\ \mathrm{d}^{2N}\theta \end{aligned} \tag{27}$$

where $\nu_{ijklmn}(w_{xi},w_{yj},\theta_{1k},\ldots,\theta_{4n})$ is the discretized version of the density $\rho_g$, normalized such that

$$\sum_i\sum_j\sum_k\sum_l\sum_m\sum_n\nu_{ijklmn}=N. \tag{28}$$

It was obtained by discretizing the $(w_x,w_y,\theta_1,\ldots,\theta_4)$ space into bins of volume $(\Delta w_x\cdot\Delta w_y\cdot\Delta\theta_1\cdots\Delta\theta_4)=(\Delta w)^2(\Delta\theta)^4$. Note that in Equation (27), the product in the first line is over the grains whereas the products in the second line are over the discretized intervals of each of the variables $w_x$, $w_y$, $\theta_1,\ldots,\theta_4$. For compactness we will write,

$$\Phi\{w_{\xi\alpha},\theta_{\alpha\beta}\}\left[P_{f\theta}\right]=\prod_i\cdots\prod_n\Big[\Upsilon_{i\ldots n}\cdot\Psi_{i\ldots n}\Big]^{\nu_{i\ldots n}}\mathrm{d}^{2N}\theta. \tag{29}$$

To find the most probable $\rho_g(w_x,w_y,\theta_1,\ldots,\theta_4)$ that results from the nonuniform DOS of Equation (25), we likewise discretize $\mathbb{S}_4$ into cells of volume $(\delta w_x\cdot\delta w_y\cdot\delta\theta_1\cdots\delta\theta_4)^N$ where $(\delta w)^2(\delta\theta)^4=(\Delta w)^2(\Delta\theta)^4/S$, where $S$ is a large integer and $S>>\nu_{i\ldots n}\forall\ (i,\ldots,n)$. The number of cells in $\mathbb{S}_4$ which map to a particular set $\{\nu_{i\ldots n}\}$ can be estimated by

explicit counting,

$$\omega\{\nu_{i\ldots n}\} = \prod_i \cdots \prod_n \left[\frac{(S-1+\nu_{i\ldots n})!}{(S-1)!\ (\nu_{i\ldots n})!}\right] \left(\sum_i \cdots \sum_n \nu_{i\ldots n}\right)! \tag{30}$$

and in the limit as $S \to \infty$ the estimate becomes exact. However, because $\mathbb{S}_4$ is an assembly space, the axes can be relabeled $N!$ different ways to represent the same combination of grains. Removing this physically meaningless repetition, we omit the factorial of the sums in the second line of Equation (30),

$$\tilde{\omega}\{\nu_{i\ldots n}\} = \prod_i \cdots \prod_n \left[\frac{(S-1+\nu_{i\ldots n})!}{(S-1)!\ (\nu_{i\ldots n})!}\right], \tag{31}$$

where the tilde on $\tilde{\omega}$ indicates that this is the "correct Boltzmann counting" for an assembly space, in which the grains are indistinguishable.

The number of states $\Omega$ in the ensemble mapping to the distribution $\{\nu_{i\ldots n}\}$ is therefore $\tilde{\omega}\{\nu_{i\ldots n}\}$ times the DOS in those cells of $\mathbb{S}_4$,

$$\Omega\{\nu_{i\ldots n}\} = \prod_i \cdots \prod_n \left[\frac{(S-1+\nu_{i\ldots n})!}{(S-1)!\ (\nu_{i\ldots n})!}\right]\ N!\ \left[\Upsilon_{i\ldots n}\Psi_{i\ldots n}\right]^{\nu_{i\ldots n}}\ \mathrm{d}^{2N}\theta \tag{32}$$

where we have used the notation of Equation (29) to express the DOS. Taking the logarithm, it may be maximized with respect to $\nu_{p\ldots u}$. If we discretize the joint distribution of fabric $P_{4\theta}(\theta_1, \ldots, \theta_4) \to \mu_{klmn}(\theta_k, \ldots, \theta_n)$ such that $\sum_k \cdots \sum_n \mu_{klmn} = N$, then each value of $\mu_{klmn}\ \forall\ (k, \ldots, n)$ is a conserved quantity according to the definition of the ensemble in which fabric is specified. The conservation of $W_x$, $W_y$ and $\mu_{klmn}$ are enforced via Lagrange multipliers $\lambda_x$, $\lambda_y$ and $\gamma_{klmn}$ respectively.

$$\frac{\partial}{\partial \nu_{p\ldots u}}\left[\ln\Omega\{\nu_{i\ldots n}\} - \lambda_x\left(\sum_i \cdots \sum_n \nu_{i\ldots n} w_{xi}\right) - \lambda_y\left(\sum_i \cdots \sum_n \nu_{i\ldots n} w_{yj}\right) - \sum_k \cdots \sum_n \gamma_{k\ldots n}\left(\sum_i \sum_j \nu_{i\ldots n}\right)\right] = 0 \tag{33}$$

The calculus is performed using Stirling's approximation and an expansion of the logarithm in a Taylor series of $\nu_{i\ldots n}$ where necessary. Taking the limit for $S \to \infty$ while conserving $N$ and then taking the continuum limit obtains

$$\rho_g(w_x, w_y, \theta_\beta) = \Upsilon\left(w_x, w_y, \theta_\beta\right)\Psi\left(w_x, w_y, \theta_\beta\right)\ G(\theta_\beta)\ e^{-\lambda_x w_x - \lambda_y w_y} \tag{34}$$

where the Fabric Partition Factor $G(\theta_\beta) = G(\theta_1, \ldots, \theta_4)$ derives from $\exp(-\gamma_{r\ldots u})$ in the continuum limit.

Note that $\lambda_x$ and $\lambda_y$ should not be confused with the decay constants of the exponential tails in the empirical distributions. Most (if not all) of the exponential behavior in Equation (34) is contained in the form of $\Upsilon$ because it is a functional of $P_{f\theta}(f, \theta)$. It will be shown in a numerical solution of the isotropic case using an approximation method (later in this paper) that the value of $\lambda_x = \lambda_y$ is approximately zero. This should not be the case in general, however because these two parameters provide the only information about stress anisotropy in the equation.

The Fabric Partition Factor $G$, along with $\Upsilon$ and $\Psi$, determines the partition of fabric between the $(w_x, w_y)$ "modes". Integrating Equation (34) over $w_x$ and $w_y$

$$\begin{aligned} P_{4\theta}(\theta_\beta) &= G(\theta_\beta) \iint_0^\infty \mathrm{d}^2 w \ \Upsilon \Psi e^{-\lambda_x w_x - \lambda_y w_y} \\ &= G(\theta_\beta)\ H(\theta_\beta). \end{aligned} \tag{35}$$

Assuming the standard result of statistical mechanics, one form of $P_{f\theta}$ will be found in the overwhelming majority of the occupied phase space, and so in the thermodynamic limit we may treat fabric as if it is partitioned by $G$ with a fixed form in all of phase space. This factor is not a function of $w_x$ or $w_y$. However, the partition is not an equipartition because of the influence of $\Upsilon$ and $\Psi$. The former is variable over the range of angle configurations within each mode, and the second is a truncating factor which limits the range of angle configurations differently for each mode.

### 3.8 The Recursive Transport Equation

Equations (26) and (34) form a recursion of $P_{f\theta}$ and $\rho_g$, the "transport" equation. This can be written explicitly by inserting equation (26) into (34),

$$\begin{aligned}\rho_g(w_x, w_y, \theta_1, \ldots, \theta_4) \;=\; & \prod_{\beta=1}^{4} \Theta\left[f_\beta(\cdot)\right]\; G(\theta_\beta)\; e^{-\lambda_x w_x - \lambda_y w_y} \\ & \times \iiiint_o^\infty \mathrm{d}^4 f \prod_{\gamma=1}^{4} \Big[P_{f\theta}(f_\gamma, \theta_\gamma \mid \rho_g)\Big]^{1/2} \\ & \times\; \delta\left(w_x - w_x^{\text{right}}(\cdot)\right) \delta\left(w_x - w_x^{\text{left}}(\cdot)\right) \\ & \times\; \delta\left(w_y - w_y^{\text{top}}(\cdot)\right) \delta\left(w_y - w_y^{\text{bott.}}(\cdot)\right) \end{aligned} \tag{36}$$

This transport equation can be solved numerically choosing $\lambda_x$, $\lambda_y$, and $G(\theta_\beta)$ as required to maintain the specified $W_x$, $W_y$ and $P_{4\theta}$.

The development of this transport equation is the principle result of this dissertation and the remaining space shall be devoted to testing it by working out its numerical predictions and comparing them to empirical data.

# CHAPTER 4

# THE MEAN STRUCTURE APPROXIMATION

## 4.1 Modified Separability in the DOS

The transport equation can be solved using Monte Carlo integration. Efforts are underway to obtain the numerical solution, which shall be presented in a future publication. For the present an approximation will be introduced, simplifying the recursion equation while yet providing sufficient accuracy to demonstrate the principle organizational features of the ensemble. This approximation also has value in its own right because it will integrate out the fabric, thereby isolating and identifying the principle features of nonuniformity in the Cartesian loads, $w_x$ and $w_y$. This will provide insight into the nature of the DOS and the resulting $P_f(f)$.

The goal in this section is to obtain a modified separability in the DOS,

$$\rho_g(w_x, w_y, \theta_\beta) \approx \rho_w(w_x, w_y)\ \rho_\theta(\theta_\beta)\ \Psi(w_x, w_y, \theta_\beta). \tag{37}$$

The physical idea is that, while $\rho_w(w_x, w_y)$ and $\rho_\theta(\theta_\beta)$ are correlated and hence the DOS is not truly separable, the correlations arise mainly because nature removes the unstable configurations, which is the function of $\Psi$. Comparing Equations 34 and 37, we find $\Psi$ in each and we identify $\rho_\theta(\theta_\beta) = G(\theta_\beta)$. Equating the remaining terms requires that we blur out the angular dependence in $\Upsilon$,

$$\Upsilon(w_x, w_y, \theta_\beta) \approx \overline{\Upsilon}(w_x, w_y) \tag{38}$$

so that

$$\rho_w(w_x, w_y) = \overline{\Upsilon}(w_x, w_y)\ e^{-\lambda_x w_x - \lambda_y w_y} \tag{39}$$

To be a valid characterization of the DOS, Equation 38 should apply to the great majority of stable grain configurations; it need not apply to all of them. Whereas $\Psi$ is a

truncating factor in the DOS, defining the region where individual grains are stable, $\Upsilon$ is a scaling factor in the DOS, indicating how often particular grain configurations will occur in the ensemble based upon the probability that they can satisfy Newton's third law with their neighbors. Equation (38) claims that this scaling is strongly dependent upon the values of $w_x$ and $w_y$; but when varying the contact angles it does not vary too much over the *majority* of that configuration space.

To investigate the meaning of the approximation, some manipulation of Equation 22 shows that,

$$\begin{aligned}\Upsilon(w_x, w_y, \theta_\beta) &= \iiiint_0^\infty \mathrm{d}^4 w \left[P^\star_{4w4\theta}(w_\xi^{\text{hem.}}, \theta_\beta)\right]^{\frac{1}{2}} \delta\left(w_x - w_x^{\text{right}}\right)\ \delta\left(w_y - w_y^{\text{top}}\right) \\ &\quad \times \delta\left(w_x - w_x^{\text{left}}\right)\ \delta\left(w_y - w_y^{\text{bott.}}\right) \end{aligned} \tag{40}$$

where,

$$\begin{aligned} P^\star_{4w4\theta}(w_\xi^{\text{hem.}}, \theta_\beta) &\triangleq P^\star_{4w4\theta}(w_x^{\text{right}}, w_x^{\text{left}}, w_y^{\text{top}}, w_y^{\text{bott.}}, \theta_1, \ldots, \theta_4) \\ &= \iiiint_0^\infty \mathrm{d}^4 f \prod_{\beta=1}^{4} P_{f\theta}\left(f_\beta, \theta_\beta\right) \\ &\quad \times \delta\left(w_x^{\text{right}} - w_x^{\text{right}}(\cdot)\right)\ \delta\left(w_x^{\text{left}} - w_x^{\text{left}}(\cdot)\right) \\ &\quad \times \delta\left(w_y^{\text{top}} - w_y^{\text{top}}(\cdot)\right)\ \delta\left(w_y^{\text{bott.}} - w_y^{\text{bott.}}(\cdot)\right). \end{aligned} \tag{41}$$

$P^\star_{4w4\theta}$ can be interpreted as the joint distribution of *attempted* loads and contact angles that $\{\mathcal{C}_i \mid P_{f\theta}\}$ (all permutations of grains having some specified $P_{f\theta}$) *attempts* to place on any one grain, without removing the $\mathcal{C}_i$ that violate Newton's second law. The star indicates that this is only a conceptual distribution, not found in nature. Because it is a mean-field calculation, the strong intra-grain correlation found in real grains has been eliminated. This is illustrated in Figure 11, where the mean-field is calculated over the union of the four circles, but the stable grains occur only in their intersection. Because of the vastly weakened correlations over this expanded region, we make the assumption,

$$\begin{aligned} P^\star_{4w4\theta}(w_\xi^{\text{hem.}}, \theta_\beta) &\approx P^\star_{4w}(w_\xi^{\text{hem.}})/16\pi^4 \\ &\approx P^\star_{2w}(w_x^{\text{right}}, w_y^{\text{top}}) P^\star_{2w}(w_x^{\text{left}}, w_y^{\text{bott.}})/16\pi^4. \end{aligned} \tag{42}$$

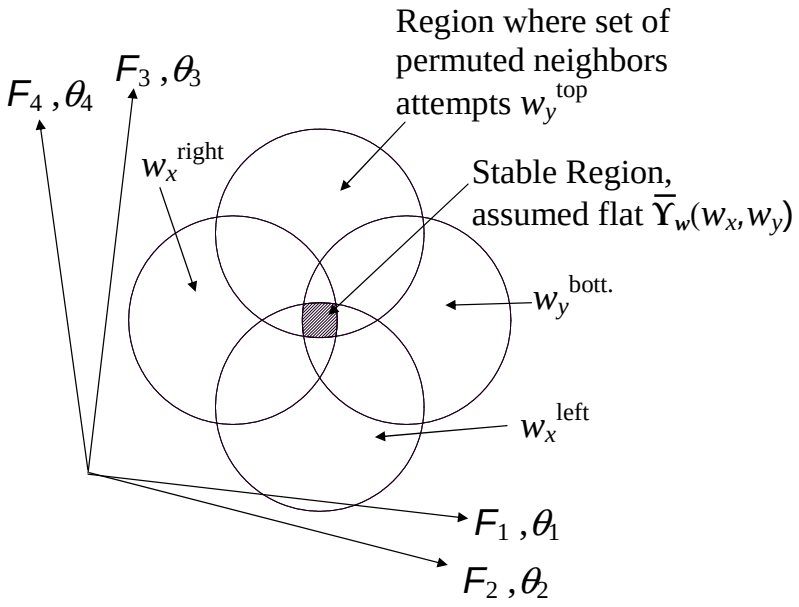


Figure 11: Schematic diagram of the Mean Structure Approximation.

We note that this argument explains the nature of the approximation but does not rigorously justify it. It shall be justified on the basis of the empirical results, later. Using this in Equation 40, we obtain

$$\Upsilon(w_x, w_y, \theta_\beta) \approx P^\star_{2w}(w_x, w_y)/4\pi^2 \triangleq \overline{\Upsilon}(w_x, w_y). \tag{43}$$

This shall be called the "Mean Structure Approximation." $P^\star_{2w}(w_x, w_y)$ may be viewed as a mean-field calculation of *attempted* loads that the ensemble of permutations attempts to place on a grain's upper and right hemispheres (for example). It must be emphasized that this is not a mean-field calculation of loads *actually* placed on the grains, but rather it is the approximate scale measuring how often particular modes will satisfy Newton's third law and therefore occur in the ensemble. It gives us the approximate effect of Newton's third law after having decoupled the strong intra-grain effects of Newton's second law. Thus, we see that the essence of the MSA is that it effects a decoupling of Newton's second and third laws in the form of the DOS.

Using this approximation, we project the DOS in $\mathbb{S}_4 \rightarrow \mathbb{S}_5$, where the latter is the subspace $\{w_{x\alpha}, w_{y\alpha}\}$. The projection is performed by integrating Equation (34) across

all the angle axes,

$$P_{2w}(w_x, w_y) = e^{-\lambda_x w_x - \lambda_y w_y} \iiiint_0^{2\pi} \mathrm{d}^4\theta \; G(\theta_\beta) \; \Psi\left(w_x, w_y, \theta_\beta\right) \; \Upsilon\left(w_x, w_y, \theta_\beta\right) \tag{44}$$

Using the MSA,

$$P_{2w}(w_x, w_y) = e^{-\lambda_x w_x - \lambda_y w_y} \; \overline{\Upsilon}\left(w_x, w_y\right) \iiiint_0^{2\pi} \mathrm{d}^4\theta \; G(\theta_\beta) \; \Psi\left(w_x, w_y, \theta_\beta\right), \tag{45}$$

which allows us to define,

$$\overline{\Psi}(w_x, w_y) = \iiiint_0^{2\pi} \mathrm{d}^4\theta \; G(\theta_\beta) \; \prod_{\gamma=1}^{4} \Theta\Big[f_\gamma(\cdot)\Big] \tag{46}$$

so that we may write,

$$P_{2w}(w_x, w_y) = e^{-\lambda_x w_x - \lambda_y w_y} \; \overline{\Upsilon}\left(w_x, w_y\right) \; \overline{\Psi}\left(w_x, w_y\right). \tag{47}$$

Writing the DOS projected into $\mathbb{S}_5$,

$$\begin{aligned} \tilde{\rho}^{(5)}\{w_{x\alpha}, w_{y\alpha}\} \;\; &= \;\; N! \prod_\alpha \; \overline{\Upsilon}(w_{x\alpha}, w_{y\alpha}) \; \overline{\Psi}(w_{x\alpha}, w_{y\alpha}) \\ &\quad \times \; \delta\left(\sum_\alpha w_{x\alpha} - W_x\right) \; \delta\left(\sum_\alpha w_{y\alpha} - W_y\right). \end{aligned} \tag{48}$$

We may identify $\overline{\Psi}(w_x, w_y)$ as the "Grain Factor" and $\overline{\Upsilon}(w_x, w_y)$ as the "Structure Factor." These are the primary features of nonuniformity in the $(w_x, w_y)$ axes of the DOS. Whereas $\overline{\Psi}$ derives from the configuration space of *individual* grains (cohesionless Newton's second law), $\overline{\Upsilon}$ derives from the configuration space of grains connecting together to form a packing structure (Newton's third law). These two factors were so-named because their separability (in the MSA) and their roles may be considered somewhat analogous to the separability and roles of the atomic form factor and structure factor of x-ray crystallography.

The meaning of $\overline{\Psi}$ can be illustrated easily through a change of variables. We notice that for rigid, cohesionless grains there is no inherent force scale and hence grain stability

must be independent of the overall scale of the forces. Thus it is convenient to change variables,[1]

$$s_\alpha = \frac{w_{x\alpha} - w_{y\alpha}}{w_{x\alpha} + w_{y\alpha}}, \qquad t_\alpha = \frac{w_{x\alpha} + w_{y\alpha}}{2}. \tag{49}$$

While grain pressure $t$ is analogous to hydrostatic pressure at the grain scale, the shear ratio $s$ is related to the local shear stress at the grain scale. The stability of the $\alpha^{\text{th}}$ grain is a function of $s_\alpha$ and the four contact angles, $\{\theta_\beta\}_\alpha$, only. With the Jacobian $J = t$, Equation (44) can also be written,

$$P_{st}(s,t) = \overline{\Upsilon}_{st}(s,t)\overline{\Psi}_s(s)e^{-(\lambda_x+\lambda_y)t-(\lambda_x-\lambda_y)st} \tag{50}$$

where the notation has been introduced,

$$\begin{aligned} \overline{\Upsilon}_{st}(s,t) &= t\ \overline{\Upsilon}[(1+s)t,(1-s)t] \\ &= (w_x+w_y)\ \overline{\Upsilon}(w_x,w_y)/2, \end{aligned} \tag{51}$$

and,

$$\begin{aligned} \overline{\Psi}_s(s) &= \overline{\Psi}[(1+s)t,(1-s)t] \\ &= \overline{\Psi}(w_x,w_y). \end{aligned} \tag{52}$$

Note that $\Theta$ in Equation (46) is insensitive to the scale of $f_\gamma$ and cares only whether it is positive or negative, and hence the $t$ does not appear as an argument of $\overline{\Psi}_s(s)$.

In these coordinates Equation (46) may be solved very efficiently by Monte Carlo integration. This has been performed for the case of quartered isotropy (see Section 3.3). In the MSA, $\overline{\Upsilon}$ does not affect the fabric partition, and hence it is easy to find the fabric partition factor. The product of the weighting for the quartering bias with the weighting for the fabric partition was obtained empirically by adjusting as required in a Fourier decomposition to achieve approximate isotropy $P_\theta(\theta) \approx 1/2\pi$. The numerical result for

[1]Note in contrast to the definition in Reference [2], $t$ has now been divided by 2 to permit its identity with hydrostatic pressure.

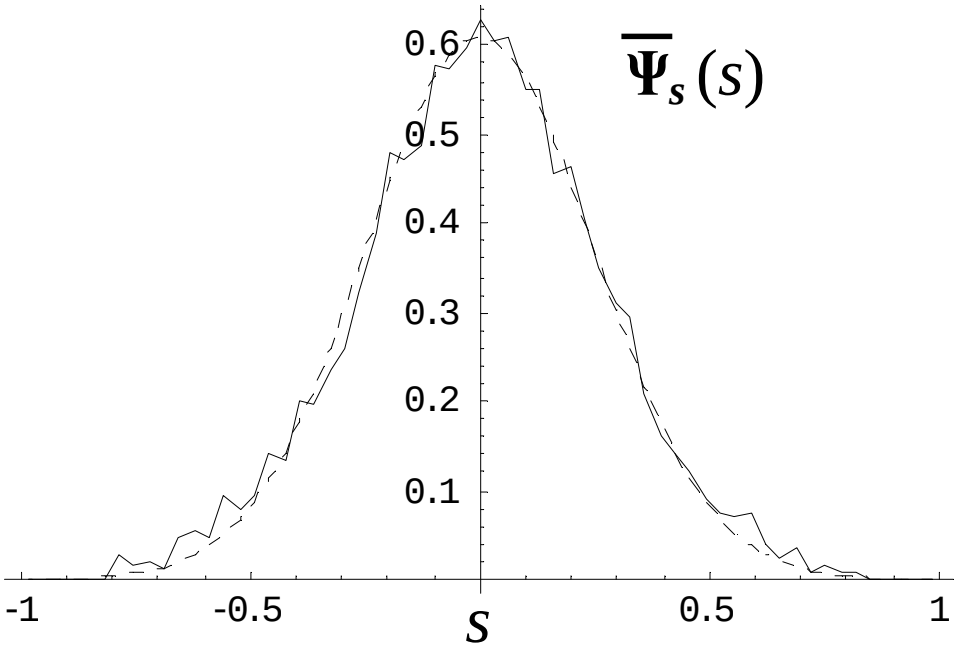


Figure 12: Grain factor $\Psi(s)$. Solid line—numerical solution of MSTE. Dashed line—functional fit per Equation 53.

that case is fit well by a Gaussian,

$$\overline{\Psi}_s(s) = \sqrt{c/\pi}\ e^{-cs^2}, \quad |s| \leq 1 \tag{53}$$

with $c = 8$. It is shown in Figure (12) with the fit as the dashed curve. This indicates that in the isotropic case the volume of a grain's stability space is a Gaussian function of the individual grain's load-anisotropy, $s$.

In contrast to the simplicity of the above result, the form of $\overline{\Upsilon}$ depends upon $P_{f\theta}$ and hence can only be found by solving the transport equation.

Finally, we note that in the MSA we can now write $\rho_g$ with modified separability,

$$\rho_g(w_x, w_y, \theta_\beta) \approx \left[\overline{\Upsilon}(w_{x\alpha}, w_{y\alpha})\ e^{-\lambda_x w_x - \lambda_y w_y}\right] \cdot G(\theta_\beta) \cdot \Psi\left(w_x, w_y, \theta_\beta\right) \tag{54}$$

### 4.2 The Mean Structure Transport Equation

Just as Equation (34) can be solved recursively, giving us the recursive "transport" equation, so can Equation (47) be solved recursively, giving us the "Mean Structure

Transport Equation" or MSTE.

To develop the MSTE, we convert the load distribution of Equation (47) into a contact force distribution. This cannot be done simply by collapsing $P_{2w}$ since it does not contain sufficient information. However, the variables may be changed if we first obtain the joint conditional distribution $C_{f\theta}\,(f, \theta \mid w_x, w_y)$, so that,

$$P_{f\theta}(f,\theta) = \iint_0^\infty \mathrm{d}^2 w \;\; C_{f\theta}(f,\theta \mid w_x, w_y)\; P_{2w}(w_x, w_y). \tag{55}$$

This distribution can be obtained easily through the same change of variables introduced previously, $(w_x, w_y) \rightarrow (s,t)$, because $C_{f\theta}\,(f,\theta \mid s,t) = t \cdot C_{f\theta}\,(tf,\theta \mid s,1)$ and the conditional dependency is reducible to the $s$ variable, alone. This may obtained by straightforward integration,

$$\begin{aligned} C_{f\theta}\,(f,\theta \mid s,1) \;\; &= \;\; \frac{1}{4}\sum_{\gamma=1}^{4} \iiiint_0^{2\pi} \mathrm{d}^4\theta \; G(\theta_\beta)\; \delta(\theta - \theta_\gamma)\; \delta\Big[f - f_\gamma(s,1,\theta_1,\ldots,\theta_4)\Big] \\ &\quad \times \prod_{\eta=1}^{4} \Theta\Big[f_\eta(s,1,\theta_1,\ldots,\theta_4)\Big] \end{aligned} \tag{56}$$

where only one term of the sum is needed in many cases due to the symmetries of the ensemble. This reflects the MSA because it assumes that all grains in the same $(s,t)$ mode contribute to the integral according to the same weight. It can be found by very easy Monte Carlo integration, and the result for the case of isotropy, $C_{f\theta}(f,\theta \mid s,1) = C_f(f \mid s,1)/2\pi$, is shown in Figure (13). Horizontal cross sections through this plot represent the conditional distribution for $f$, where white represents higher probability density. The vertical axis represents its dependence upon the $s$ variable and the entire plot is shown for a fixed $t = 1$. Varying $t$ only rescales the $f$ axis. Note that the horizontal axis is normalized by the average contact force magnitude, which was found to be $\langle f \rangle = 0.39$ when $t = 1$.

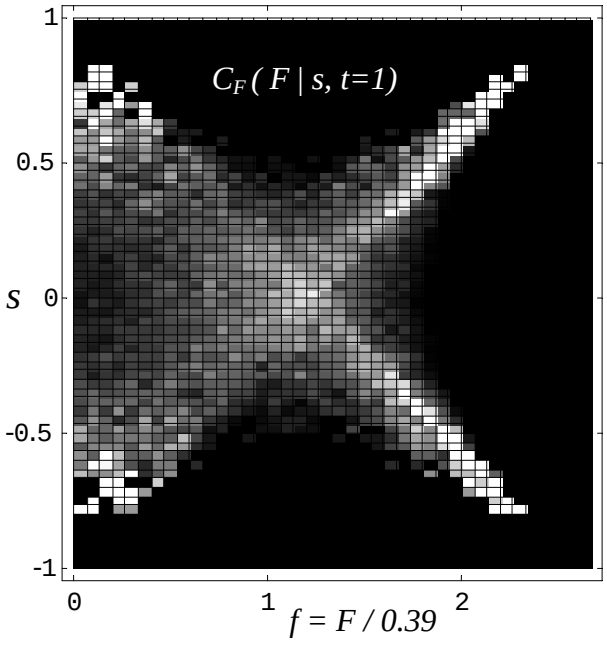


Figure 13: $C_f(f \mid s,t)$ with $t = 1$.

Combining this distribution with Equation (47) and the definitions of $C_{f\theta}$, $\overline{\Psi}$ and $\overline{\Upsilon}$,

$$P_{f\theta}(f,\theta) = \frac{1}{16\pi^2}\sum_{\gamma=1}^{4}\iint_0^\infty \mathrm{d}^2w\; e^{-\lambda_x w_x-\lambda_y w_y}\iiiint_0^{2\pi}\mathrm{d}^4\theta\;\; G(\theta_\beta)$$
$$\times\; P^\star_{2w}(w_x,w_y)\;\delta(\theta-\theta_\gamma)\;\delta\Big[f-f_\gamma(\cdot)\Big]\;\prod_{\eta=1}^{4}\Theta\Big[f_\eta(\cdot)\Big]. \qquad (57)$$

$P^\star_{2w}(w_x,w_y)$ used in this equation may be obtained a number of ways that should be equivalent within the accuracy of the MSA. Two of these have been used in the numerical results and were shown indeed to produce identical results to within the statistical precision of the data. The first is purely consistent with the MSA, assuming no necessity for *a priori* correlation between the loads and the contact angles. Furthermore, it assumes no *a priori* correlation between $w_x$ and $w_y$. Correlations arise only after throwing out unstable grain configurations. That is, it assumes a fixed $\overline{\Upsilon}$ over the union of two circles in Figure (11), not just the intersection of all four (the gray region). Imposing $\overline{\Psi}$ then

throws out grain configurations outside of the gray region. This method is,

$$\begin{aligned} w_x &= f_1 \cos\theta_1 + f_2 \cos\theta_2, \\ w_y &= f_3 \sin\theta_3 + f_4 \sin\theta_4 \end{aligned} \tag{58}$$

(note that all four contacts are treated as if distinctly different despite the fact that an $x$-hemisphere and a $y$-hemisphere overlap in one quadrant), and

$$P^{\star}_{2w}(w_x, w_y) = P^{\star}_{wx}(w_x) P^{\star}_{wy}(w_y), \tag{59}$$

where

$$P^{\star}_{wx}(w_x) = \iint_0^{\infty} \mathrm{d}^2 f \iint_0^{2\pi} \mathrm{d}^2\theta \prod_{\beta=1}^{2} P_{f\theta}\left(f_\beta, \theta_\beta\right) \delta(w_x - f_1\cos\theta_1 - f_2\cos\theta_2), \tag{60}$$

$$P^{\star}_{wy}(w_y) = \iint_0^{\infty} \mathrm{d}^2 f \iint_0^{2\pi} \mathrm{d}^2\theta \prod_{\gamma=3}^{4} P_{f\theta}\left(f_\gamma, \theta_\gamma\right) \delta(w_y - f_3\sin\theta_3 - f_4\sin\theta_4). \tag{61}$$

The second method attempts greater fidelity to the micromechanics by imposing *a priori* correlation between $w_x$, $w_y$ and $\{\theta_\beta\}$. If the MSA is valid, then imposing these correlations should be largely superfluous. Expressed here for the case of quartered fabric, the second method is

$$\begin{aligned} w_x &= f_1 \cos\theta_1 + f_2 \cos\theta_2, \\ w_y &= f_2 \sin\theta_2 + f_3 \sin\theta_3 \end{aligned} \tag{62}$$

(note the shared contact $\vec{f}_2$), and

$$\begin{aligned} P^{\star}_{2w3\theta}(w_x, w_y, \theta_\beta) = \iiint_0^{\infty} \mathrm{d}^3 f \prod_{\gamma=1}^{3} P_{f\theta}\left(f_\gamma, \theta_\gamma\right) \\ \times \delta(w_x - f_1\cos\theta_1 - f_2\cos\theta_2)\ \delta(w_y - f_2\sin\theta_2 - f_3\sin\theta_3). \end{aligned} \tag{63}$$

Inserting either of these forms of $P^{\star}_{2w}$ into Equation (57) produces an MSA recursion equation in $P_{f\theta}$, which is the MSTE. It can be simplified by taking advantage of the various symmetries of the ensemble.

The two different forms of $P^{\star}_{2w}$ produce two different forms of the MSTE. This is striking because one form of $P^{\star}_{2w}$ contains $(P_{f\theta})^3$ whereas the other contains $(P_{f\theta})^4$. The ability of these two very different transport equations to produce the same $P_{f\theta}$ depends upon the validity of the MSA.

# CHAPTER 5

# PREDICTIONS OF THE THEORY

This chapter numerically solves the simplified transport equation (that is, the Mean Structure Transport Equation, or MSTE) and makes predictions about the various distributions that we should expect to find in a disordered granular packing. Some of the predicted distributions are for statistics that had never been measured before in any simulation or experiment, whether by the author or by others, and so the subsequent empirical test of them (reported in the next chapter) constituted a real test of the theory's predictions.

The MSTE was solved in a Monte Carlo process for the case of isotropic stress and fabric, but with one further simplification. It was found that $\lambda_x$ and $\lambda_y$ were not exactly zero in the MSA, although they were very tiny $\sim 0.01$ so that the exponential factors were not exactly unity but were nevertheless negligible. Therefore, rather than implementing the exponential weighting exactly, the forces were simply rescaled with a flat factor in each iteration to prevent incremental growth. This approach is reasonable because the phase space for rigid grains has no inherent force scale, the growth was very small, and the growth was balanced in the $x$ and $y$ components. Hence, the form of the DOS should not be greatly affected by this flat rescaling.

The MSTE was shown to converge efficiently to the same stationary state after beginning from several different initial distributions. The original work was performed with MATHEMATICA solving for approximately $5,500$ grains. These results are presented in this chapter. Subsequent efforts with Fortran demonstrate that converged solutions can be found for a million contacts in about 1 minute on a desktop computer. It is quite easy

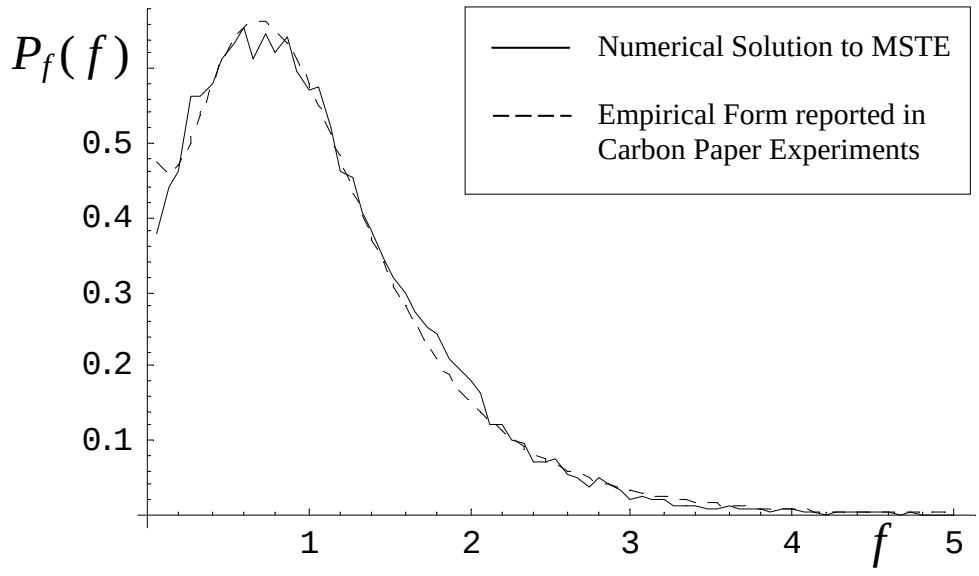


Figure 14: (Solid Line) $P_f(f)$ resulting from Monte Carlo solution of the MSTE. (Dashed Line) Fit to $P_f(f)$ using functional form obtained in the carbon paper experiments reported in [9].

to obtain data sets of $10^{10}$ grains or greater, making it possible to study joint or conditional distributions of three or more variables with smooth statistics using only a desktop computer. For some applications this provides a tremendous computational advantage over the fully dynamic simulations.

## 5.1 Numerical Results

Here, the following nomenclature is used. The vector magnitude of the contact forces are denoted by $F$, their distribution is $P_F(F)$, and their mean is $\langle F \rangle$. The corresponding normalized force magnitudes are $f = F/\langle F \rangle$, which have a distribution $P_f(f) = \langle F \rangle P_F(f \langle F \rangle)$. The Cartesian force components in the $x$ direction are denoted by $F_x$, their distribution is $P_X(F_x)$, and their mean is $\langle F_x \rangle$. The corresponding normalized Cartesian forces are $f_x = F_x/\langle F_x \rangle$, which have a distribution $P_x(f_x) = \langle F_x \rangle P_X(f_x \langle F_x \rangle)$.

### *5.1.1 Force Magnitudes*

The $P_f(f)$ resulting from the MSTE using Equation 61 is shown in Figure (14) and semi

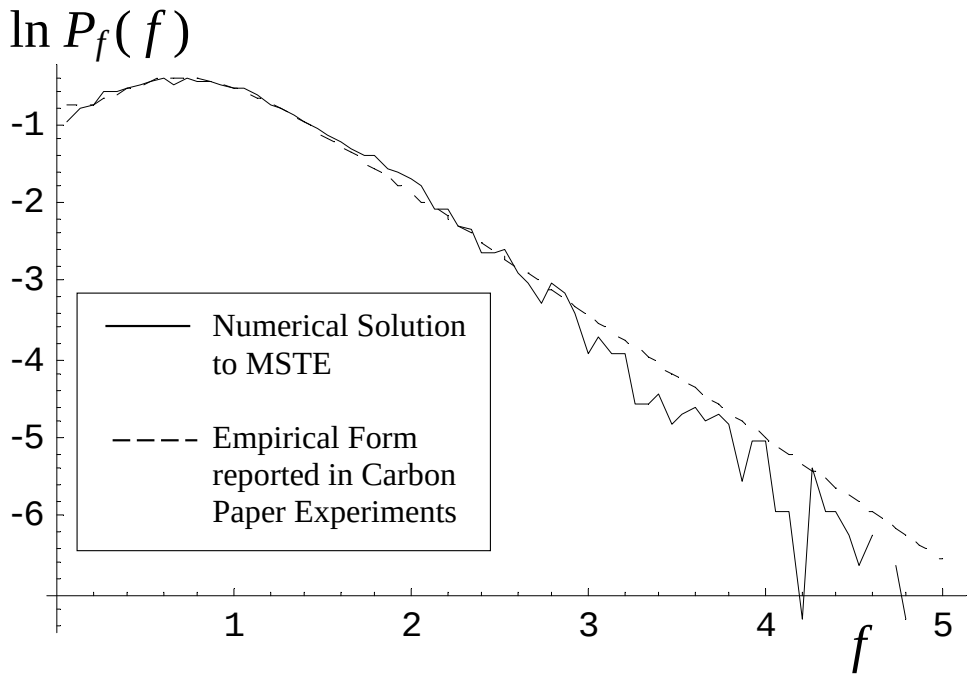


Figure 15: (Solid Line) Semi logarithmic $P_f(f)$ resulting from Monte Carlo solution of the MSTE. (Dashed Line) Fit to $P_f(f)$ using functional form obtained in the carbon paper experiments reported in [9].

logarithmically in Figure (15). It has all the key characteristics of granular contact force distributions: a nonzero probability density for zero force, a peak just below $f = 1$, and an exponential tail. A fit, shown as the smooth curve in Figure (14), was obtained using the form proposed by the Chicago group for their carbon-paper experiments [9],

$$P_f(f) = a\left(1 - be^{-cf^2}\right)e^{-df}. \tag{64}$$

Using the values $a = 3.28$, $b = 0.85$, $c = 1.56$, and $d = 1.56$, the fit is good and is in quantitative agreement with the range of values reported from both experiments and numerical simulations.

### *5.1.2 Cartesian Components*

For the special case of true isotropy in which

$$P_{F\theta}(F,\theta) = P_F(F)P_\theta(\theta) = P_F(F)/2\pi, \tag{65}$$

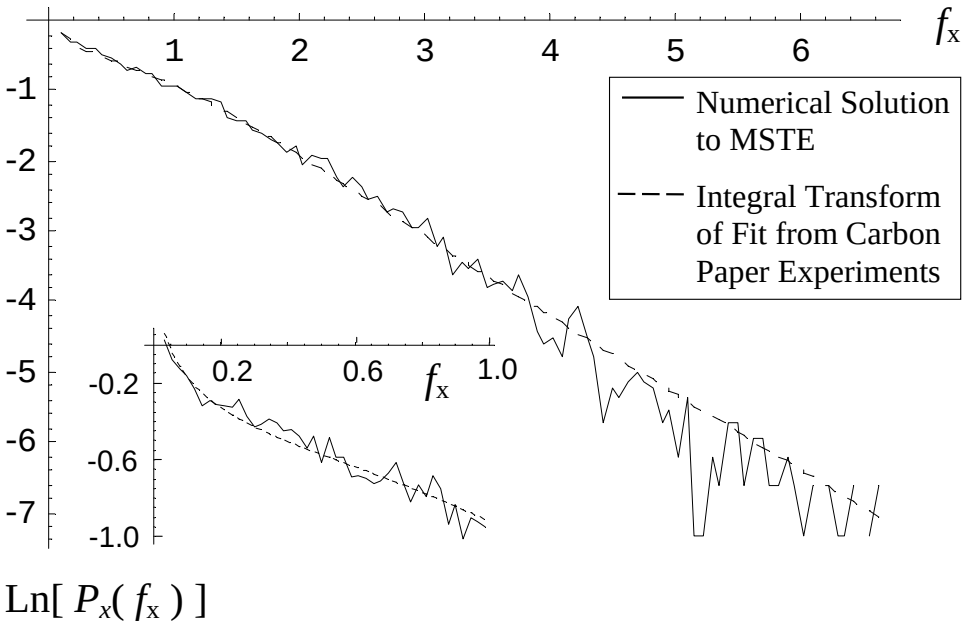


Figure 16: (Solid Line) Semi-logarithmic $P_x(f_x)$ resulting from Monte Carlo solution of the MSTE. (Dashed Line) Semi-empirical fit described in the text. (Inset) Semi logarithmic behavior of the same two curves below $f_x = 1$.

changing variables to Cartesian components $F_x = F\cos\theta$ is effected in probability theory by the straightforward

$$P_X(F_x) = \int_0^{2\pi} \mathrm{d}\theta \int_0^{\infty} \mathrm{d}F \; \frac{P_F(F)}{2\pi} \delta(F_x - F\cos\theta), \tag{66}$$

or by evaluating the inner integral and expressing as normalized forces,

$$P_x(f_x) = \frac{2}{\pi}\frac{\langle F\rangle}{\langle F_x\rangle} \int_0^{\frac{\pi}{2}} \mathrm{d}\theta \; P_f(f_x \sec\theta)\sec\theta, \tag{67}$$

where the symmetries of isotropy were used to reduce the range of integration in $\theta$. Numerically integrating this [38] with the $P_f(f)$ of Equation (64) yields the smooth line in Figure (16). It fits the numerical Cartesian component data from the transport algorithm (shown in the same figure) over the entire range. The semi logarithmic inset shows the behavior below $f_x = 1$. It has a singularity at $f_x = 0$ and is monotonically decreasing as demonstrated in numerical simulations [38]. It is not purely exponential, the two knees being indicative of a summation of $n^{\text{th}}$ order Modified Bessel Functions of

the Second Kind, $K_n(\beta_x f_x)$, functions that result naturally [43] when exponential forms are used for $P_f(f)$ in Equation (67).

### *5.1.3 Functional Forms*

The only problem with the fit shown in Figure (14) occurs in the region of very small forces, $f \lesssim 0.2$. This is the same region in which the form of Equation (64) could not be experimentally verified due to calibration limits. A better fit can be obtained using another form so that it fits excellently over the entire range including $f << 1$. This will be accomplished starting with the observation noted above, that the two knees in Figure (16) are indicative of $K_n(\beta_x f_x)$. These two knees appear very dramatically in a rotation of the coordinates, a rotation which is most easily understood if performed manually by lifting the edge of the page toward the eye and rotating it so that the line of sight is parallel to the segments of the graph in Figure (16). The fit to $P_f(f)$ will therefore be accomplished by fitting the natural forms to $P_x(f_x)$ and then mathematically inverting the transformation of Equation (67). The simplest fit to within the statistical accuracy of this data set appears to be of the form,

$$P_x(f_x) = C_1 \sum_{n=0}^{2} a_n f_x^n K_n(\beta_x f_x) \tag{68}$$

with $a_0 = 2$, $a_1 = -2$, $a_2 = 11$, and $\beta_x = \pi/2$, and where $C_1$ is for normalization. The fit is excellent over the entire range, displaying all the correct knees and piecewise slopes as shown in Figure (17)(top). The shape of the knee closest to $f_x = 0$ could be obtained only by including a $K_0$ term. This term has infinite probability density for $f_x = 0$, but the singularity is very narrow and hence cannot usually be seen in a finite set of empirical data that has been aggregated into bins of finite width.[1]

The transformation integral which is the inverse of Equation (67) cannot be deduced by probability theory because $f_x$ and $\theta$ are not statistically independent. Therefore,

[1] A definite integral over the singularity converges producing a finite probability as expected, so the singularity in the probability *density* is not a problem.

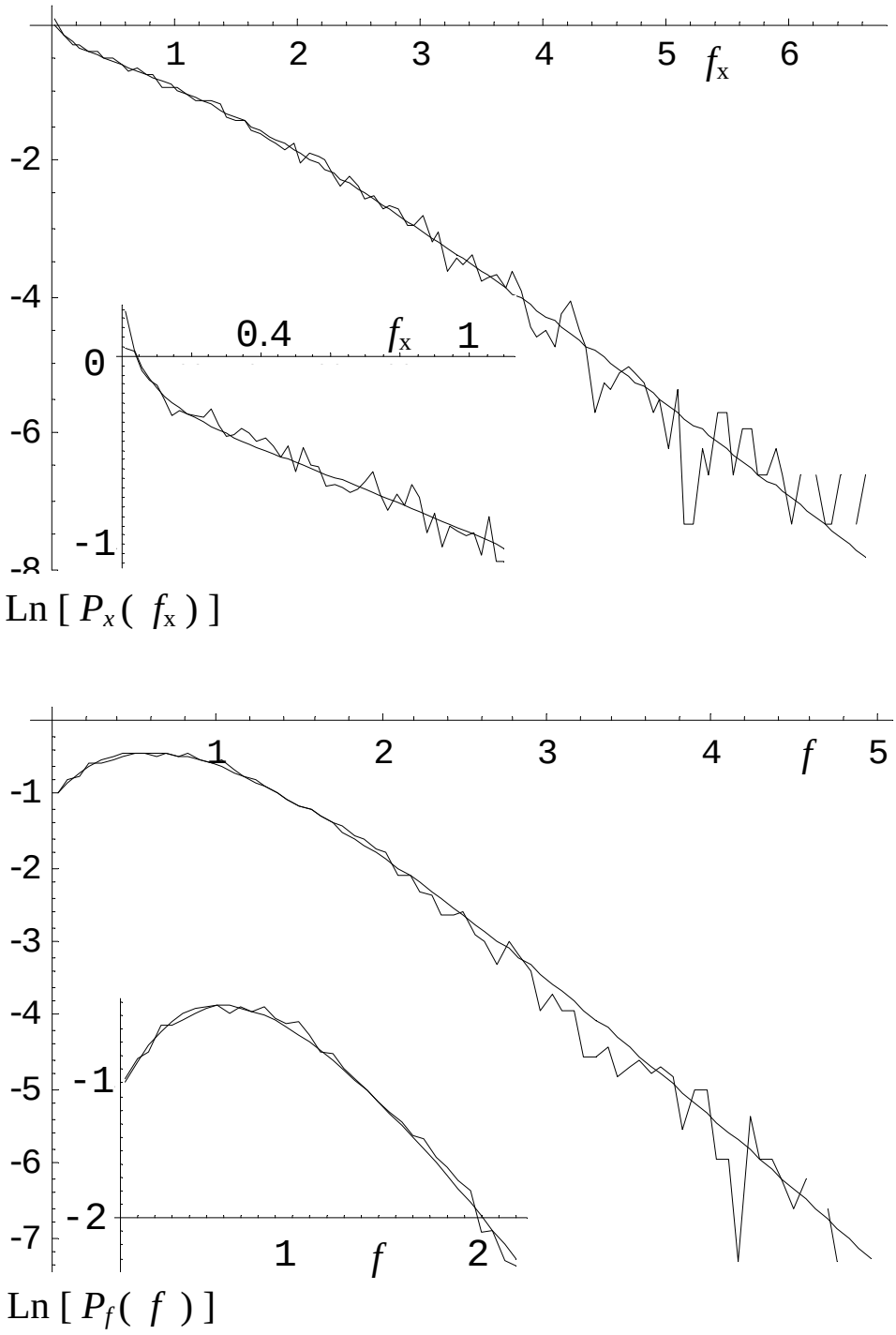


Figure 17: $P_x(f_x)$ and $P_f(f)$ resulting from Monte Carlo solution of the MSTE. (Smooth curves) Fits to these distributions using the natural functional forms as suggested in the text. (Top) Semi logarithmic $P_x(f_x)$; inset showing behavior below $f_x = 1$. (Bottom) Semi logarithmic $P_f(f)$; inset showing behavior below $f = 2$.

inverting the change of variables to go from $(f_x, \theta) \rightarrow (f, \theta)$ is not trivial, even in this isotropic case. Nevertheless, the exact relationship was derived recently by Youngquist using an approach that is similar to the mathematics of X-Ray Tomography [43]. The result is,

$$P_F(F) = \frac{1}{F} \int_0^{\frac{\pi}{2}} \mathrm{d}\theta \; P_X(F \sec\theta) \csc^2\theta, \tag{69}$$

or, in normalized forces,

$$P_f(f) = \frac{\langle F_x \rangle}{\langle F \rangle} \frac{1}{f} \int_0^{\frac{\pi}{2}} \mathrm{d}\theta \; P_x(f \sec\theta) \csc^2\theta. \tag{70}$$

This relationship is fascinating because we know that $F_x = F\cos\theta$ and therefore $F_x \leq F$ for all $\theta$; however, this relationship computes $F$ in terms of $F_x = F\sec\theta$ so that $F_x \geq F$ for all $\theta$. This says that the probability of finding a contact force magnitude $F$ is a weighted sum over the probabilities for all the Cartesian components $F_x$ that are too large to be relevant. Nevertheless it is mathematically correct.

Using Equation (68) in Equation (70), we obtain,

$$P_f(f) = \frac{\pi C_2}{2} e^{-\beta f} \sum_{n=0}^{2} b_n \langle F \rangle^n f^n \tag{71}$$

with $C_2 = C_1$, $b_0 = a_0$, $b_1 = \pi a_1/2 + a_2$, $b_2 = \pi a_2/2$, and $\beta = \beta_x \langle F \rangle / \langle F_x \rangle \approx (\pi/2)^2$. This result fits the numerical data from the MSTE excellently over the entire range of $f$ as shown in Figure (17)(bottom). It exactly matches the finite and nonzero value of $P_F(0) = \frac{\pi}{2} C_1 a_0$ that occurred in the numerical data, so we see that the $a_0$ term that made $P_x(f_x \rightarrow 0)$ infinite is the same $b_0$ term that makes $P_f(0)$ nonzero and finite. The linear plots of Equations (68) and (71) are shown in Figure (18) in order to show that the curve fits are truly good in the region of weak forces, even without the compression of a logarithmic axis.

### *5.1.4 Cartesian Loads*

Figure (19) shows semi-logarithmically the Cartesian Load distribution $P_w(w)$ produced by the MSTE, computed for several different rotations of the Cartesian axes. These

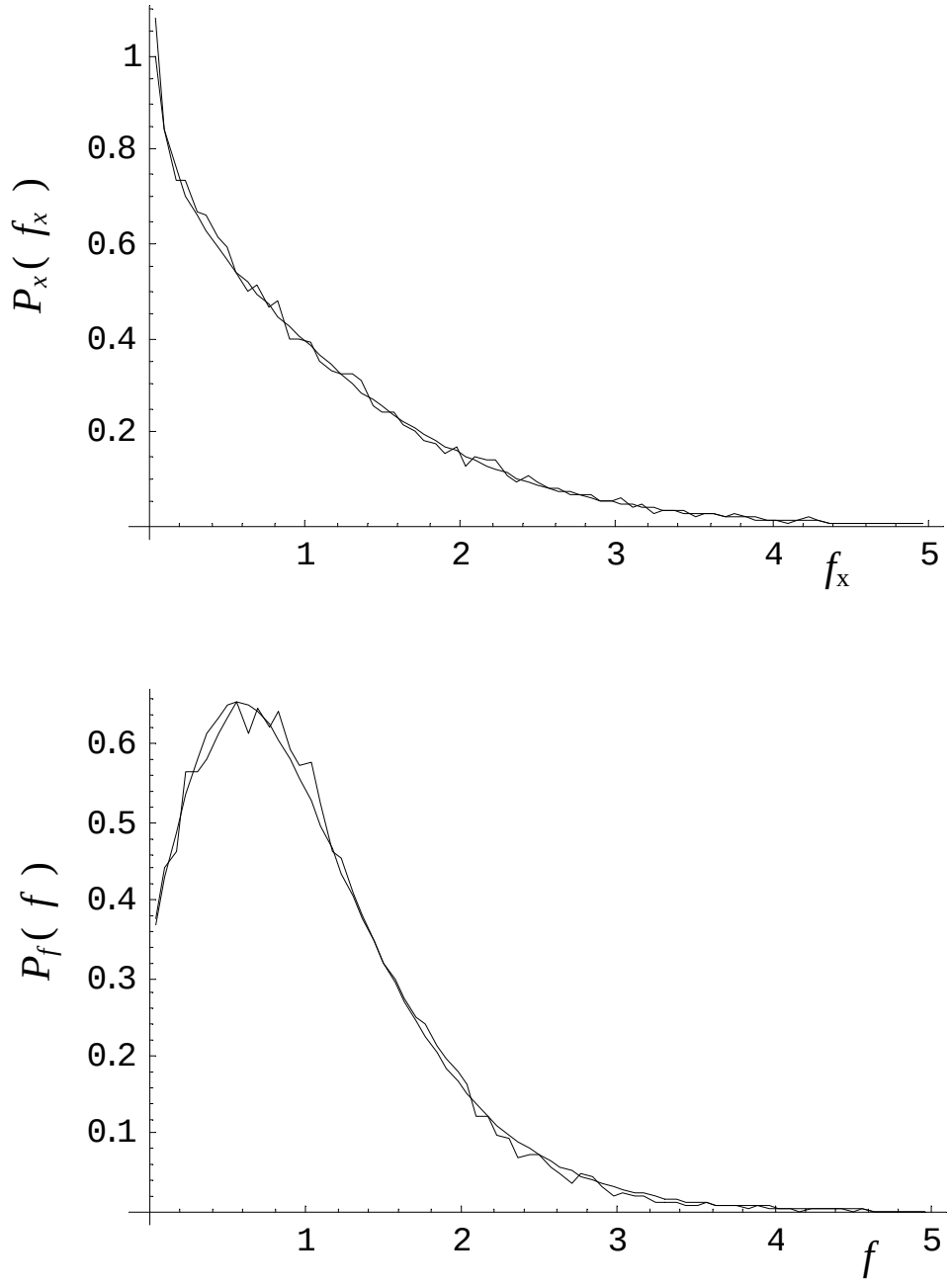


Figure 18: Linear plots of $P_x(f_x)$ and $P_f(f)$ resulting from Monte Carlo solution of the MSTE. (Smooth curves) Fits to these distributions using the natural functional forms as suggested in the text. (Top) $P_x(f_x)$. (Bottom) $P_f(f)$.

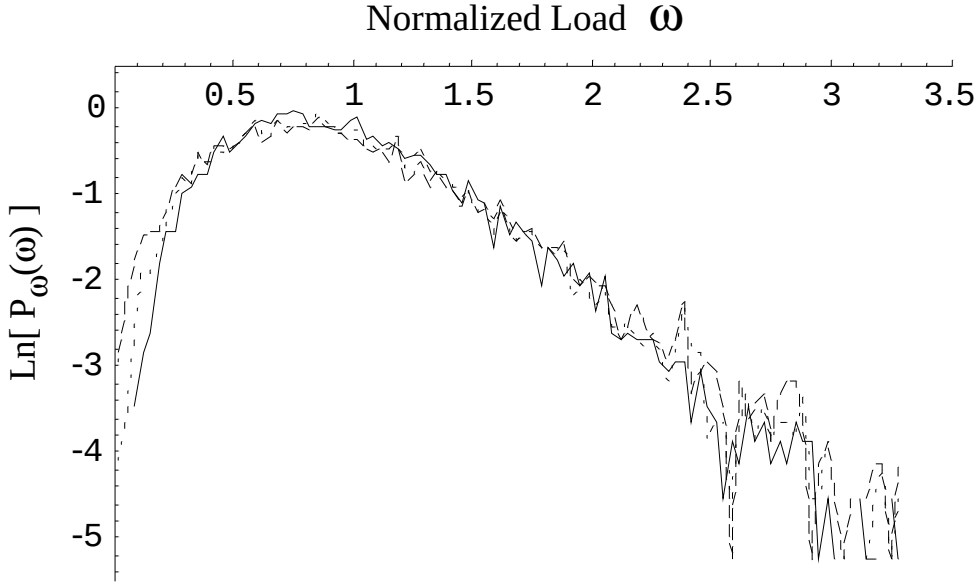


Figure 19: $P_w(w)$ in the $x$ or $y$ direction unrotated (solid line), rotated $\pi/6$ radians (dotted line), and $\pi/4$ radians (dashed line).

distributions have an exponential tail and a peak near $w \approx 1$. The near similarity of the rotated plots indicates approximate rotational symmetry for this nearly isotropic model, despite its quartered fabric. The variation in the region of weak loads is the result of that quartering. In the unrotated axes, wherein the grains have exactly two contacts on each hemisphere, we find $P_w(w) \to 0$ as $w \to 0$ in agreement with the $q$ model. We may fit $P_w(w)$ in these unrotated axes to an exponential with a power law prefactor,

$$P_w\left(w_x\right) = \left(\frac{w_x}{\langle w_x \rangle}\right)^{\alpha} e^{-\beta w_x / \langle w_x \rangle}. \tag{72}$$

If the distribution of $F_x$ had been purely exponential and if there had been no correlation between adjacent values of $F_x$ on the same grain, then this should have had values of $\alpha = 1.0$, $\beta = 2.0$, and $\langle w_x \rangle = 2 \langle F_x \rangle$ as in the uniform $q$ model. We do find an excellent fit over the entire curve using this form, and we do find that $\langle w_x \rangle = 2 \langle F_x \rangle$, but the fit is obtained with the values $\alpha = 3$ and $\beta = 4$.

By comparison, when the Cartesian axes are rotated the grains in this model may have 1, 2 or 3 contacts on the sampled hemisphere instead of the strict 2 contacts per

hemisphere (1 contact per quadrant) that was defined for the unrotated axes. The $P_w(w)$ for these rotated axes are also shown in Figure (19). They begin with a *finite* probability density for zero force instead of beginning at zero, and the finite value is maximized when the rotation is $\pi/4$ radians because this is where we obtain the maximum fraction of grains having something other than 2 contacts on the hemisphere. It was found in numerical simulations [40, 38] that when the grains in the bulk are segregated into separate populations having one, two, or three contacts on one side of the grain, respectively, then the Cartesian weight on the grains which support two or three others has a $P_w(w)$ which does go to zero probability for $w \to 0$. It is the population which supports only one contact which has a nonzero $P_w(w)$ because the load in that case is closely related to $P_f(f)$, which itself is nonzero at zero force. Thus, the MSTE results are in agreement with this aspect of the simulation data, as well.

### *5.1.5 Shear Ratios and Grain Pressures*

The distribution shear ratios $s$ and grain pressures $t$ resulting from the transport method are fit excellently by

$$P_{st}(s,t) = A\cos\left(\frac{\pi}{2}s\right)\left(\frac{t}{\langle t\rangle}\right)^4 e^{-5t/\langle t\rangle}e^{-8s^2}. \tag{73}$$

Thus, by comparing Equations (53) and (50) with $\lambda_x = \lambda_y = 0$, the structure factor can be identified,

$$\overline{\Upsilon}_{st}(s,t) = \cos\left(\frac{\pi}{2}s\right)\left(\frac{t}{\langle t\rangle}\right)^4 e^{-5t/\langle t\rangle} \triangleq \overline{\Upsilon}_s(s)\ \overline{\Upsilon}_t(t). \tag{74}$$

$\overline{\Upsilon}_t$ and $\overline{\Upsilon}_s$ resulting from the transport method are shown in Figure (5.1.5) with smooth curves from Equation (74). These are normalized by $\langle w_x\rangle = \langle w_y\rangle = \langle t\rangle = 1$.

From Equation 73 we may note that

$$P_{st}(s,t) = P_s(s)P_t(t), \tag{75}$$

which implies that the grain pressure $t$ and shear ratio $s$ are statistically independent

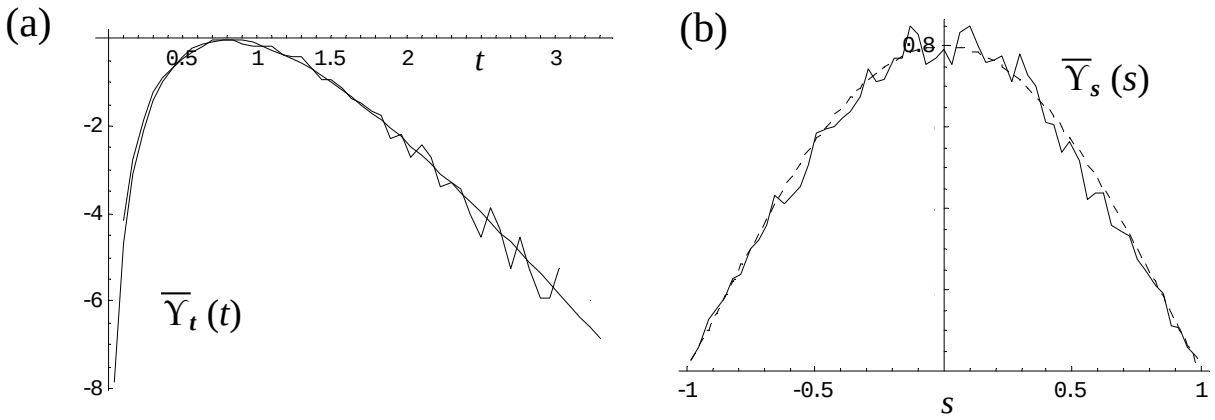


Figure 20: Structure factor from the MSTM: (Left) semi logarithmic $\Upsilon_t(t)$, (Right) $\Upsilon_s(s)$.

in the DOS, at least to MSA accuracy. If true, this is an important finding because it indicates a simplicity in the form of the DOS.

### 5.2 Empirical Test of the MSA

The numerical solution of the MSTE helps validate the usefulness of the MSA in three ways.

First, the results produced by the MSA appear to be in excellent agreement with the empirical data available in the published literature. This will be explored in more detail in the next chapter presenting the results of a focused empirical test of the theory.

Second, two different sampling schemes were implemented as presented in Equations (61) and (63). The results for $P_f(f)$ were identical to within the statistical precision of the data, as shown in Figure (21). Note that for clarity each curve shown is actually a functional fit to the numerical solution of the corresponding case and not the actual, noisy data. Each curve fit was obtained without comparison to the other until after both had been finalized. The resulting close similarity shows that the distributions are insensitive to the existence or nonexistence of correlations between the Cartesian loads and the contact angles, and this is the essence of the MSA.

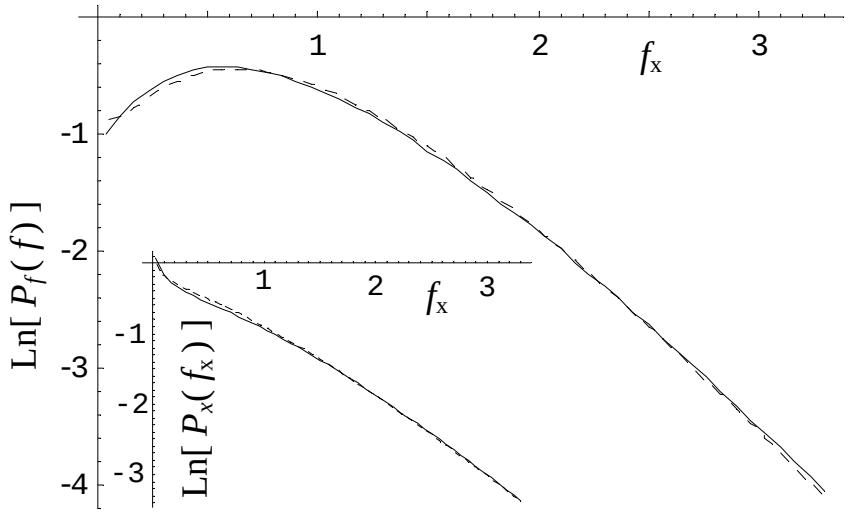


Figure 21: $P_f(f)$ (large plot) and $P_x(f_x)$ (inset) resulting from the MSTM in two different sampling methods.

Third, the values of $\Upsilon$ have been calculated according to Equation (19). The conditional distribution $P_\Upsilon(\Upsilon \mid s,t)$ was calculated for various fixed values of $s$ and $t$ and these are presented in Figure (22) for $s = 0$ and $s = 0.6$ with several values of $t$. For some values of $s$ and $t$, the ratio $\Upsilon^{(\max)}/\overline{\Upsilon}$ is as high as 3 (or greater) and $\Upsilon^{(\min)}/\overline{\Upsilon}$ is as small as 1/3 (or lower). This means that some grain configurations $\{s_i, t_i, \theta_{ij}\}$ will occur three times too often or only 1/3 often enough in the MSA ensemble compared to the exact Edwards ensemble. This effect is most pronounced when $t$ is high and $s$ is low. However, high values of $t$ are rare to begin with. Furthermore, the distribution for each pair of values $(s,t)$ is localized with a clear peak and so the majority of grain configurations will have a value of $\Upsilon$ that is *relatively* not very far from $\overline{\Upsilon}$ while being distinctly separate from the $\overline{\Upsilon}$ for other values of $(s,t)$. These latter considerations imply that the MSA does characterize the organization in the DOS qualitatively, but more effort is needed to show whether it is quantitatively sufficient.

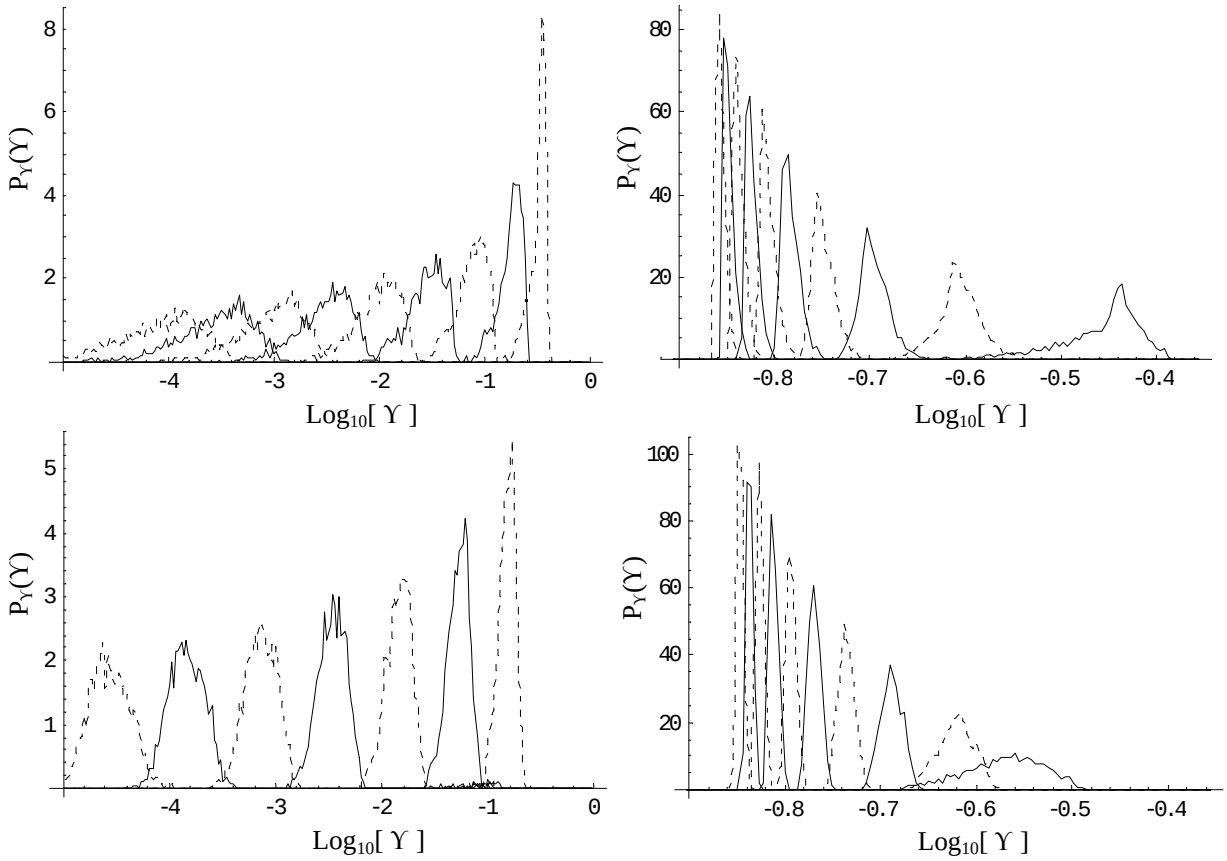


Top Left, s=0. From left to right, t=10 (dashed), 9 (solid), 8 (dashed), 7 (solid), 6 (dashed), 5 (solid), 4 (dashed), 3 (solid), and 2 (dashed).

Top Right, s=0. From left to right, t=1/10 (dashed), 1/9 (solid), 1/8 (dashed), 1/7 (solid), 1/6 (dashed), 1/5 (solid), 1/4 (dashed), 1/3 (solid), 1/2 (dashed), and 1 (solid).

Bottom Left, s=0.6. From left to right, t=8 (dashed), 7 (solid), 6 (dashed), 5 (solid), 4 (dashed), 3 (solid), and 2 (dashed).

Bottom Right, s=0.6. From left to right, t=1/10 (dashed), 1/9 (solid), 1/8 (dashed), 1/7 (solid), 1/6 (dashed), 1/5 (solid), 1/4 (dashed), 1/3 (solid), 1/2 (dashed), and 1 (solid).

Figure 22: Distribution of values of $\Upsilon(s,t,\theta_j)$ for fixed value of $s$ and several fixed values of $t$.

## 5.3 Summary of Predictions

Although the numerical solution of the MSTE compared well with the empirically-fitted form of $P_f(f)$ from the carbon paper experiments [9], that did not provide a good test of the theory since that form was obtained in cases with gravity, friction, and measurements taken exclusively along the container boundary. At the time that the MSTE was first solved, no other functional forms were available in the published literature for an accurate comparison. The next chapter will present the results of new data obtained specifically to test the predictions of the MSTE.

The following predictions of the MSTE will be tested in the next chapter: $P_f(f)$, $P_x(f_x)$, $P_s(s)$, $P_t(t)$, and the statistical independence between the $s$ and $t$ state variables. It should be noted that the predicted distributions have no free parameters; all parameters such as the decay constants are predicted by the theory and therefore the distributions cannot be adjusted *ad hoc* to make them fit the empirical data.

# CHAPTER 6

# EMPIRICAL TEST OF THE THEORY

To compare the theory with empirical data, the software code that numerically solves the MSTE in MATHEMATICA was converted to Fortran code to gain greater efficiency and produce smoother data sets. A fully converged data set of 10 billion grains was obtained and analyzed in just a few hours of processing time on a desktop computer. For the remainder of this chapter, "the theory" refers to this solution. The theory shall be compared to an empirical data set produced by numerical simulation, which solves the dynamics explicitly for a single packing.

## 6.1 Discrete Element Modeling as a Test of the Theory

Discrete element modeling (DEM) simulations [52] were performed for two-dimensional, packings of 17,000 grains. The software used for this was PFC2D, or Particle Flow Code in Two Dimensions [53]. A portion of a typical DEM packing in PFC2D is shown in Figure 1. Pains were taken to mimic the idealizations of this theory as far as practically achievable. This is the key difference between the DEM results presented here and the simulation results presented elsewhere by others and the reason why this modeling was needed. These efforts, as well as the remaining differences between the DEM and theory, are described below.

First, the isotropic case in fabric and stress is achieved by randomly placing the grains into a square test cell without gravity and then slowly rescaling all of the grain diameters simultaneously until the packing jams. During that rescaling process the grains shove each other around and Newton's laws govern the dynamics grain-by-grain until the packing settles into a metastable state.

Second, the grain properties were idealized. Obviously these grains were selected to be

round and frictionless to match the theory. However, it is not possible in DEM to model perfect rigidity of these grains; there must be an overlap of grains at the contact points (a microscopic strain) to decide the magnitude of the repulsive force between neighbors. A linear spring contact law was selected for this purpose, although technically the form of the law (linear spring versus Herzian, and so on) is immaterial. That is because, as argued in Chapter 2, the isostatic contact force network becomes insensitive to the form of the contact law (or work function) in the limit of vanishing strains. Varying the value of the spring constant also has no effect in the same limit other than to trivially rescale all the forces in the packing. The relevant parameter in this limit is the purely geometric packing fraction. By simultaneously rescaling the diameters of all the grains slightly larger or smaller as required, the packing fraction was fine-tuned just to the point of jamming/unjamming, staying slightly jammed but with minimal overlap of the contacts to mimic perfect grain rigidity as closely as possible.

Third, the theory had been simplified by ignoring the packings' boundaries, working in the bulk in the thermodynamic limit. This is actually an important feature of realism in the theory and has great value toward eventually predicting realistic macroscopic behaviors of packings in nature. This is because real packings in nature contain a vastly larger number of grains than is accommodated in most physics experiments and simulations. Hence, the effects of a boundary are vastly de-emphasized in nature's statistics relative to the empirical data sets that are small and include the boundary. To similarly de-emphasize boundary effects in the DEM data, grains near the container walls were discarded from the statistical analysis. It was discovered that failing to do so significantly skews the statistics. The boundary layer was chosen somewhat arbitrarily to be four grain diameters in width along each wall. This was based on the insight developed elsewhere [54] that geometric memory of the boundary vanishes at about four grain diameters distance for 3D packings. The assumptions here are that 2D packings lose geometric correlation at roughly the same distance, and that $P_f(f)$ loses memory of

the boundary at about the same distance as the geometry. Future studies should do a more careful analysis to quantify the evolution of $P_f(f)$ moving from the boundary to the bulk.

A place where the analysis differs from the DEM is the idea that a frictionless packing may be simultaneously monodisperse (all grain diameters identical) and amorphous (not crystalline). Although this is geometrically possible, it does not typically occur in dynamic simulations of round, frictionless grains because they tend to crystallize very easily. The grains tend to slide until they form three-grain triangles that are very stable, and these triangles then accumulate into a widespread, hexagonal lattice with just a few defect boundaries percolating across the packing. This crystallization can be prevented a number of ways. The most effective is to give the grains a dispersity of diameters. In the present work the simulated packing's grains were distributed between 1.0 and 1.5 units of diameter. This makes the simulation more disordered and more like the sandpiles of nature in contrast to a monodisperse idealization. However, the monodispersity of the theory in Chapter 3 is not expected to have much of a deleterious effect. Even if polydispersity had been used in the theory it would not have explicitly affected the equations anywhere. It does affect the number of grains per volume, which helps set the scale of the stress tensor, but nowhere was that tensor used explicitly. Also, polydispersity would be evident in $P_{4\theta}$ because then steric exclusion should have been blurred over some range of angles rather than discretely fixed at $\pi/3$ radians. The effect of this is truly minor and we freely choose to ignore it for the sake of simplicity. Finally, larger grains should have a slightly larger average number of contacts $\langle Z \rangle$ than smaller grains, so we should expect some statistical effect in the contact force network due to this. However, the theory already makes a more sweeping simplification in $Z$ than the effects of monodispersity, as it assigns every grain the constant $Z = 4$. The author does not expect monodispersity versus polydispersity to have much of an effect by comparison to this.

The theory's assumption of $Z = 4$ for every grain will have a significant effect on the

DOS. This assumption cannot really be justified from first principles but was adopted only to make the theory solvable. In contrast, dynamic simulations of two dimensional, frictionless packings develop three major populations of grains having $Z = 3$, $Z = 4$, and $Z = 5$, respectively. Nevertheless, the theory will be very clearly validated in the next section, and the contrast of the three $Z$ populations will serve to produce significant, new insights into the nature of granular packings. Those insights will be very helpful as we generalize $Z$ in future versions of the theory.

Finally, the ideal is that all rattlers—grains that are not locally jammed but are free to rattle around within their local cage of neighboring grains—will be identified and removed from the data set because their contact forces are dynamic and transitory, not representative of the statistical mechanics of a static packing. In practice removing the rattlers is difficult. The simple method adopted here was to exclude grains having two or fewer contacts, since those grains cannot be among the stable ones in the absence of friction.

## 6.2 Modeling Results Compared to the Ensemble Theory

Figure 23 shows $P_f(f)$ obtained from the theory and from the DEM data including all grains having $Z > 2$. The agreement is even better when only $Z = 4$ grains are included as shown in Figure 24. These are in such remarkable agreement that we may claim that the theory's prediction is proven correct. Figure 25 shows $P_x(f_x)$ obtained from the theory and from the DEM data including all grains having $Z > 2$. Figure 26 shows the comparison for the $Z = 4$ population of the DEM. Again, the prediction has been proven correct. The form of $P_x(f_x)$ shows the two knees that are characteristic of modified Bessel functions of the second kind. In the isotropic case $P_f(f)$ can be analytically derived from $P_x(f_x)$ using Youngquist's transform [43], and the functional form that results when $P_x(f_x)$ is composed of modified Bessel functions of the second kind is an exponential with a polynomial prefactor as discussed in Section 5.1.0.3. This provides additional

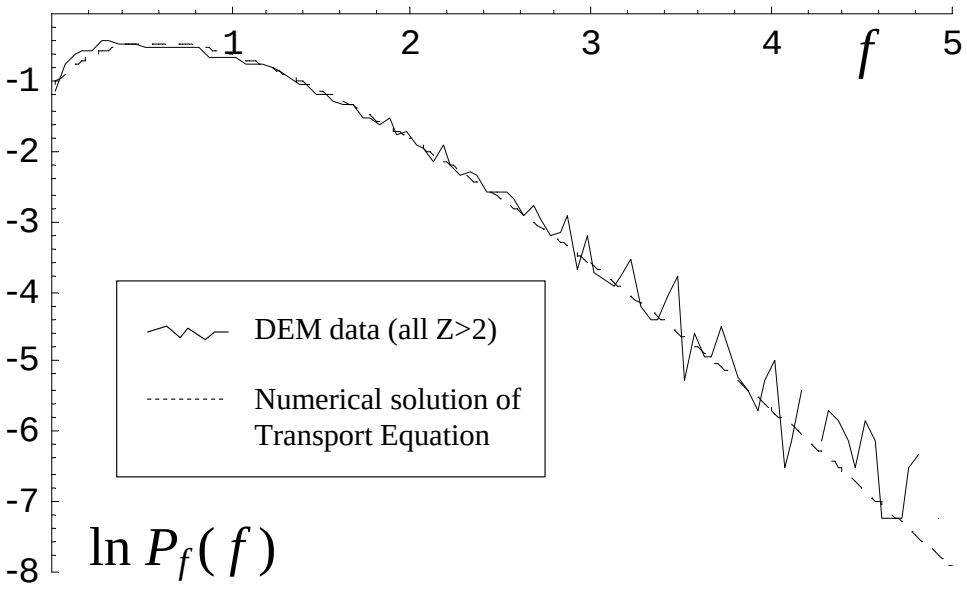


Figure 23: Semi logarithmic $P_f(f)$ obtained in numerical solution of the transport equation and from DEM data, all $Z > 2$.

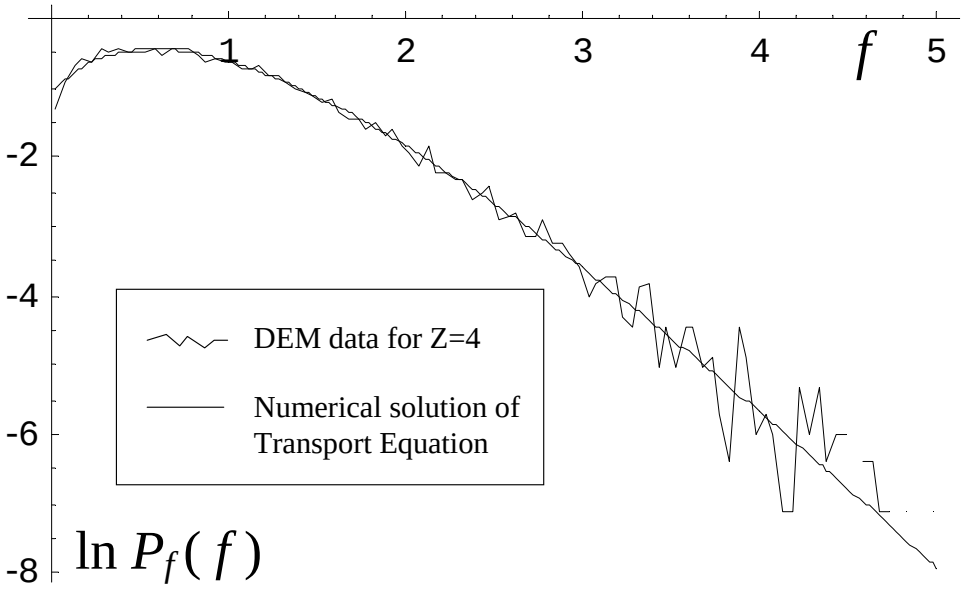


Figure 24: Semi logarithmic $P_f(f)$ obtained in numerical solution of the transport equation and from $Z = 4$ population of DEM.

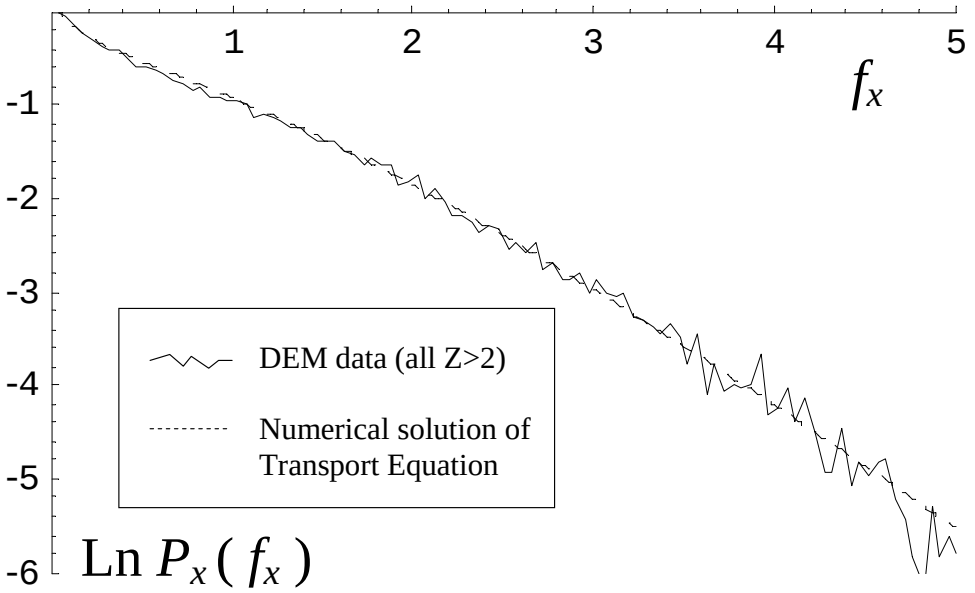


Figure 25: Semi logarithmic $P_x(f_x)$ obtained in numerical solution of the transport equation and from DEM data, all $Z > 2$.

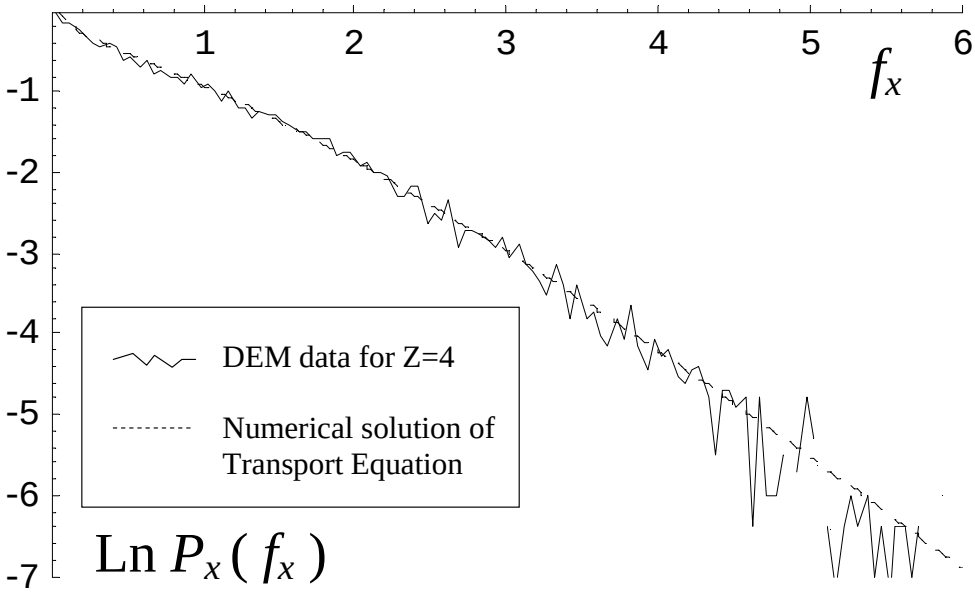


Figure 26: Semi logarithmic $P_x(f_x)$ obtained in numerical solution of the transport equation and from $Z = 4$ population of DEM data.

evidence that the tail really is asymptotically exponential.

The DOS parameters $s$ and $t$ have been examined for statistical independence and it appears that they are not independent. However, the grains in the DEM have been sorted into separate populations by $Z$ so that,

$$P_{st}(s,t) = \sum_{Z=3}^{5} n_Z P_{st}^{(Z)}(s,t) \tag{76}$$

where $n_Z$ is the fraction of grains within each $Z$ population and $P_{st}^{(Z)}(s,t)$ is the distribution of each population taken separately. Then, we find that the $s$ and $t$ parameters are statistically independent within each population considered separately,

$$P_{st}^{(Z)}(s,t) = P_s^{(Z)}(s) P_t^{(Z)}(t) \tag{77}$$

for each value of $Z$. This implies that the DOS has a remarkably simplistic form, which was unexpected in view of the disorder apparent in Figure 1.

Figure 27 compares the distribution of the shear ratio $P_s(s)$ from the theory's prediction and the DEM data. The agreement is quite good, even without sorting by $Z$. Since the theory assumed $Z = 4$ we wish to test whether the other $Z$ populations fit the same form. For comparison we use the functional form that was fitted to the MSTE solution,

$$P_s(s) = \cos(\pi s/2)\, e^{-8s^2}. \tag{78}$$

Remarkably, we find that the same form fits all three populations reasonably well after we make one parameter change,

$$P_s(s) = \cos(\pi s/2)\, e^{-s^2/2\sigma^2} \tag{79}$$

where the standard deviation $\sigma = 1/Z$. This form compared to all three $Z$ populations is shown in Figure 28. The fit is increasingly better with increasing $Z$, probably because Newton's second and third laws are less coupled when there are more contacts.

For the conditions of isotropy reflected in these distributions, $P_s(s)$ emphasizes the values of $s$ close to zero and de-emphasizes the values of $s$ near the positive and negative extremes. On the other hand, we can see by the definition of $s$ in Equation 49

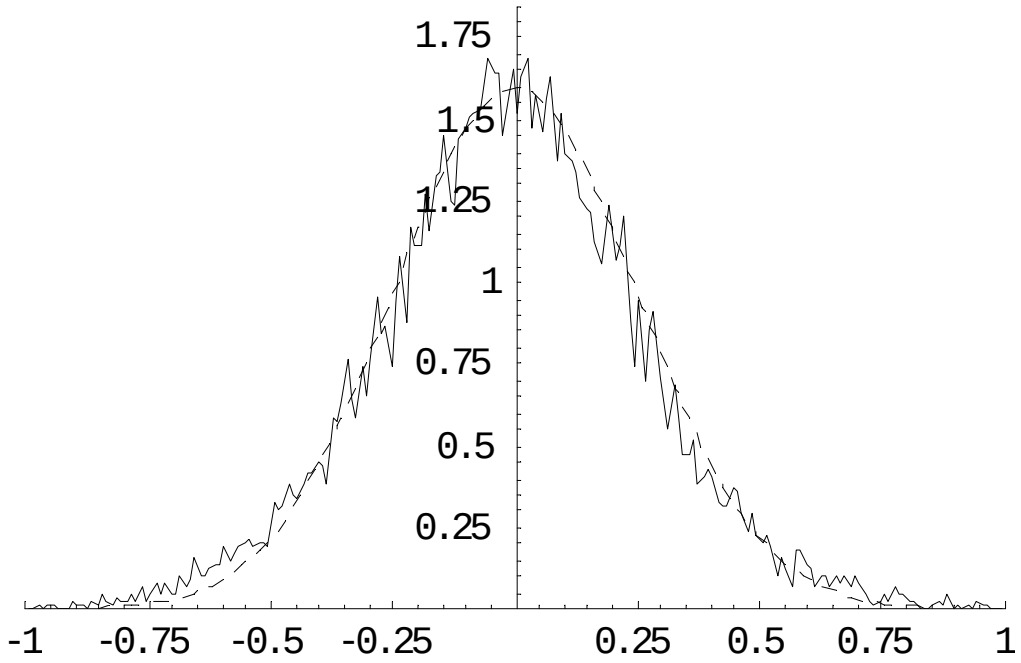


Figure 27: $P_s(s)$ obtained in numerical solution of the transport equation and from DEM data including all grains having $Z > 2$.

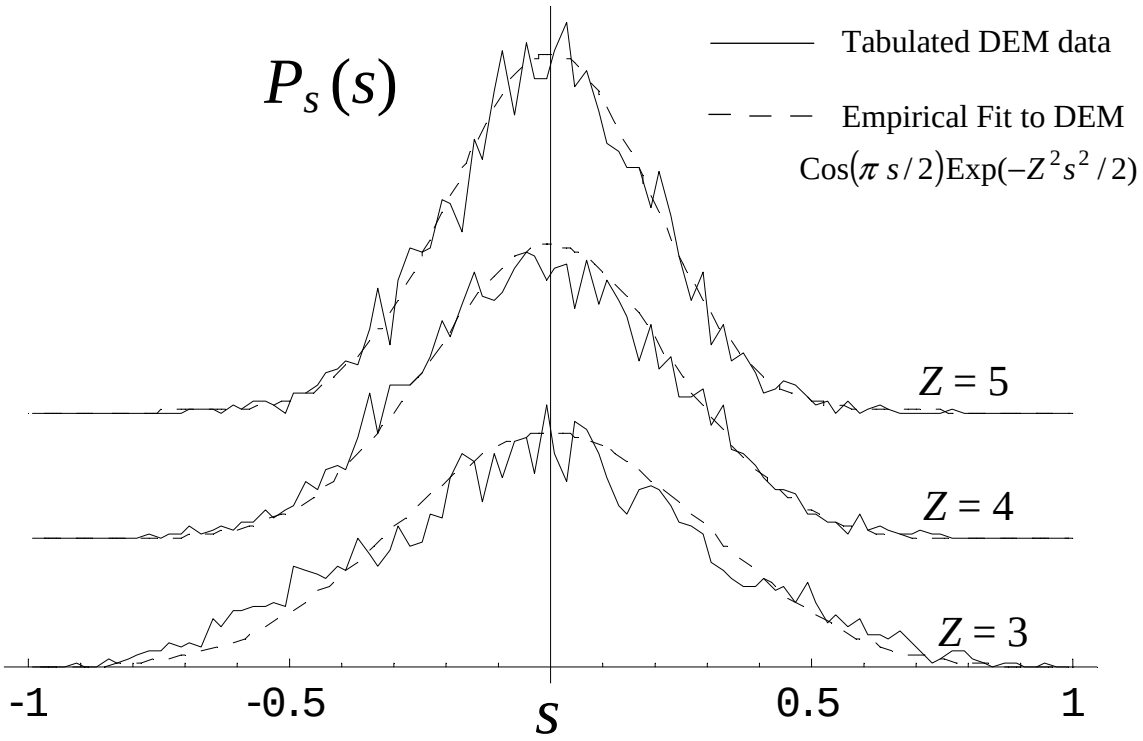


Figure 28: $P_s(s)$ in DEM data segregated by $Z$.

that packings with anisotropic stress tensors $W_x \neq W_y$ must have a form of $P_s(s)$ that emphasizes one of the two extremes, either emphasizing positive $s$ when $W_x > W_y$ or negative $s$ when $W_x < W_y$. Remembering this as we review $C(f \mid s,t)$ in Figure 13, we see that the DOS discriminates against weak values of $f$ under conditions of isotropy when $s$ is predominantly midrange, but the DOS increases the occurrences of weak $f$ for anisotropic conditions. Hence, we see the reason for the rise in $P_f(f)$ to a peak when the packing is isotropic, and the reason why $P_f(f)$ evolves to larger values of $P_f(0)$ and a monotonically decreasing form when the packing becomes anisotropic. The simplistic argument in Chapter 2 showed that this behavior is the result Newton's second law in the absence of tensile forces injecting a bias against weak forces. The more general results produced through solving the transport equation have now shown that Newton's second law produces the grain factor, and it is this grain factor that controls these behaviors. This does not produce any clearer insight than what Chapter 2 had provided, but it shows that the argument in Chapter 2 and the more general solution are in substantial agreement.

Examining the distribution of grain pressures, $P_t(t)$, Figure 29 compares the $Z = 4$ population of the DEM with the theory's prediction. Figure 30 makes the same comparison semi logarithmically. These demonstrate good agreement. However, the DEM data with all $Z$ populations included does not match the theory's predictions very well due to the presence of the $Z = 3$ and $Z = 5$ grains. Nevertheless, as was done for $P_s(s)$, an interesting comparison can be made between all these populations by finding a functional fit and parameterizing it in terms of $Z$. A function that fits the theory's prediction reasonably well over the region of experimental interest ($0 \leq t \lesssim 3$), is

$$P_t(t) = t^{\beta-1}e^{-\beta t} \tag{80}$$

with $\beta = 5$. After segregating the DEM data by $Z$ we find that all three populations do fit this same form as shown in Figures 31 and 32, but using $\beta = 2Z - 4$. The origin of

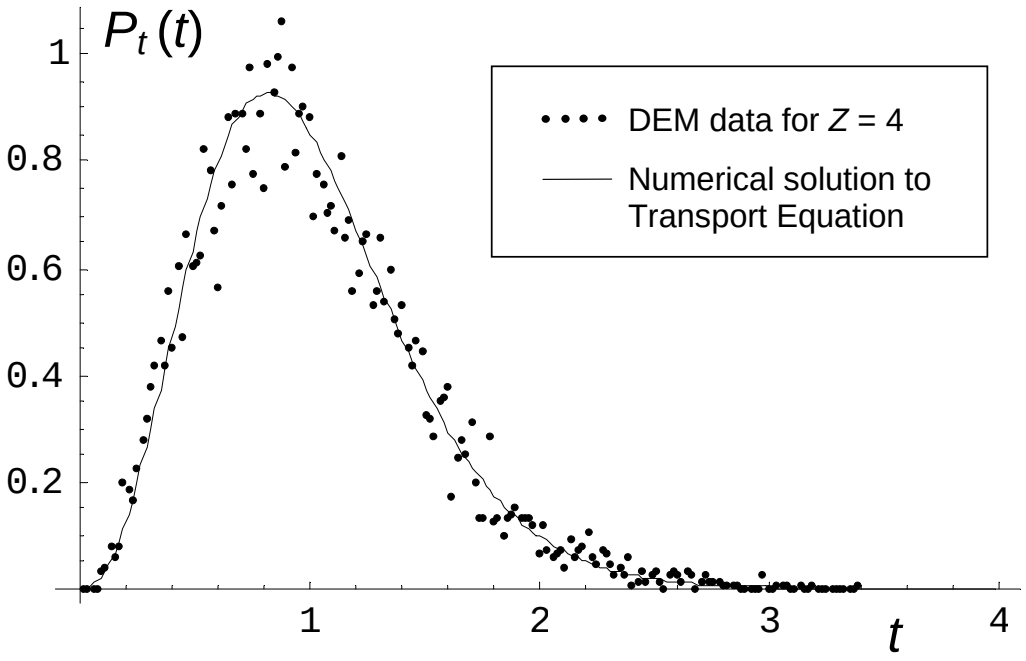


Figure 29: $P_t(t)$ obtained from numerical solution of the transport equation and from DEM data including only grains having $Z = 4$.

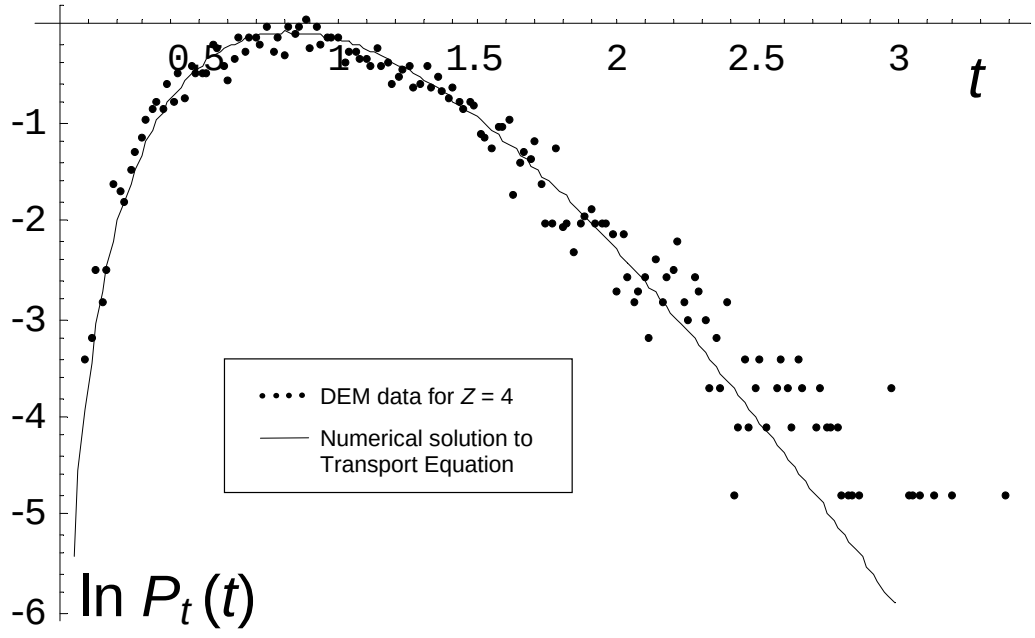


Figure 30: Semi logarithmic comparison of $P_t(t)$ obtained from numerical solution of the transport equation and from DEM data including only grains having $Z = 4$.

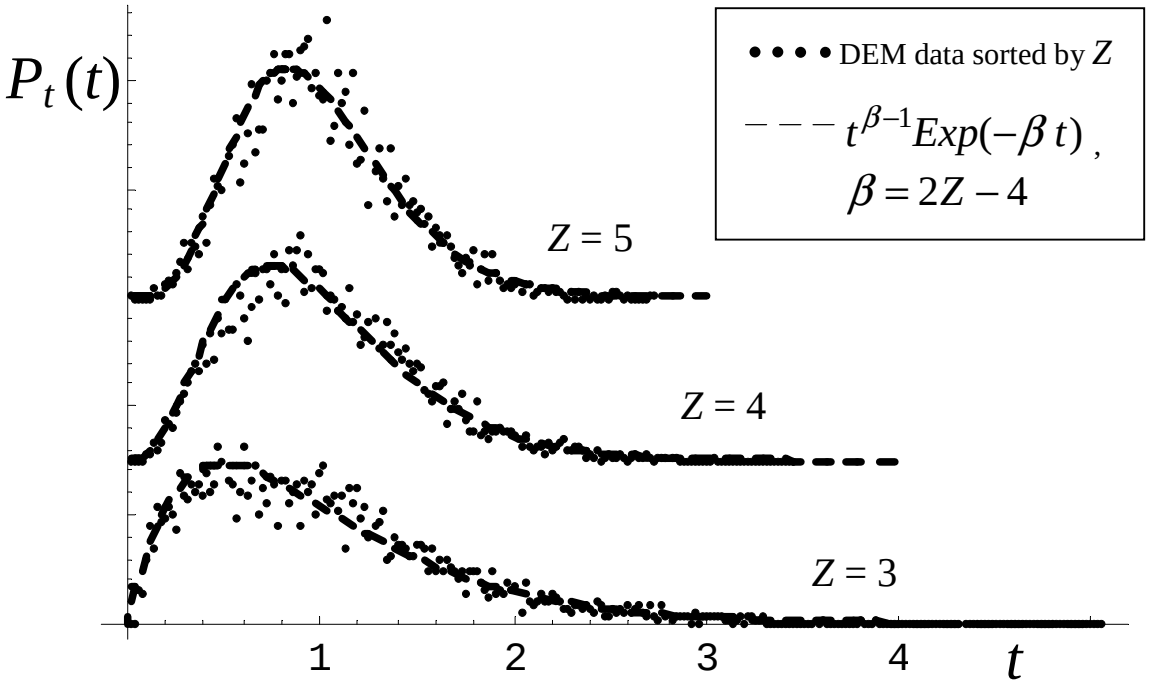


Figure 31: $P_t(t)$ in the DEM, segregated by $Z$.

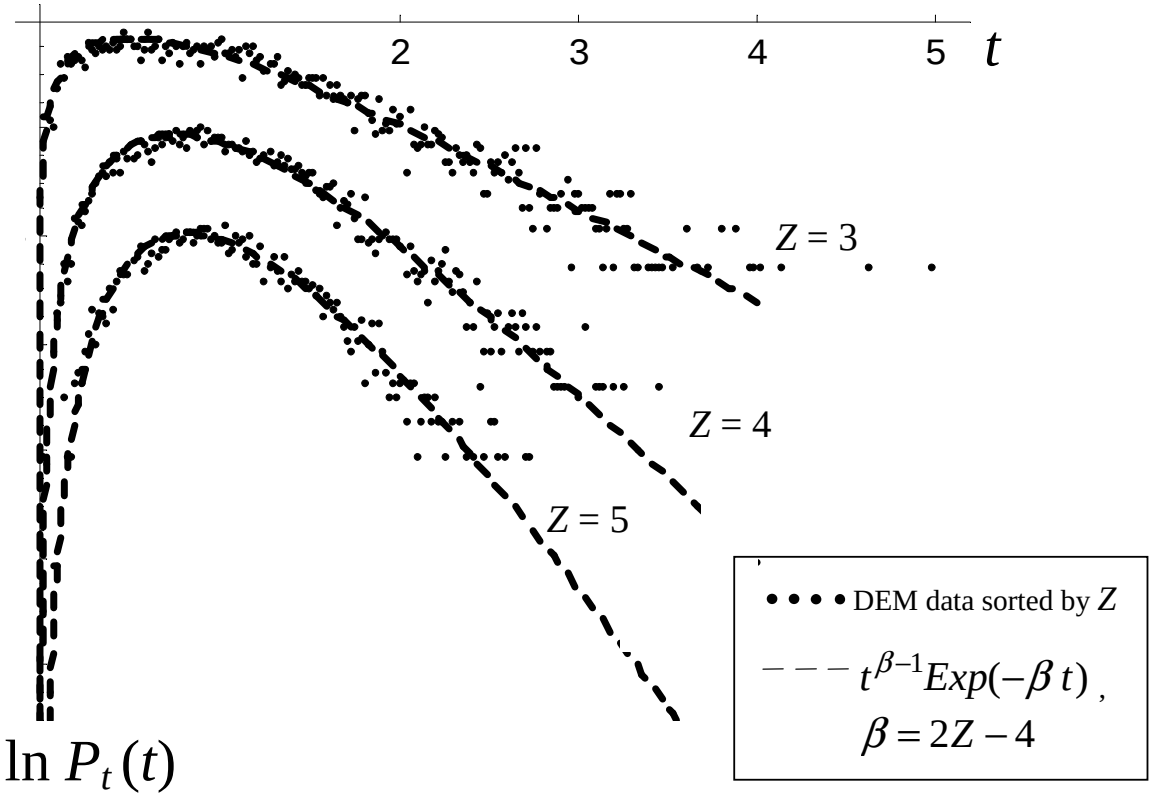


Figure 32: Semi logarithmic $P_t(t)$ in the DEM, segregated by $Z$.

this form for $\beta$ is not known. Neither is it known why $\beta = 5$ in the theory but $\beta = 4$ for the $Z = 4$ case in the DEM data. Surprisingly the decay constants of the tails in $P_f(f)$ and $P_x(f_x)$ are in perfect agreement between theory and DEM, and these are scaled by the decay constant in the tail in $t$. So whatever the origin of $\beta$ may be it appears that the theory is correct insofar as the fixed $Z = 4$ approximation is concerned, but it needs to be generalized to allow for the interactions of all three $Z$ populations. It is clear that the theory has incorporated all of the correct physics because it has predicted the basic form of $P_t(t)$ over the region of experimental interest not only for the $Z = 4$ population but for all three populations such that a simple parameter change is able to fit them all.

Equation 80 is very interesting. This is the distribution that would result if $t$ were composed of a sum of distinct contributions

$$t = \sum_{i=1}^{\beta} \tau_i \tag{81}$$

where the $\tau_i$ are statistically independent and canonical. It is tempting to assume that each $\tau_i$ is associated with one of the grain's contact forces. However, $\beta \neq Z$ in general, and so the number of contacts on each grain does not equal the number of contributions to its grain pressure. On the other hand, $\langle\beta\rangle = \langle Z\rangle$ if and only if $\langle Z\rangle = 4$, which happens to be correct since the packing is isostatic. Thus, is seems that these putative canonical variables are associated with the contacts in the packing, but not locally in the number of contacts around each grain. This is reminiscent of the eigenmodes of vibration in a mass-spring network, where the number of eigenmodes is equal to the number of springs, but the eigenmodes are not locally correlated to the individual springs. It seems to the author that these features of the DOS are too elegant to be coincidental and hence they are suggestive of the existence of some basis change that will produce a canonical picture in $\tau_i$.

# CHAPTER 7

## SUMMARY AND CONCLUSIONS

Beginning with Edwards' flat measure in $\{\zeta_i\}$ and Edwards' probability functional for contact forces $\{\vec{f}^{\alpha}\}$, a transport equation was derived that can be solved numerically to predict the density of single grain states in idealized granular packings. This transport equation was simplified by decoupling Newton's second and third laws in the *Mean Structure Approximation* (MSA). The simplified transport equation, or *Mean Structure Transport Equation* (MSTE) was then solved and this produced a predicted density of single grain states along with all the associated distributions including $P_f(f)$. The predictions of the theory were compared with discrete element modeling (DEM) of a static granular packing. The DEM was carefully formulated to allow an idealized comparison with the theory. This produced $P_f(f)$ and $P_x(f_x)$ that were in outstanding agreement with the theory. Although the theory was based upon $Z = 4$ for every grain in the packing, the predicted the forms for $P_s(s)$ and $P_t(t)$ were found to be correct not only for the $Z = 4$ grains, but also for the other $Z$ populations as well (over the range of experimental interest) when only a simple parameter change was implemented based on $Z$. Furthermore, the transport equation predicted statistical independence between $s$ and $t$, and when the grains were sorted into separate $Z$ populations the $s$ and $t$ data were found to be statistically independent for each $Z$ considered separately. The DOS can therefore be written to good approximation in the following simple form,

$$\rho_g(s,t,\theta_\beta) \;=\; \cos(\pi s/2)\sum_{Z=3}^{5} n_Z t^{2Z-5} e^{-(2Z-4)t-Z^2s^2/2}\; G(\theta_\beta)\;\prod_{\gamma=1}^{4}\Theta\left[f_\gamma(\cdot)\right] \qquad (82)$$

where the only parameters to be provided empirically are the $n_Z$.

In solving the theory several features in the DOS were identified with the physics that produce them. It was Newton's second law that produced the Grain Factor $\overline{\Psi}$,

while Newton's third law produced the Structure Factor $\overline{\Upsilon}$. The relatively weak coupling between Newton's second and third laws in the correlations of the forces render these factors separable to good approximation. The rising slope in $P_f(f)$ in the region of weak forces is due to a bias against weak forces that exists in an isotropic packing.

These results have shown that Edwards' flat measure is sufficient to produce the correct distribution of forces in granular packings. Therefore, Edwards' hypothesis has passed another, significant test demonstrating that it may be the correct starting point for a complete theory of granular mechanics. Furthermore, this work uncovered an elegant, underlying pattern in the form of the DOS. Although granular materials are "messy" and disordered, they demonstrate the same type of statistical simplicity that is found in the typical ergodic systems of thermal statistical mechanics. This important result contributes to the increasing body of evidence that statistical mechanics will ultimately be successful in explaining granular materials.

## REFERENCES


[1] * P.T. Metzger, Phys. Rev. E **69**, 053301 (2004) [4].

[2] * P.T. Metzger, Phys. Rev. E **70**, 051303 (2004) [4].

[3] * P.T. Metzger and C.M. Donahue, to appear in Phys. Rev. Lett. (2005) [4].

[4] The three items marked by asterisks (*), above, form the basis of this dissertation. The remaining items, below, are works by others that provide the background and the supporting data for the present work.

[5] T. Halsely and A. Mehta, eds. *Challenges in Granular Physics*, (World Scientific, New Jersey, 2002).

[6] G. Ristow, *Pattern Formation in Granular Materials*, Springer Tracts in Modern Physics **164** (Springer, New York, 2000).

[7] J.P. Bouchaud, in *Slow Relaxations and Nonequilibrium Dynamics in Condensed Matter, Les Houches Session LXXVII*, edited by J.-L. Barrat, M.V. Feigelman, J. Kurchan, and J. Dalibard, NATO ASI Series (Springer Verlag, New York, 2003), pp. 141-2.

[8] J.H. Prevost R. Popescu, Electronic Journal of Geotechnical Engineering **1**, http://www.ejge.com (1996).

[9] D.M. Mueth, H.M. Jaeger, and S.R. Nagel, Phys. Rev. E **57**, 3164 (1998); D.L. Blair, N.W. Mueggenburg, A.H. Marshall, H.M. Jaeger, and S. R. Nagel, Phys. Rev. E **63**, 041304 (2001).

[10] D.W. Howell, R.P. Behringer, and C.T. Veje, Chaos **9**,559 (1999).

[11] F. Radjai, D.E. Wolf, M. Jean, and J.-J. Moreau, Phys. Rev. Lett. **80**, 61 (1998); F. Radjai and D.E. Wolf, Gran. Mat. **1**, 3 (1998).

[12] A.J. Liu and S.R. Nagel, Nature **396**, 21 (1998); M.E. Cates, J.P. Wittmer, J.-P. Bouchaud, and P. Claudin, Chaos **9**, 511 (1999).

[13] C.S. O'Hern, L.E. Silbert, A.J. Liu, and S.R. Nagel, Phys. Rev. E **68**, 011306 (2003).

[14] M.E. Cates, J.P. Wittmer, J.-P. Bouchaud, and P. Claudin, Phys. Rev. Lett. **81**, 1841 (1998).

[15] S.F. Edwards and R.B.S. Oakeshott, Physica A **157**, 1080 (1989).

[16] L. Rothenburg and A.P.S. Selvadurai in *Mechanics of Structured Media*, edited by A.P.S. Selvadurai (Elsevier Scientific, New York, 1981), p.469.

[17] K. Bagi, in *Powders & Grains 97*, edited by Behringer and Jenkins (Balkema, Rotterdam, 1997), pp. 251-54; K. Bagi, Gran. Mat. **5**, 45 (2003).

[18] N.P. Kruyt, L. Rothenburg, Int. J. Solids Struct. **39**, 571 (2002); N.P. Kruyt, Int. J. Solids Struct. **40**, 3537 (2003).

[19] A.H.W. Ngan, Phys. Rev. E **68**, 011301 (2003).

[20] S.F. Edwards and D.V. Grinev, Gran. Mat. **4**, 147 (2003).

[21] J.M. Erikson, N.W. Mueggenburg, H.M. Jaeger, and S.R. Nagel, Phys. Rev. E **66**, 040301(R) (2002).

[22] O. Tsoungui, D. Vallet and J.-C. Charmet in *Physics of Dry Granular Media*, ed. by H.J. Herrman, J.-P. Hori, and S. Luding (Kluwer Academic, Boston, 1998), pp. 149–154.

[23] J. Brujić, S.F. Edwards, I. Hopkinson, and H.A. Makse, Physica A **327**, 201 (2003).

[24] J. Brujić, S.F. Edwards, D.V. Grinev, I. Hopkinson, D. Brujić, and H.A. Makse, Faraday Disc. **123**, 207 (2002).

[25] F. Radjai, M. Jean, J.-J. Moreau, and S. Roux, Phys. Rev. Lett. **77**, 274 (1996).

[26] F. Radjai, S. Roux, and J.-J. Moreau, Chaos **9**, 544 (1999).

[27] C.S. O'Hern, S.A. Langer, A.J. Liu, and S.R. Nagel, Phys. Rev. Lett. **86**, 111 (2001).

[28] S.J. Antony, Phys. Rev. E **63**, 011302 (2001).

[29] C. Thornton, Kona **15**, 81 (1997).

[30] L.E. Silbert, G.S. Grest, and J.W. Landry, Phys. Rev. E **66**, 061303 (2002).

[31] J.W. Landry, G.S. Grest, L.E. Silbert, and S.J. Plimpton, Phys. Rev. E **67**, 041303 (2003).

[32] C.S. O'Hern, S.A. Langer, A.J. Liu, and S.R. Nagel, Phys. Rev. Lett. **88**, 075507 (2002).

[33] H.A. Makse, D.L. Johnson, and L.M. Schwartz, Phys. Rev. Lett. **84**, 4160 (2000).

[34] J.H. Snoeijer, T.J.H. Vlugt, M. van Hecke, and W. van Saarloos, Phys. Rev. Lett. **92**, 054302 (2004).

[35] A.V. Tkachenko and T.A. Witten, Phys. Rev. E **60**, 687 (1999); L.E. Silbert, D. Ertaş, G.S. Grest, T.C. Halsey, and D. Levine, Phys. Rev. E **65**, 031304 (2002); A. Kasahara and H. Nakanishi, J. Phys. Soc. Jpn. **73**, 789 (2004).

[36] C.-h. Liu, S.R. Nagel, D.A. Schecter, S.N. Coppersmith, S. Majumdar, O. Narayan, and T.A. Witten, Science **269**, 513 (1995).

[37] S.N. Coppersmith, C.-h. Liu, S. Majumdar, O. Narayan, and T.A. Witten, Phys. Rev. E **53**, 4673 (1996).

[38] J.H. Snoeijer, M. van Hecke, E. Somfai, and W. van Saarloos, Phys. Rev. E **70**, 011301 (2004).

[39] C. Eloy and E. Clément, J. Phys. I (France) **7**, 1541 (1997); E.B. Pitman, Phys. Rev. E **57**, 3170 (1998); M. Nicodemi, Phys. Rev. Lett. **80**, 1340 (1998); J.E.S. Socolar, Phys. Rev. E **57**, 3204 (1998); M.L. Nguyen and S.N. Coppersmith, Phys. Rev. E **59**, 5870 (1999); M.G. Sexton, J.E.S. Socolar, D.G. Schaeffer, Phys. Rev. E **60**, 1999 (1999); M.L. Nguyen and S.N. Coppersmith, Phys. Rev. E **62**, 5248 (2000); O. Narayan, Phys. Rev. E **63**, 010301 (2000); T. Aste, T. Di Matteo, and E.G. d'Agliano, J. Phys. Cond. Mat. **14**, 2391 (2002).

[40] J.H. Snoeijer, M. van Hecke, E. Somfai, and W. van Saarloos, Phys. Rev. E **67**, 030302(R) (2003).

[41] J.H. Snoeijer, T.J.H. Vlugt, W.G. Ellenbroek, M. van Hecke, J.M.J. van Leeuwen, Phys. Rev. E **70**, 061306 (2004).

[42] A.V. Tkachenko and T.A. Witten, Phys. Rev. E **62**, 2510 (2000).

[43] R.C. Youngquist, P.T. Metzger, and K.N. Kilts, to appear in SIAM J. Appl. Math. (unpublished).

[44] A. Mehta and S.F. Edwards, Physica A **157**, 1091 (1989); C.C. Mounfield and S.F. Edwards, Physica A **210**, 279 (1994); S.F. Edwards and C.C. Mounfield, Physica A **210**, 290 (1994); C.C. Mounfield and S.F. Edwards, Physica A **210**, 301 (1994); S.F. Edwards and D.V. Grinev, Phys. Rev. E **58**, 4758 (1998); S.F. Edwards, J. Non-Cryst. Solids **293-295**, 279 (2001); A. Coniglio and M. Nicodemi, Physica A **296**, 451 (2001); S.F. Edwards and D.V. Grinev, Adv. Phys. **51**, 1669 (2002); R. Blumenfeld and S.F. Edwards, Phys. Rev. Lett. **90**, 114303 (2003); J. Brujić, S.F. Edwards and D.V. Grinev, Phil. Trans. R. Soc. Lond. A **361**, 741 (2003); S.F. Edwards, D.V. Grinev and J. Brujić, Physica A **330**, 61 (2003); A. Coniglio, A. Fierro, and M. Nicodemi, Physica D **193**, 292 (2004).

[45] A. Barrat, J. Kurchan, V. Loreto and M. Sellitto, Phys. Rev. Lett. **85**, 5034 (2000); A. Barrat, J. Kurchan, V. Loreto and M. Sellitto, Phys. Rev. E **63**, 051301 (2001); J. Berg, S. Franz, and M. Sellitto, Eur. Phys. J. B **26**, 349 (2002); V. Colizza, A. Barrat, and V. Loreto, Phys. Rev. E **65**, 050301(R) (2002); A. Fierro, M. Nicodemi, and A. Coniglio, Phys. Rev. E **66**, 061301 (2002); J.J. Brey and A. Prados, Phys. Rev. E **68**, 051302 (2003); AG. Trajus and P. Viot, Phys. Rev. E **69**, 011307 (2004).

[46] H.A. Makse and J. Kurchan, Nature **415**, 614 (2002).

[47] S.F. Edwards and C.C. Mounfield, Physica A **226**, 1 (1996); C.C. Mounfield and S.F. Edwards , Physica A **226**, 12 (1996); S.F. Edwards and C.C. Mounfield, Physica A **226**, 25 (1996); S.F. Edwards, Physica A **249**, 226 (1998); S.F. Edwards, Philos. Mag. A **77**, 1293 (1998); S.F. Edwards and D.V. Grinev, Phys. Rev. Lett. **82**, 5397 (1999); S.F. Edwards and D.V. Grinev, Chaos **9**, 551 (1999); S.F. Edwards and D.V. Grinev, Physica A **263**, 545 (1999); R.C. Ball and D.V. Grinev, Physica A **292**, 167 (2001); S.F. Edwards and D.V. Grinev, Physica A **294**, 57 (2001); S.F. Edwards and D.V. Grinev, Physica A **302**, 162 (2001); R. Blumenfeld, cond-mat/0312313 (unpublished); R. Blumenfeld, cond-mat/0402556 (unpublished).

[48] J.-P. Bouchaud, P. Claudin, D. Levine, and M. Otto, Eur. Phys. J. E **4**, 451 (2001); M. Otto, J.-P. Bouchaud, P. Claudin, and J.E.S. Socolar, Phys. Rev. E **67**, 031302 (2003); J.E.S. Socolar, Discrete Cont. Dyn. B **3**, 601 (2003); J.-P. Bouchaud, M.E. Cates, and J.P. Wittmer, Phys. Rev. E **57**, 4441 (1998); J. Geng, D. Howell, E. Longhi, R.P. Behringer, G. Reydellet, L. Vanel, E. Clément, and S. Luding, Phys. Rev. Lett. **87**, 035506 (2001); D. Serero, G. Reydellet, P. Claudin, É. Clément, and D. Levine, Eur. Phys. J. E **6**, 169 (2001); C.F. Moukarzel, J. Phys. Cond. Mat. **14**, (2002); N.W. Mueggenburg, H.M. Jaeger, and S.R. Nagel, Phys. Rev. E **66**, 031304 (2002); L. Breton, P. Claudin, É. Clément, and J.-D. Zucker Europhys. Lett. **60**, 813 (2002); J. Geng, G. Reydellet, E. Clément, and R.P. Behringer, Physica D **182**, 274 (2003).

[49] A.V. Tkachenko and T.A. Witten, Phys. Rev. E **60**, 687 (1998); L. Vanel, D. Howell, D. Clark, R.P. Behringer, and E. Clément, Phys. Rev. E **60** R5040 (1999); J. Rajchenback, Phys. Rev. E **63**, 041301 (2001); J. Geng, E. Longhi, R.P. Behringer, and D.W. Howell, Phys. Rev. E **64**, 060301(R) (2001).

[50] S. McNamara and H. Herrman, cond-mat/0404297 (unpublished).

[51] H. Troadec, F. Radjai, S. Roux, and J.C. Charmet, Phys. Rev. E **66**, 041305 (2002).

[52] P.A. Cundall and O.D.L. Strack, Géotechniqe, **29**, 47 (1979).

[53] *PFC2D Theory and Background*, Second Ed.(Itasca Consulting Group, Minneaspolis, 2002).

[54] G.T. Seidler, G. Martinez, L.H. Seeley, K.H. Kim, E.A. Behne, S. Zaranek, B.D. Chapman, S.M. Heald, and D.L. Brewe, Phys. Review E **62**, 8175 (2000).